

**EXAMINATION OF A MICROMECHANICS BASED FAILURE CRITERION
FOR NON-CRIMP FIBER REINFORCED COMPOSITE LAMINATES**

by
EMRE FIRLAR

Submitted to the Graduate School of Engineering and Natural Sciences
in partial fulfillment of
the requirements for the degree of
Master of Science

Sabanci University
Spring 2008

EXAMINATION OF A MICROMECHANICS BASED FAILURE CRITERION FOR
NON-CRIMP FIBER REINFORCED COMPOSITE LAMINATES

APPROVED BY:

Assist Prof. Dr. Melih Papila.....
(Dissertation Supervisor)

Assoc. Prof. Dr. Mehmet Ali Gülgün

Prof. Dr. Yusuf Menciloğlu.....

Assist Prof. Dr. Mehmet Yıldız.....

Assist Prof. Dr. Nuri Ersoy.....

DATE OF APPROVAL: 22.07.08

© Emre Fırlar 2008
All Rights Reserved

EXAMINATION OF A MICROMECHANICS BASED FAILURE CRITERION FOR NON-CRIMP FIBER REINFORCED COMPOSITE LAMINATES

Emre Fırlar

Materials Science and Engineering, M. Sc. Thesis, 2008

Thesis Advisor: Assist. Prof. Melih Papila

Keywords: micromechanics of failure, finite element modeling, non-crimp fiber reinforced composite laminates

ABSTRACT

Warp-knit non-crimp fabric (NCF) reinforced polymer matrix composites manufactured by vacuum infusion (VI) have become appealing for structural applications, particularly in automotive parts, wind turbine blade production and marine industry. Their efficient and optimal use in structural design relies on the accuracy of the selected failure criterion typically specific to fiber reinforced composites. Experimental studies are conducted in order to measure the accuracy of the methodology of the applied failure criterion.

This thesis focuses on a failure criterion via finite element based micromechanics, typically referred as micromechanics of failure (MMF) and its experimental assessment for NCF reinforced polymer matrix composites. Glass fiber NCF/Vinyl ester unidirectional (UD) and multidirectional (MD) laminates are produced by VI. The mechanical properties of laminates with their constituent materials, i.e. the glass fiber and cured vinyl ester, are also measured to be used in micromechanics computations. Representative Volume Element (RVE) of a single fiber embedded in the polymer matrix at measured fiber volume fraction is modeled in MSC. PATRAN and solved in MD. NASTRAN for elastic constants. This RVE is also used for calculating the stress amplification factors within the RVE at several nodes. Back calculations of the glass fiber and cured resin strength by multiplying the ply average stresses at failure (experimental) with the maximum stress amplification factor are compared with the tested strength of constituents. They match well indicating the efficiency and accuracy of MMF in predicting the failure of NCF laminated composites and suggest that MMF can be implemented in design optimization of laminated composites against failure.

KIVRIMSIZ ELYAF TAKVİYELİ KOMPOZİT LAMİNATLAR İÇİN MİKROMEKANİK BAZLI KIRILMA KRİTERİNİN İNCELENMESİ

Emre Fırlar

Malzeme Bilimi ve Mühendisliği, Yüksek Lisans Tezi, 2008

Tez Danışmanı: Yar. Doç. Dr. Melih Papila

**Anahtar Kelimeler: kırılma mikromekaniği, sonlu elemanlar modellemesi,
kırırmsız elyaf takviyeli kompozit laminatlar**

ÖZET

İplik dikimi ile kat düzleminde paralel tutturulmuş elyaflardan oluşan, kırırmsız elyaf takviye dokumalar ve vakum infüzyon yöntemi ile üretilen polimer matris elyaf takviye kompozit yapılar otomotiv, rüzgar türbini ve deniz taşıt endüstrisinde sık kullanılır hale gelmiştir. Bu tip malzemelerin verimli ve en iyi şekilde yapısal tasarımlarda kullanılması, elyaf takviyeli kompozit yapılara özel geliştirilen/önerilen kırılma kriterinin etkinliğine bağlıdır. Kullanılacak olan kırılma kriterinin verimliliğinin değerlendirilmesi için deneysel çalışmalar önemli yer tutmaktadır.

Bu tezde, kırılma mikromekaniği olarak bilinen, sonlu elemanlar yöntemi esaslı mikromekanik çözümlerlerin kullanıldığı kırılma kriterinin ve bu kriterin kırırmsız elyaf takviyeli polimer matrisli kompozitler üzerinde deneysel olarak değerlendirilmesi üzerinde odaklanılmıştır. Kırırmsız cam elyaf/vinil esterden yapılmış tek ve çok yönlü laminatlar vakum infüzyon yöntemi ile üretilmiştir. Laminatların hammaddeleri için, cam elyaf ve reaksiyon süreci tamamlanarak sertleştirilmiş vinil ester numunelerin deneysel tespit edilen mekanik özellikleri mikromekanik hesaplamalarında kullanılmıştır. Ortasına elyaf gömülü olarak hazırlanmış temsili hacim elemanı MSC. PATRAN' da modellenmiş ve de MD. NASTRAN' da malzemenin elastik sabitlerinin elde edilmesi amacı ile çözdürülmüştür. Bu temsili hacim elemanı, çeşitli noktalarda gerilme artış katsayılarının bulunması sırasında da kullanılmıştır. Her bir laminadaki ortalama kırılma gerilmesi ile hesaplanmış olan gerilme artış katsayısı çarpımları ile bulunan elyaf ve reçine mukavemetleri, deneysel olarak bulunan değerler ile karşılaştırılmıştır. Bulgular, kırırmsız elyaf takviyeli kompozit laminatların kırılmasının tahmininde kullanılan mikromekanik esaslı kırılma kriterinin tutarlılığını ve doğruluğunu göstermiştir. Elde edilen sonuçlar mikromekanik esaslı bu kırılma kriterinin kompozit laminatların kırılmaya karşı tasarımlarının eniyileştirilmesi için kullanılabileceğini göstermektedir.

ACKNOWLEDGEMENT

The author is very grateful to his supervisor **Dr. Melih Papila** for his invaluable support and guidance during the Master's period.

I also thank to **Dr. Mehmet Ali Gülgün** for his great help in the Scanning Electron Microscopy (SEM) and Optical Microscope Imaging. **Dr. Güllü Kızıldaş** helped also a lot in the Finite Element Modeling (FEM) during my thesis.

My colleagues during my thesis were **Firuze Okyay, Cihan Pirimoğlu, Alp Araz, Sabri Kurum** and **Kaan Bilge**. If it wasn't for them, I couldn't make so many experiments in such a short period of time. **Gülay Bozoklu, Cahit Dalgiçdir, Gökhan Kaçar, Özge Malay, Vanya Uluç, Seren Yüksel, Can Kartoğlu, Firuze Okyay, Murat Mülayim, Zuhale Taşdemir, Eren Şimsek, Anastassia Zakhariouta, Burcu Saner, Cenk Gümece, Canan Dağdeviren** and **Erdem Öğüt** do share the same air with me in the Materials Science and Engineering Laboratories and I admit that a graduate study period wouldn't be so enjoyable, unless I was with them during my graduate study.

Mehmet Güler and **Süleyman Tutkun**, in the mechanical workshop, have also great help in my thesis as far as my tests are concerned. The specimen preparation for my mechanical tests wouldn't be easy unless we had them present in our faculty.

I am also thankful to **Çağrı Doğan** from **BIAS Engineering** for the assistance in FEM Modeling and **METYX Co.** for the supply of constituent materials in the composite production. **Cam Elyaf Co.** also helped a lot in glass fiber testing.

Special thanks are addressed to **TEMSA** and **The Scientific and Technological Research Council of Turkey (TUBITAK)** for the financial support.

TABLE OF CONTENTS

Overview of the Thesis	1
CHAPTER 1	3
1 INTRODUCTION	3
1.1 Vacuum Infusion.....	3
1.2 Non-Crimp Fiber Reinforcement.....	8
1.3 Micromechanics based Failure Criterion.....	10
2 MATERIALS AND MANUFACTURING	16
3 EXPERIMENTAL METHODS	23
3.1 Mechanical Testing.....	23
3.1.1 Tensile Testing of the Fiber	23
3.1.2 Tensile Testing of the Resin	25
3.1.3 Tensile Testing of the Laminates.....	25
3.2 Determination of Fiber Volume Fraction	26
4 COMPUTATIONAL METHODS	28
4.1 Semi – empirical Mechanistic Micromechanics for Elastic Constant Prediction....	30
4.1.1 Halpin – Tsai.....	30
4.1.2 Chamis	31
4.1.3 Rule of Mixture (ROM).....	31
4.2 FEM based Micromechanics for Elastic Constant Prediction	32
4.3 FEM based Failure Criterion	36
4.3.1 Methodology involving Application of Unit Strains [2], [3] (Option 1)....	37
4.3.2 Methodology involving Application of Unit Stress [4] (Option 2)	44
5 RESULTS.....	51
5.1 Case Study 1 (Examination of composites having loosely warp-knitted 600, 1200 and 2400TEX non-crimp reinforcement)	51
5.1.1 Mechanical Properties of the Constituent Materials.....	51
5.1.2 Mechanical Testing of the Laminates.....	54
5.1.3 Determination of Fiber Volume Fraction	57

5.1.4	Micromechanical Predictions using Monte Carlo Technique.....	58
5.1.5	Back Calculation of Strength Values of Constituents	60
5.2	Case Study 2 (Axial Strength Prediction of the UD Laminate by tightly warp-knitted NCF: Application of Back Calculation Methodology).....	63
5.2.1	Mechanical Testing of the Constituent Materials.....	64
5.2.2	Mechanical Examination of the UD Composite Laminates	64
5.2.3	Determination of Fiber Volume Fraction	66
5.2.4	Back Calculation of Strength Values of Constituents	67
5.3	Case Study 3(Verification of the Strength of Fiber and Resin of Laminates with 1200TEX fiber reinforcement having $((0/90)_3)_s$ stacking sequence).....	68
5.3.1	Mechanical Examination of the Laminates	69
5.3.2	Determination of Fiber Volume Fraction	69
5.3.3	Classical Lamination Theory via FEM.....	70
6	DISCUSSION.....	72
7	SUGGESTIONS.....	78
8	REFERENCES.....	79
9	APPENDIX	83
9.1	Case Study 1	83
9.2	Case Study 2	88
9.3	Case Study 3	92

LIST OF FIGURES

Figure 1.1- Performance vs. production volumes of composite manufacturing methods	5
Figure 1.2- Production techniques vs. production volume and component size	6
Figure 1.3- Typical view of non-crimp Fibers.....	9
Figure 1.4- The waviness of the fibers and individual fibers in the bundle [15].....	10
Figure 1.5- a) Brittle failure, b) Brittle failure with fiber pull-out, c) Brittle failure with fiber debonding and/or matrix failure	12
Figure 1.6- General methodology in micromechanics for composite laminates	15
Figure 2.1- A typical epoxy based vinyl ester	16
Figure 2.2- Uncured vinyl ester	17
Figure 2.3- Cured vinyl ester	17
Figure 2.4- Cross-sectional view of a laminate with 600 TEX fibers	18
Figure 2.5- Cross-sectional view of a laminate with 1200 TEX fibers	19
Figure 2.6- Cross-sectional view of a laminate with 2400 TEX fibers	19
Figure 2.7- Unidirectional dry glass fiber reinforcement a) with no lateral glass fibers to knit on b) with fraction of glass fibers laterally placed and knit on.	20
Figure 2.8- A typical vacuum infusion process	21
Figure 3.1- Zwick UTM at Cam Elyaf Co. for the testing of fiber bundles	24
Figure 3.2- Specimen dimensions of resin for tensile testing according to ASTM D638	25
Figure 3.3- Zwick Z100 UTM at Sabanci University for testing of polymers and composite laminates.....	26
Figure 4.1- Axes conversion from ply to laminate	28
Figure 4.2- Possible Representative Volume Elements a) Single cube, b) Multiple cube, c) Hexagonal, d) Diamond, e) Quarter hexagonal and f) Quarter diamond, where the white part shows the matrix and the red part shows the reinforcement.....	33
Figure 4.3- The representative volume element: square array type(where red part is for the fiber and the white part is for the resin).....	35
Figure 4.4- Critical points in the structure.....	38
Figure 4.5- Top-bottom view in the Material Property Prediction.....	39
Figure 4.6- Unit strains are applied to each RVE. a)Unit strain in X direction is applied and resulting strain distribution in X direction is given b) Unit strain in Y direction is applied and resulting strain distribution in Y direction is given c) Unit strain in Z direction is applied and resulting strain distribution in Z direction is given d) Unit strain in XY direction is applied and resulting strain distribution in XY direction is given e) Unit strain in XZ direction is applied and resulting strain distribution in XZ direction is given f) Unit strain in YZ direction is applied and resulting strain distribution in YZ direction is given.....	43

Figure 4.7-The multiple point constraints on each face of RVE	44
Figure 4.8- Resulting amplified stress values for Case 1 a) Stresses are applied in x direction and resulting corresponding stress values in x direction b) Stresses are applied in y direction and resulting corresponding stress values in y direction	45
Figure 4.9- Stress Amplification Distribution Deformation in direction 2, when unit stresses are applied in 2 direction [3].....	46
Figure 4.10- Resulting amplified stress values for Case 2 a) Stresses are applied in x direction and resulting corresponding stress values in x direction b) Stresses are applied in y direction and resulting corresponding stress values in y direction	47
Figure 4.11- Stress Amplification Distribution Deformation in direction 2, when unit stresses are applied in 2 direction	47
Figure 4.12- Comparison of amplified stress values in X direction for Case 1 resulting from both application of unit strains and stresses in X direction.....	48
Figure 4.13- Comparison of amplified stress values in Y direction for Case 1 resulting from both application of unit strains and stresses in Y direction.....	48
Figure 4.14- Comparison of amplified stress values in X direction for Case 2 resulting from both application of unit strains and stresses in X direction.....	49
Figure 4.15- Comparison of amplified stress values in Y direction for Case 2 resulting from both application of unit strains and stresses in Y direction.....	49
Figure 5.1- Tension test of 600TEX glass fibers	52
Figure 5.2- Tension test of 1200TEX glass fibers	52
Figure 5.3- Tension test of 2400TEX glass fibers	53
Figure 5.4- Tension test of the cured Crystic Scott Bader T671 vinyl ester resin.....	53
Figure 5.5- Longitudinal tension test of (0) ₈ laminates with 600TEX fibers.....	54
Figure 5.6- Longitudinal tension test of (0) ₈ laminates with 1200TEX fibers,.....	55
Figure 5.7- Longitudinal tension test of (0) ₈ laminates with 2400TEX fibers	55
Figure 5.8- Transverse tension test of (0) ₈ laminates with 600TEX fibers	56
Figure 5.9- Transverse tension test of (0) ₈ laminates with 1200TEX fibers	56
Figure 5.10- Transverse tension test of (0) ₈ laminates with 2400TEX fibers	57
Figure 5.11- Comparison of experimental and computed values modulus of laminates - transverse moduli a) Experimental vs inverse ROM, b)Experimental vs Halpin-Tsai, c) Experimental vs Chamis and d) Longitudinal modulus experimental vs predicted ..	59
Figure 5.12- Comparison of experimental and back calculated fiber strength values....	62
Figure 5.13- Comparison of experimental and back calculated resin strength values ...	63
Figure 5.14- Tension test of Scott Bader Crystic T676 NA vacuum infusion resin.....	64
Figure 5.15- Longitudinal tension test of (0) ₁₂ UD laminates	65
Figure 5.16- Transverse tension test of (0) ₁₂ UD laminates	65
Figure 5.17- Comparison of predicted and experimental fiber strength values both with reduced (effective) and unreduced (overall) fiber volume fractions	67
Figure 5.18- Tension testing of ((0/90) ₃) _s laminates.....	69

Figure 6.1- Waviness of fiber bundles in the structure and resin pockets prevents the efficiency of isostress condition. 76

LIST OF TABLES

Table 1.1- Comparison of expenses required for different manufacturing processes	6
Table 1.2- Typical failure modes of glass and carbon fiber reinforced polymer composites	11
Table 1.3- Test cases for different micromechanical models	13
Table 2.1- Measured diameters of individual fibers	20
Table 2.2- Laminate constituents with ply stacking	22
Table 3.1- Specimen dimensions for laminates to be used in tensile testing.....	25
Table 4.1- Axial and transverse modulus equations of semi - empirical models	31
Table 4.2- The applied boundary conditions to the representative volume elements.....	34
Table 4.3- Properties of constituents for the verification of the methods described by Barbero.....	35
Table 4.4- The Comparison of the values found via FEM Method and the ones given in Barbero.....	36
Table 4.5- Unit strain values are applied for each condition	37
Table 4.6- The list of critical points in the structure.....	38
Table 4.7- The properties of the constituents used in case 1	45
Table 4.8- The properties of the constituents used in case 2	46
Table 5.1- Minimum and maximum values stiffness and fiber volume fraction of fibers used in the MC Simulations.....	58
Table 5.2- Minimum and maximum stiffness values of the resin used in the MC Simulations	58
Table 5.3- Stiffness predictions via Monte Carlo Simulation	59
Table 5.4- Comparison of strength values of the fibers with the values found via back calculation.....	61
Table 5.5- Comparison of strength values of the resin with the values found via back calculation.....	62
Table 5.6- Comparison of predicted and experimental fiber strength values both with overall and effective fiber volume fractions	67
Table 5.7- Elastic Moduli of biaxial reinforced laminates obtained via UTM Device...	69
Table 5.8- Laminate Properties predicted via CLT	70
Table 5.9- Prediction of fiber strength in ((0/90) ₃) _s laminates	70
Table 5.10- Prediction of resin strength in ((0/90) ₃) _s laminates	71
Table 9.1- Stiffness values of the loosely warp knitted fibers and Crystic Scott Bader T671 vinyl ester resin	83
Table 9.2- Longitudinal and transverse stiffness values of laminates with UD reinforcement having loosely warp knitted fibers and Crystic Scott Bader T671 vinyl ester resin	84

Table 9.3- Fiber volume fractions of UD reinforcement having loosely warp knitted fibers and Crystic Scott Bader T671 vinyl ester resin	84
Table 9.4- Elastic moduli and stiffness of Crystic Scott BaderT671 vinyl ester resin	88
Table 9.5- Axial and transverse moduli of UD laminates	89
Table 9.6- Fiber volume fraction of biaxial reinforced laminates	94
Table 9.7- Axial and transverse moduli of UD laminates	95

LIST OF SYMBOLS

Subscripts 1, 2, 3	directions for material axes where 1 refers to the longitudinal, and 2 and 3 refer to transverse directions
Subscripts x, y, z	directions in the global axes where x refers the longitudinal, and y and z for transverse directions
Subscript m	matrix material
Subscript f	fiber material
V_f	fiber volume fraction
E_f	elastic modulus of fiber
E_m	elastic modulus of matrix
σ_f	strength of fiber
σ_m	strength of matrix
G_f	shear modulus of fibers
G_m	shear modulus of matrix
ν_f	Poisson's ratio of fiber
ν_m	Poisson's ratio of matrix
ε	strain
$u_{x,y,z}$	displacements in x, y and z directions
C_{ij}	stiffness tensors
S_{ij}	compliance tensors
σ_{ij}	stress tensors
Subscript L	longitudinal direction
Subscript T	transverse direction
Upper dash $\bar{\quad}$	average Value

LIST OF ABBREVIATIONS

NCF	Non-Crimp Fibers
FEM	Finite Element Methodology
CLT	Classical Lamination Theory
TEX	Grams of Fiber in one kilometer Length
UD	Unidirectional
BD	Bidirectional
FRP	Fiber Reinforced Polymer
ASTM	American Society for Testing and Materials
IF1, 2	Inter-fiber positions 1, 2
IS	Interstitial Position
M1-8	Positions 1-8 in Matrix
F1-9	Positions 1-9 in Fiber
RVE	Representative Volume Element
AF	Amplification Factor

*To my beloved family
Bahar, Musa, Süheyda, Burak and Mine*

Overview of the Thesis

One of the focus points in this thesis is the non-crimp fabric (NCF) reinforcement for composites. Use of warp-knit NCF has increased in structural applications of fiber reinforced plastics (FRP) made by resin flow/wetting processes such as resin transfer molding (RTM) and vacuum infusion (VI). These processes are particularly appealing to automotive making, wind turbine blade production and marine industry as they are more economical than autoclave molding, and provide much better quality than hand wet lay-up technique. Use of NCF, furthermore addresses the high material cost, like the one of high quality pre-preg materials without significant sacrifice in in-plane capability, unlike woven type reinforcement. In short the NCF and VI somewhat combine attributes of unidirectional pre-preg tapes at much reduced cost.

The second essential element here is finite element based micromechanics of failure (MMF). One of the most vivid research topics regarding mechanical behavior of the fiber reinforced composites is fracture or failure criteria and their implementations in design. Despite the significant amount of work and various criteria already proposed, there is still need for improvement on the available criteria or proposition of new criteria. It is primarily because in composite materials that there exist numerous types of failure, such as fiber pull-out, fracture of fiber, matrix cracking, delamination etc. In addition, the available criteria usually were demonstrated / proposed in case of specified lay-ups and loading type, rather than being validated for any scenario. Micromechanics based failure criteria/analysis has gotten considerable attention recently and several methods proposed and implemented in predicting even the progression of the failure in composite materials. The available data however appears to be concentrated on the composites made by pre-pregs.

As the title implies, the thesis is focused on these two elements and combines them by the following objectives:

- To exercise the finite element based micromechanics analysis of the fiber reinforced composites by unidirectional and bidirectional ply stacking

- To demonstrate the efficiency of the micromechanics based failure analysis in NCF composite laminates.

In the first chapter, a brief introduction regarding the vacuum infusion, non-crimp reinforcement and an MMF based failure criterion are given. The second chapter presents the materials and description of the laminates along with the vacuum infusion steps that were followed for the laminate production. Next chapter describes the experiments for the determination of mechanical properties of both the laminates and constituents and fiber volume fraction of the constituents. In the fourth chapter, the computational methods including both the semi-empirical and FEM based elastic constant prediction models are explained. It presents a novel FEM based failure criterion recently implemented by Ha and his co-workers. In the fifth chapter, the results are given for three case studies. The conclusions are discussed in the sixth chapter. Finally, the suggestions will be given in the seventh chapter.

In this study, the variability or uncertainty in the material properties are taken into consideration. Statistics of the experimental results and associated bounds for all computations are also reported. Two types of NCF reinforcements with three different TEX values and two types of resin were used with varying stacking in the case studies. In the first case study, the effects of TEX on the final mechanical properties of unidirectional reinforced laminates were examined [1]. The stress amplification factors are calculated [2], [3], [4] and back calculation methodology [3], [4] is applied to these laminates with different TEX values in order to estimate the strength of both the fiber and resin. In the second case study, the back calculation methodology on a laminate with another type of fabric is examined. In the final study, the modulus of $((0/90)_3)_s$ laminate is tried to be predicted via FEM and back calculation method is applied to predict the strength of both fiber and resin[5].

CHAPTER 1

1 INTRODUCTION

1.1 Vacuum Infusion

Vacuum infusion (VI) is one of the easiest and cheapest composite laminate manufacturing methods. It requires cheap tooling and low craftsmanship. The basic mechanism can be described as the conveyance of the resin through the reinforcement which is accomplished with the application of vacuum. VI appeared in the 1940s with the name of Marco Process. Due to the environmental legislation in 1970s and 1980s, the amount of emitted styrene was reduced from 100 to 25 or 20ppm in Western Countries. The firms using open-mold processes had to use ventilation systems in order to remove the styrene output from the process and additional filters help in the removal of emitted styrene. As the development regarding the elimination of the styrene after the environmental legislation proceeds, VI has become a strong competitor to open mold processes like hand lay-up and spray-up. The companies divert into the vacuum infusion method in the 1990s due to this elimination of this poisonous product. Although this technology was started to be used in 1940s, there are many unknowns in this technique. The introduction of the vacuum infusion also results in high quality final products. This high quality lets the manufacturers in the aviation and aerospace use these products in the high-tech goods.

Vacuum infusion is a derivation of the resin transfer molding technique (RTM). A typical resin transfer molding process is done as the placement of fibers into the mold

and after that the mold is closed and resin is conveyed through the fibers via an injector, resulting in impregnation of the fibers. With the application of desired pressure and temperature, the resin is cured and after the laminate becomes completely solid, the laminate is taken out of the mold [6]. The final products manufactured via RTM are known to be stiff and strong, which necessitates a more expensive tooling so as to be compared with other methods. This drawback was overcome with the usage of vacuum in the vacuum infusion method. The application of the pressure gradient for the flow of the resin determines the type of the injection technique. In the case of vacuum infusion the pressure gradient is created by vacuum on the outlet port. In the RTM technique the resin injection tank is under desired pressure. In RTM (with a pressurized resin tank and an outlet at ambient pressure), a leak in the mold would just result in resin spillage. Besides, air will flow into the mold much easier than resin will flow out of the mold (i.e., the viscosity of air is much smaller than the viscosity of the resin) [6]. So, when a laminate with certain volume fraction of fiber is required with a regular quality (not for use in high-tech applications like aerospace), the vacuum infusion method becomes a strong competitor.

Laminate Manufacturing Methods via Resin Conveyance

There are several derivatives of Vacuum Infusion. In Structural Reaction Injection Molding (SRIM), the two types of resin, which are typically polyurethanes with low viscosity, are mixed and sent to the reinforcement cavity [7]. In the Vacuum Assisted Resin Injection (VARI), the mold is stayed strong, and the amounts of the voids in the laminates are reduced with the application of vacuum. In the Resin Film Infusion (RFI) method, the resin is conveyed through the fibers as film pellets with an increase in heat resulting in a lower viscosity, which helps resin to flow through the thickness [8]. In the Seeman Composite Resin Infusion Molding Process (SCRIMP) process, the dry fibers are placed in a mold with a core and they are covered with a flexible vacuum bag and a SCRIMP cloth. With the application of the vacuum, the catalyzed resin is sent to the mold [9]. VI is used mainly in the manufacturing of the fiber reinforced polymers

(FRP). There is no clear boundary between RTM and vacuum infusion. The way of the pressure application and tooling mainly determine the technique.

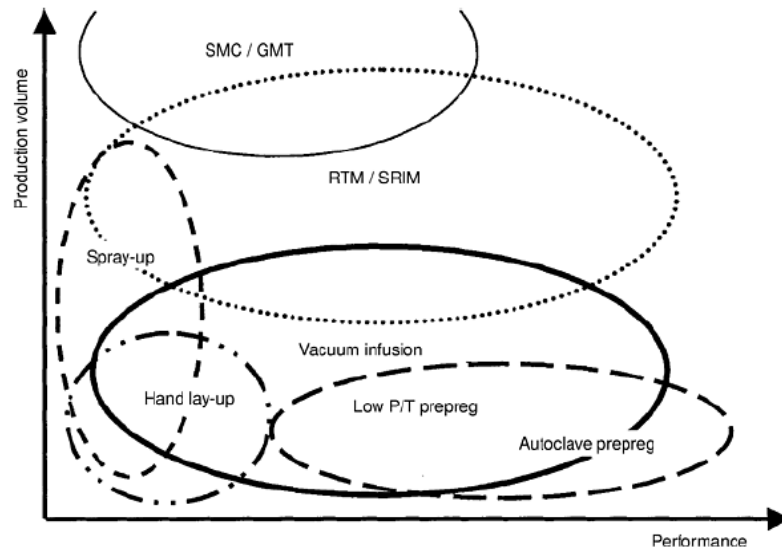


Figure 1.1- Performance vs. production volumes of composite manufacturing methods

Typical Properties of Vacuum Infusion Process

Three-dimensional curved, shell-like structures and closed hollow parts can be manufactured via this method. The most crucial issues that limit the size of the structure are practicality and accessibility to place the dry reinforcement in the mold system. Sharp edges may disturb the flow pattern of the resin and variations of the thickness result in the change in the flow of the resin. Several types of cores and inserts can also be placed in the structure constructed via vacuum infusion. The fiber content in the composite structure manufactured via vacuum infusion varies from 15% to 65%. The type of mold, resin and fiber determine the surface finish of the structure. Mainly, the surface which is in contact with the mold has a good surface finish. It is difficult to obtain a net shape in vacuum infusion. During the removal of the structure from the mold, there appear several places consisting of only resin and some places where the alignment of fibers is disturbed, both of which have to be trimmed.

Table 1.1 gives the economical point of view of several composite manufacturing methods. As also seen in the table below and figure 1.1, the vacuum infusion process is a cost-effective method.

Table 1.1- Comparison of expenses required for different manufacturing processes

	Vacuum Infusion	RTM	Hand Lay-Up	Spray Lay-Up	Low P/T Pre-preg	Autoclave Pre-preg
Workshop Requirements	\$\$	\$\$	\$\$\$\$	\$\$\$\$	\$\$\$	\$\$\$
Equipment	\$\$	\$\$\$	\$	\$\$	\$\$\$	\$\$\$\$\$
Tooling	\$\$	\$\$\$\$	\$\$	\$\$	\$\$	\$\$\$
Ancillary Materials	\$\$\$	\$\$	\$	\$	\$\$\$	\$\$\$
Raw Materials	\$\$	\$\$	\$\$	\$	\$\$\$	\$\$\$\$
Labor	\$\$	\$	\$\$	\$	\$\$\$	\$\$\$

In a typical vacuum infusion setup, a vacuum pump and a resin trap are required. Tooling for vacuum infusion, hand lay-up, spray-up, and low pressure and temperature pre-preg can be simple and relatively cheap when compared with the autoclave pre-preg and RTM. Vacuum infusion requires a foil, sealant tape, tubes, peel-ply, flow media and hoses. VI involves more expensive reinforcement materials than spray-up, but is much cheaper than pre-pregging materials. Glass, carbon and aramid fibers are generally used as the reinforcing materials. Epoxy, vinyl ester and polyester are the commonly used resin materials. The ancillary materials used only once are foil, sealant tape, tubes, and hoses and discarded after demolding.

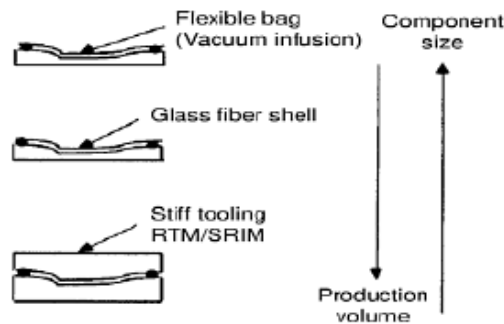


Figure 1.2- Production techniques vs. production volume and component size

As seen in figure 1.2, bigger components can be made with the VI method, whereas higher production volume can be obtained by means of RTM method. With the usage of glass fiber shell and application of some vacuum at the resin inlet, a compromise can be made between the component size and production volume.

Parameters affecting Resin Conveyance

For a quick and efficient resin conveyance, the viscosity of the resin and flow distance should be low, permeability of the reinforcement and the applied pressure difference should be high [10].

Advantages

Vacuum infusion is a cheaper solution to RTM, since the stiff and strong molds and injector are not needed. Since bigger geometries require bigger molds, the high amount of tooling is removed when the vacuum infusion is preferred. This method has also a lot of advantages when compared with manufacturing with the pre-pregs since pre-pregs require being kept at lower temperatures and are more expensive than the constituents used in vacuum infusion. Vacuum infusion process is not only cheaper when compared to resin transfer tooling, but also it is easier to conduct. Another advantage of VI is that the mold does not require prior heating and it is done at room temperature according to the type of the resin used. Details about the whole vacuum infusion process are given in Materials and Manufacturing Chapter. The geometry size and production volume comparison of several composite manufacturing techniques are given in figure 1.2. When the elimination of the styrene emission is concerned, vacuum infusion is also by far more environmental friendlier technique so as to be compared with the open mold techniques like spray-up and hand lay-up techniques. The quality of the laminate is better when compared to these two open mold techniques since higher

impregnation and higher fiber contents are obtained with this method. Besides, there is no limitation for the use of different type of fibers [11].

Disadvantages

The layup stacking should be of utmost carefulness placed in order to avoid the angle tolerance of the plies. If it cannot be removed, then the change in angle of ply may result in lower modulus and strength values. Another crucial fact is that the air should be completely removed before the resin transportation through the structure starts and it should be guaranteed that no holes are present on the vacuum bag and no open spots to air near the hose entrance and exit are present throughout the whole laminate. Besides, the good surface finish is difficult to achieve since the exothermic curing process makes large shrinkages inside the structure, which affects not only the final finish, but also the final strength and modulus values. In addition to these, the cleaner and releasing liquids, catalysts and hardeners, resins are hazardous to human health and the manufacturing should be done very carefully. Handling with the fiber reinforcement is also hazardous since the individual fibers are hard to notice with naked eye and can result in eye and skin damage.

1.2 Non-Crimp Fiber Reinforcement

As the less weight and improved mechanical properties are required for the structural elements, use of composite materials has become inevitable in various key industries such as aerospace and automotive. The most crucial desired properties of the composite structures are high stiffness and strength, lightweight, improved corrosion resistance and lowered maintenance for transportation and structural elements [12], [13]. Very stiff and strong composites can be obtained using autoclaves which is an expensive process since the energy consumed and time spent during the production of composites via autoclaves are very high. The unidirectional (UD) pre-pregs, readily

resin impregnated layers of fiber reinforcement used for this method have limited shelf/pot life, require being kept at lower temperatures and have high cost. To substitute the expensive UD pre-preg option without sacrificing its superior in-plane mechanical behavior, non-crimp fiber (NCF) reinforcements are produced. Unlike a woven fabric in which yarns are crimped due to interlacing, these multi-axial warp knitted fabrics preserve the unidirectional characteristics of each fiber layer (Figure 1.3) [14]. This form of reinforcement imitate the conventional stitched appearance with the advantage of eliminated crimping behavior [15], which results in the reduction of longitudinal modulus of the fiber tows, in turn accounts for the reduction of the longitudinal modulus of the laminate[16].

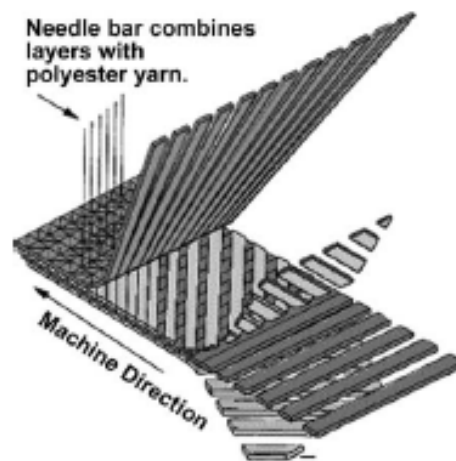


Figure 1.3- Typical view of non-crimp Fibers

The composites with NCFs can be produced via traditional hand lay-up, resin transfer molding, pultrusion, vacuum bagging, centrifugal casting and filament tape winding. The lack of obtaining very complicated shapes can be prevented by means of non-crimp fibers since they are of the form of high conformability. The non-crimp characteristic also results in the elimination of the weak compression behavior in the composite structure (Figure 1.3) [17]. As far as the shapes of the fiber bundles in NCFs are considered, the complexity is easily seen which is because of the resin pockets, surface compression during production and bundle orientation in the blanket (Figure 1.4). The wavy shape of the fiber bundles affects tensile strength and elastic modulus of

the composite structure. Final mechanical properties of the composite are directly affected by the effect of stitching and the presence of resin rich regions.

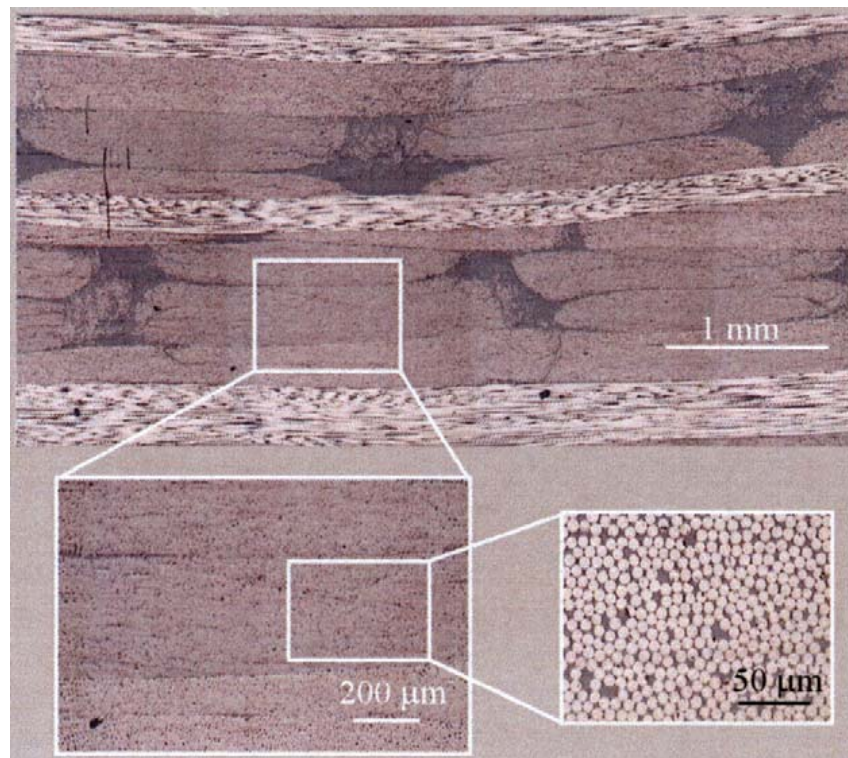


Figure 1.4- The waviness of the fibers and individual fibers in the bundle [15]

1.3 Micromechanics based Failure Criterion

Prediction of mechanical properties of composite laminates and their failure behavior are of crucial importance as they are not only used in many casual life devices, machines, but also in high-tech applications like space shuttles. That's why engineers are trying to anticipate the behavior of these laminates under different loadings without conducting many experiments since they require high cost and time. With the knowledge of the properties of constituents and the information about the volume fraction and type of reinforcements, the final behavior of the composite has always been tried to be guessed by micromechanics. It has been achieved mainly with analytical methods but as the precision come out, the trend in the industry turns to finite element

modeling. Not only the behavior of the laminate structure is guessed more precisely, changing the parameters in this method is also very easy and the visualization after computation gives a lot of information. The distribution of the micro stresses all in the fiber, matrix and fiber-matrix interface are well predicted by examining several critical nodes in the structure. For several failure criteria, stacking of plies, the elastic moduli, Poisson's ratios and volume fractions of the constituents are taken as the input data. For the prediction of strength of the laminate, the strength values of the constituents are also required. There are many factors affecting the modulus and strength of the composite structure, like, distribution, alignment and type of the fiber. All of these factors have to be taken into account in order to make a sound prediction for the mechanical properties of the composite structure.

Typical Failure Mechanisms

There are several types of laminate failure which are summarized at in table 1.2[18].

Table 1.2- Typical failure modes of glass and carbon fiber reinforced polymer composites

Type of Failure	Mechanism
Fiber Fracture	This type of failure is seen when the applied stress is higher than the tensile strength of the fiber.
Fiber Pull-Out	When fiber-matrix interface is not strong enough, this type of failure exist.
Matrix Cracking	When the applied tensile stress is higher than the tensile strength of the matrix, this failure is seen.
Fiber Buckling	If axial compressive stress is applied, this type of failure is seen.
Fiber Splitting and Radial Interface Crack	If the hoop stress in the fiber or interface region between the fiber and the matrix reaches its ultimate value, these failures can be observed.

The schematic illustrations of some of the failures listed above are given in figure 1.5[19].

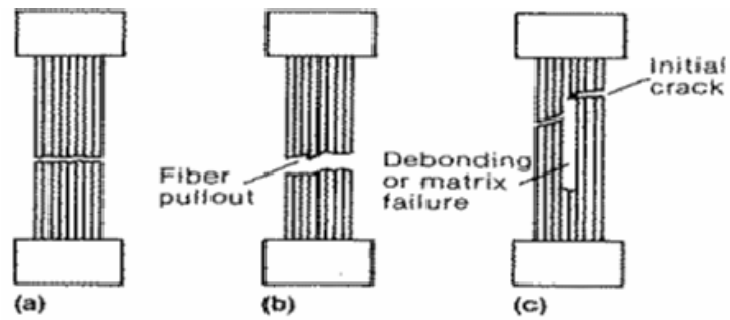


Figure 1.5- a) Brittle failure, b) Brittle failure with fiber pull-out, c) Brittle failure with fiber debonding and/or matrix failure

These failure modes are assumed to occur in the micromechanics based failure criteria given in literature. The most important and popular ones are discussed in Hinton *et al.*[20]. As stated in Hinton *et al.*, only a few can predict the failure by means of micromechanics, the most popular of which are Chamis, Hart-Smith, Rotem, Tsai, Puck, Mayes and Huang. These criteria are compared and contrasted in several test cases in Hinton *et al* which not only require different laminate lay-up but also different material properties(Table 1.3).

Table 1.3- Test cases for different micromechanical models

Laminate lay-up	Material	Test Case	Description
0°	E-glass / LY556 / HT907 / DY063	1	Biaxial failure stress envelope under transverse and shear loading (σ_y vs τ_{xy})
	T300 / BSL914C	2	Biaxial failure stress envelope under longitudinal and shear loading (σ_x vs τ_{xy})
	E-glass / MY750 / HY917 / DY063	3	Biaxial failure stress envelope under longitudinal and transverse loading v (σ_y vs σ_x)
(90° / ±30° / 90°)	E-glass / LY556 / HT907 / DY063	4	Biaxial failure stress envelope (σ_y vs σ_x)
		5	Biaxial failure stress envelope (σ_x vs τ_{xy})
(0° / ±45° / 90°)	AS4 / 3501-6	6	Biaxial failure stress envelope (σ_y vs σ_x)
		7	Stress - strain curves under uniaxial tensile loading in y direction (σ_y : $\sigma_x=1:0$)
		8	Stress - strain curves for $\sigma_y=\sigma_x=2:1$
±55°	E-glass / LY556 / HT907 / DY063	9	Biaxial failure stress envelope (σ_y vs σ_x)
		10	Stress - strain curves under uniaxial tensile loading for for $\sigma_y=\sigma_x=1:0$
		11	Stress - strain curves $\sigma_y=\sigma_x=2:1$
(0° / 90°)	E-glass / LY556 / HT907 / DY063	12	Stress - strain curves under uniaxial tensile loading for $\sigma_y=\sigma_x=0:1$
±45°	E-glass / LY556 / HT907 / DY063	13	Stress - strain curves for $\sigma_y=\sigma_x=1:1$
		14	Stress - strain curves for $\sigma_y=\sigma_x=1:-1$

Some of the criteria use linear analysis, which are Chamis, Hart-Smith and Tsai. Chamis uses Integrated Composites Analyzer (ICAN) and Composite Durability Structural Analyzer (CODSTRAN) modules to predict the biaxial failure envelopes and only CODSTRAN is used to create stress-strain curves. Chamis can predict all initial and final failures for all cases described in the table above except for case 6, since it can only predict initial failure for it. First ply strength is obtained from ICAN and ultimate tensile strength is obtained via CODSTRAN. CLT and FEM are used in this work. This methodology can identify the matrix failure. Micromechanics is used as failure criterion. Hart -Smith uses CLT to predict the failure in the structure. Hart - Smith can predict cases 1,2,3 both for initial and final failures, and 4,5,6 and 9 only final failures.

Longitudinal compressive failure and shear of fibers are evaluated in this criterion by means of Generalized Tresca Theory. Tsai uses CLT in order to compute the fiber tension and compression failures. Tsai-Wu Quadratic Theory is used in order to evaluate the failure, and a software named Mic-Mac is developed. Effect of nonlinearity comes onto surface for several cases. Nonlinearity can be primarily explained as the decrease in in-plane shear stiffness with the increase in the shear strain. Another reason for the introduction of the nonlinearity is the change of ply angle during the progression of the damage which results in the increase in the stiffness at large strains for $\pm 45^\circ$ laminates loaded in pure shear. Final reason for the nonlinearity may be the decrease in the transverse and shear moduli after initial failure. The remaining Rotem, Puck, Huang and Mayes use non-linear analysis. Rotem uses CLT to compute the failure with the Rotem Theory. An in-house program is developed in this work. Longitudinal compressive, tension and matrix failure are predicted with this work. Puck uses CLT with the Puck's Theory in his studies. A software called FRACUAN is used for this work. Fiber failure in tension and compression, interfiber failure for transverse tension, moderate transverse compression and large transverse compression failures are predicted in this criterion. Huang uses Generalized Maximum Stress with Plasticity with an in-house program. CLT is again used in this work. Fiber failure, transverse compressive failure and matrix failure are evaluated in this work. Mayes uses both CLT and FEM. Multi-Continuum Theory is used to compute the fiber and matrix failures. Tsai, Rotem, Puck, Huang and Mayes can predict all cases.

In Tay *et al.*, the amplified strain values are measured and the strain invariants are calculated in order to predict the failure[21]. In the theory of Jin *et al.* [2] and Ha *et al.* [3], the stress values amplified as a result of applied strains are evaluated. It is done as applying unit strain values to one face of a representative volume element (RVE) for the micromechanics model at a time and keeping the opposite face constant. Then, the matrices of both the stiffness of the lamina and nodal strains are obtained. With the usage of those matrices and stiffness matrices of the constituents, the amplified stress values are obtained and the possible failure regions are predicted. Alternatively, the amplified stress values can also be obtained with the method of Cai *et al.*[4], in which

the multiple point constraints are used and unit stresses are applied in order to evaluate the amplified stress values in the structure. Besides, by means of Back Calculation Methodology[4], the strength of the constituents can be retrieved if the laminate's strength values are known or vice versa. This methodology is also focused on and applied in this study as illustrated in the flowchart below:

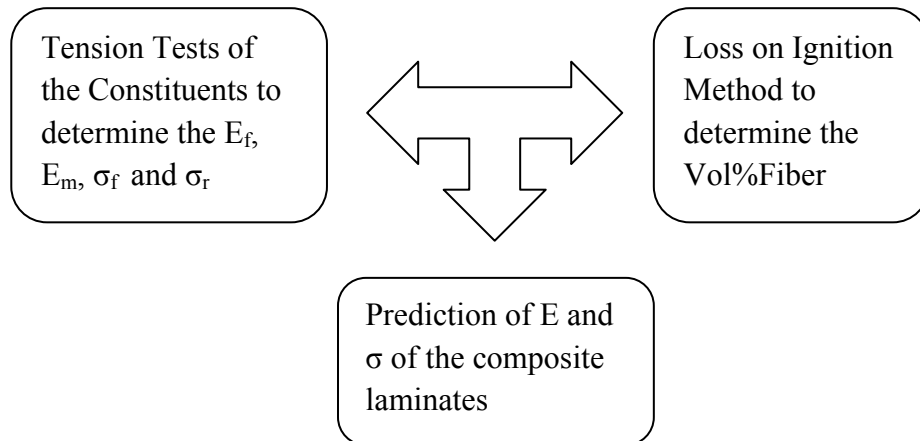


Figure 1.6- General methodology in micromechanics for composite laminates

According to the failure criterion discussed in this study, the fracture modes of the laminates appeared to be mainly the breakage of interfacial bonds and fiber pull-out.

CHAPTER 2

2 MATERIALS AND MANUFACTURING

There are two types of resin and two types of fiber reinforcement with three different TEX values used during the laminate production.

Resin: The types of resin are Crystic Scott Bader T671 and T676NA vinyl esters [22]. Vinyl ester resins have the advantage of having higher mechanical properties than polyesters. They also have very high chemical and environmental resistance. Mainly a post-cure is required for obtaining higher mechanical properties. Their disadvantages can be classified as their high styrene content, high curing shrinkage and higher price so as to be compared with polyesters. Typical view of the vinyl ester resin is given in figure 2.1. The uncured and cured vinyl esters are seen in figures 2.2 and 2.3, respectively. According to these figures, vinyl ester resins have relatively higher toughness than polyesters since the active sites are located only at the ends of the chains. Upon the application of an impact, the rest of the chain can withstand the load [23].

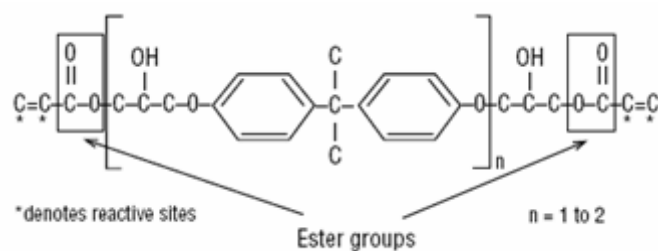


Figure 2.1- A typical epoxy based vinyl ester

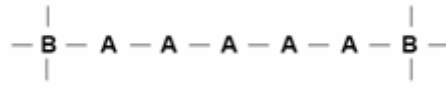


Figure 2.2- Uncured vinyl ester



Figure 2.3- Cured vinyl ester

The additives for T676NA are Accelerator D (styrene 10wt%, N-N dimethyl aniline with >89 wt %), Accelerator G (styrene >80wt %) and Butanox LPT (methyl ethyl ketone peroxide in diisobutyl phthalate). The composition of the resin is 1000ml T676NA vinyl ester, 10g Accelerator D, 20g Accelerator G and 20g Butanox LPT. The additives for the T671 are again Accelerator G and Butanox LPT. The composition of the resin is 1000ml T671 vinyl ester, 6ml of Accelerator G and 8ml of Butanox LPT.

Reinforcement: Several UD glass fiber reinforcements (like in figures 2.4, 2.5 and 2.6) made by fiber tows of different line density (weight per unit length) were used. The advantages of glass fibers are mainly their high tensile and compressive modulus and strength values. Since the ductility they have is very low, their toughness can be concluded as very low. They have low cost like £1-2/kg [24].

Experimental work was carried out using UD glass fiber reinforcements purchased from METYX Composites Co [25]. The UD dry reinforcements are formed by a special equipment that can place the tows next to each other and enables them to remain intact and stable by knitting with a small amount of fibers, typically 5-6%, but not necessarily of the same type of main reinforcing fibers in the perpendicular direction (i.e. if the UD is a 0° type, then the addition would be on the 90° direction) as shown in figure 1.3[14]. Several UD reinforcements (like in figures 2.4, 2.5 and 2.6) made by fiber tows of different line density (weight per unit length) were used. The fiber

reinforcements in this study were in the form of layers as shown in figures 2.7a and b, which involves only longitudinal fibers and transverse reinforcement in addition to the longitudinal ones, respectively. Specifically, 600 TEX, 1200 TEX and 2400 TEX glass fibers from PPG Industries, glass fibers of 600, 1200 and 2400 g/km, respectively were used[25]. The diameter of the individual glass fibers, in the tows were examined in the cross-sectional view of the laminate via Scanning Electron Microscopy (SEM) images (Figures 2.4, 2.5 and 2.6). Several individual fiber diameter measurements per each TEX and their statistics are reported in table 2.1. The diameter of individual fibers were found as 12.5 ± 1.0 , 17.1 ± 0.9 and 18.1 ± 0.8 mm for 600 TEX, 1200 TEX and 2400 TEX, respectively. The measurements indicated that there is a correlation between the TEX and the fiber diameter for the reinforcing materials used in this study. The fibers used are of two types, loosely warp-knitted and tightly warp-knitted fibers (Figures 2-7a and b). As given in table 2.1, when the number of TEX increases, the diameter of the fiber increases. The cross-sections of the laminates and the diameters of the fibers are seen in the figures below:

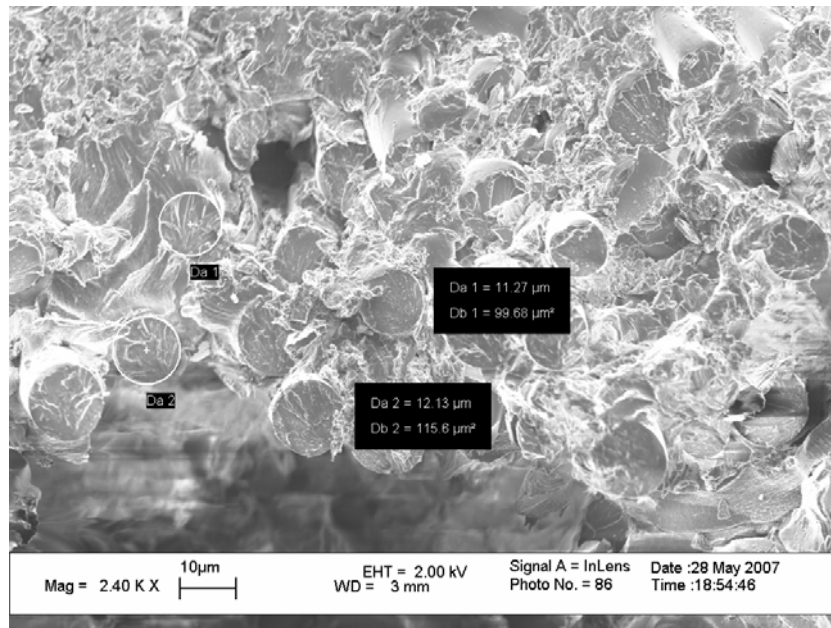


Figure 2.4- Cross-sectional view of a laminate with 600 TEX fibers

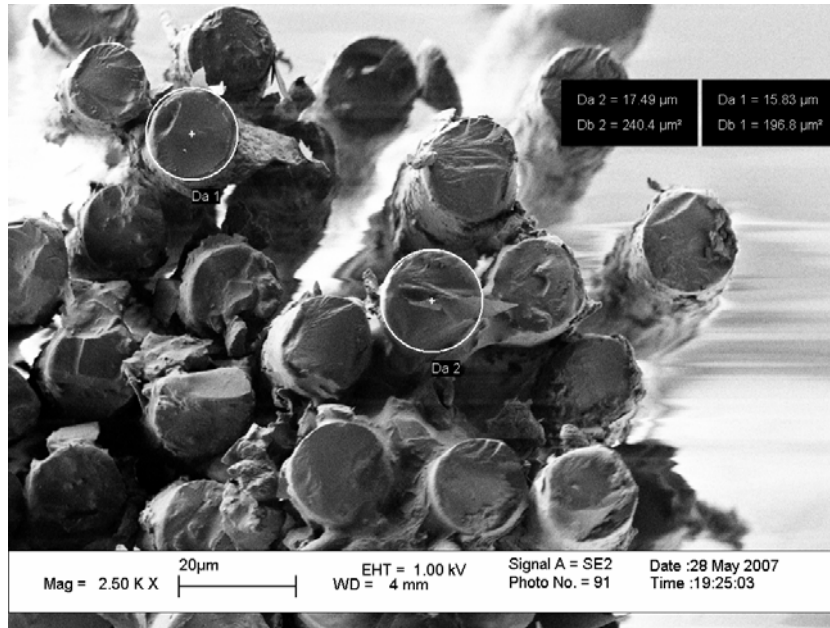


Figure 2.5- Cross-sectional view of a laminate with 1200 TEX fibers

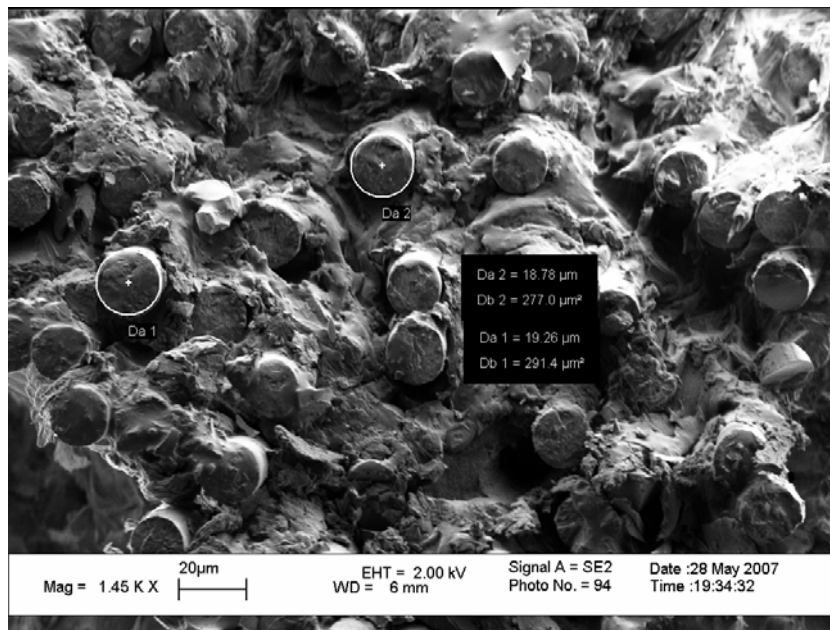


Figure 2.6- Cross-sectional view of a laminate with 2400 TEX fibers

Table 2.1- Measured diameters of individual fibers

#of Spec	Measured Diameters of Individual Fibers(in μm)		
	600 TEX	1200TEX	2400TEX
1	11.6	17.5	17.3
2	12.0	15.8	18.8
3	12.4	17.0	18.3
4	13.6	18.7	17.8
5	11.3	15.8	18.8
6	12.1	17.2	19.3
7	14.2	17.5	16.9
8	12.1	17.2	17.8
Average	12.5	17.1	18.1
Std dev	1.0	0.9	0.8

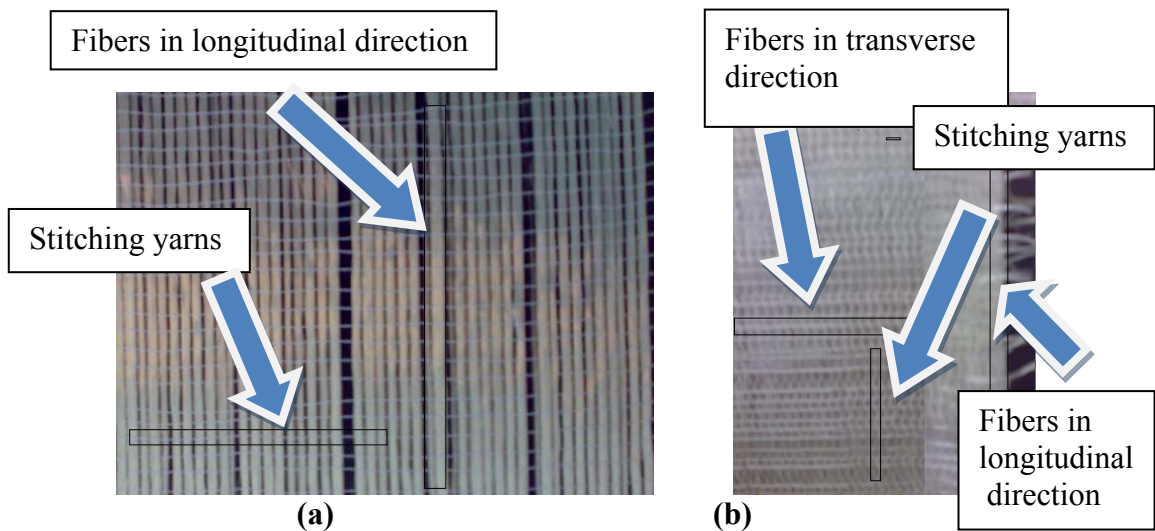


Figure 2.7- Unidirectional dry glass fiber reinforcement a) with no lateral glass fibers to knit on b) with fraction of glass fibers laterally placed and knit on.

Vacuum Infusion

The detailed procedure of the vacuum infusion method utilized for the laminate production in this work is

1. The mold is cleaned with a cleaner solvent.
2. The tape is placed in order to distinguish the boundary of the setup and to keep the vacuum bag fixed on the setup at the final stage of the setup implementation.

3. On the mold, the releasing agent is applied in order to remove the laminate easily.
4. Fiber lay-ups are cut and placed onto one another as in desired stacking.
5. The peel ply is put onto the fibers to remove the distribution media easily after the production of the laminate.
6. The distribution media is placed onto the peel ply.
7. The hose is prepared for both the connection between resin container and the laminate setup, and for the connection between the laminate setup and vacuum trap.
8. A helical hose is placed in the setup where resin enters the fiber lay-up to distribute the resin in the transverse direction.
9. The vacuum bag is placed onto the setup.
10. The vacuum is opened by keeping the hose at the resin part closed, in order to remove the initial air inside the laminate.
11. The resin is prepared and it is placed at the end of the hose which is at the inlet of the setup.
12. After the fibers are wet completely, the resin is removed from the entrance.
13. The setup is kept under vacuum as much as the curing time of the resin.
14. The vacuum is removed and the outlet from the setup is kept closed via a clamp.
15. When the curing process is completed, the distribution media is taken from the setup by means of the peel-ply.

Typical VI process is illustrated in figure 2.8[26].

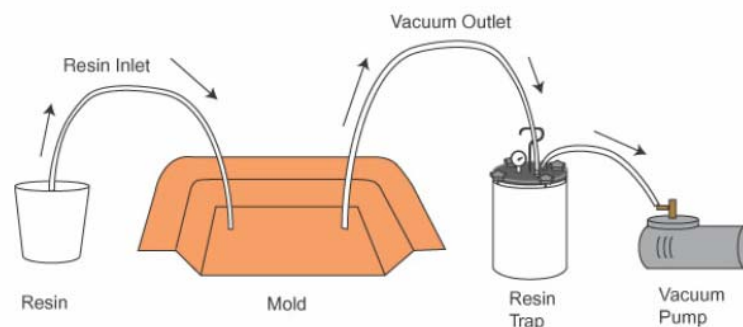


Figure 2.8- A typical vacuum infusion process

The stacking sequences for the laminates and respective constituent materials used in this work are summarized in table 2.2.

Table 2.2- Laminate constituents with ply stacking

	FIBER	RESIN	STACKING
Loosely warp-knitted	600TEX (Case 1)	Crystic Scott Bader T671 vinyl ester	(0) ₈
	1200TEX (Case 1)	Crystic Scott Bader T671 vinyl ester	(0) ₈
	2400TEX (Case 1)	Crystic Scott Bader T671 vinyl ester	(0) ₈
Tightly warp-knitted	1200TEX (Case 2)	Scott Bader Crystic T676 NA vinyl ester	(0) ₁₂
	1200TEX (Case 3)	Scott Bader Crystic T676 NA vinyl ester	((0/90) ₃) _s

CHAPTER 3

3 EXPERIMENTAL METHODS

3.1 Mechanical Testing

3.1.1 Tensile Testing of the Fiber

Mechanical testing of the fiber rovings are made in the Cam Elyaf Co. by means of the Zwick Z100 Tensile Testing Device with a special setup for fiber testing (Figure 3.1).



Figure 3.1- Zwick UTM at Cam Elyaf Co. for the testing of fiber bundles

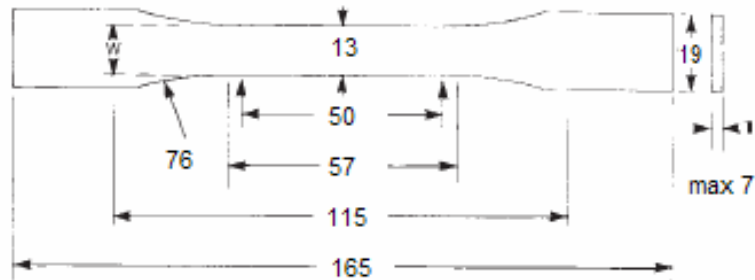
According to the factory standards, the grip to grip separation is set to 200mm and the speed of the test is set to 200mm/min. The results are obtained as kg vs. % elongation. The load (kg)/elongation (%) values obtained from the tension tests of 600, 1200 and 2400TEX fibers were converted into MPa by multiplying the kg values with factors of 42.84, 21.42 and 10.71, respectively. These conversion factors (CF) are calculated with the proposed equation:

$$CF = \frac{9.81(N / kg) * d(g / cm^3) * 0.01(cm^2 / mm^2)}{TEX (g / km) * 0.00001(km / cm)} \quad (3.1)$$

Where d=density of the fiber and TEX=number of TEX

3.1.2 Tensile Testing of the Resin

The 10kN load cells are used during our tests. The testing procedure is selected as ASTM D638 [27]. Rate of strain at the start was 0.1mm/mm.min and the speed of the test was 5mm/min. The dimension of a tensile test specimen of the resin is given in figure 3.2.



All dimensions are in mm.

Figure 3.2- Specimen dimensions of resin for tensile testing according to ASTM D638

Tensile testing of the resin is done in the Zwick Z100 UTM device (Figure 3.3).

3.1.3 Tensile Testing of the Laminates

This test is conducted according to ASTM D3039 standard [28]. The 100kN load cells were used during these tests. The speed of the testing device was set to 2mm/min. The specimen dimensions are given in table 3.1.

Table 3.1- Specimen dimensions for laminates to be used in tensile testing

Fiber Orientation	Width(in mm)	Length(in mm)
0 unidirectional	15	250
90 unidirectional	25	175
Balanced and symmetric	25	250

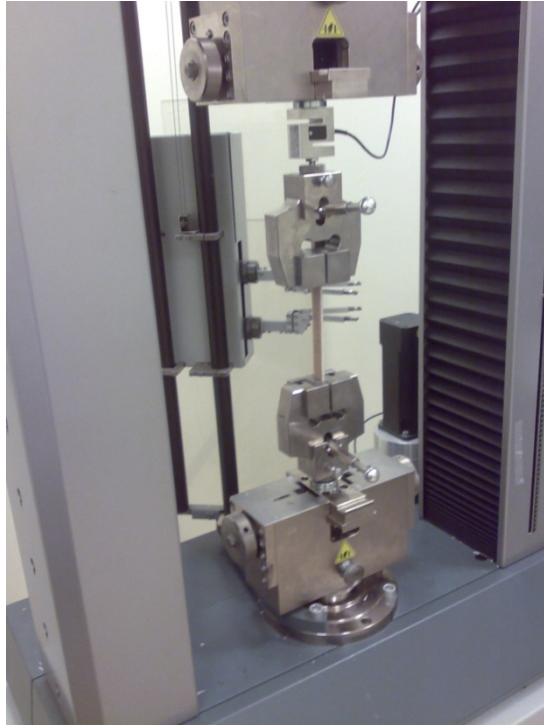


Figure 3.3- Zwick Z100 UTM at Sabanci University for testing of polymers and composite laminates

3.2 Determination of Fiber Volume Fraction

Loss on Ignition Method

The determination of the fiber volume fraction is done according to the Loss on Ignition Method found in literature as ISO1887 [29]. According to this method, first the specimen is placed in a container and its weight is measured (M_1). The weight of the container is also measured as C . Then, the specimen is heated up to 120°C in an oven open to air and kept at that temperature for 1 hour. The moisture is removed in this way and the weight is again measured (M_2). Finally, the container is heated to 650°C in the same environment and kept at that temperature for 30 minutes and again its weight is measured (M_3). The weight fraction is determined as

$$\text{Moisture} = M_1 - M_2 \quad (3.2)$$

$$W_f = \frac{M3 - C}{M2 - C} \quad (3.3)$$

The volume fraction of the fiber is then determined as

$$V_f = \frac{(M3 - C) / d_f}{(M2 - M3) / d_r + (M3 - C) / d_f} \quad (3.4)$$

Where d_f is the density of the fiber (= 2.62 g/cm³) and d_r is the density of the resin (= 1.33 g/cm³). V_f is the fiber volume fraction of the specimen.

CHAPTER 4

4 COMPUTATIONAL METHODS

Coordinate systems that are used throughout this thesis, the material coordinate system of the ply (axes 1 and 2) and the general coordinate system (axes x and y), are shown in figure 4.1.

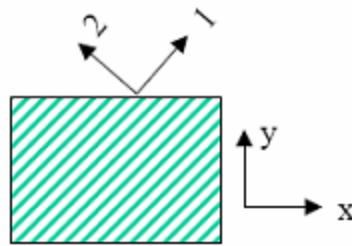
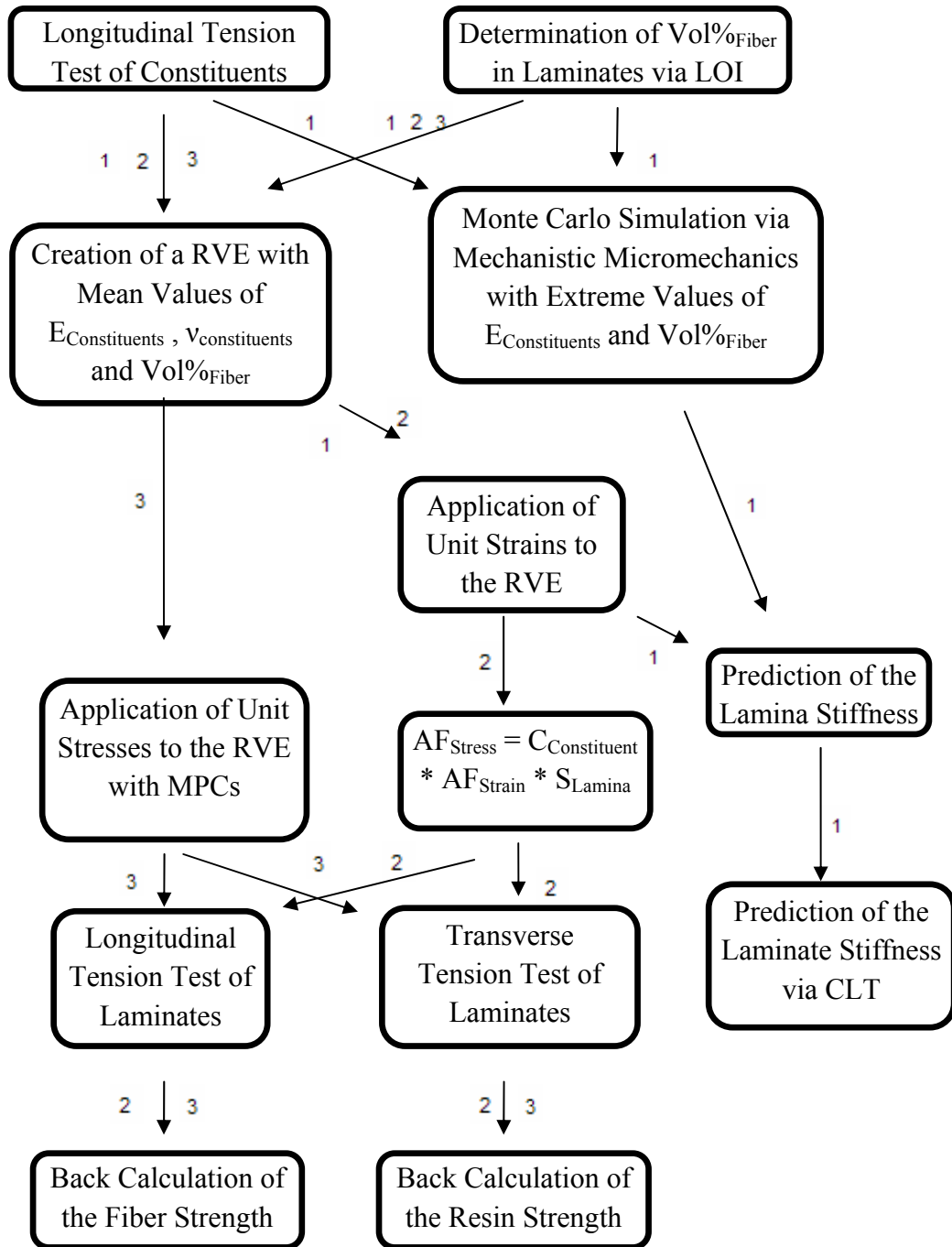


Figure 4.1- Axes conversion from ply to laminate

The methodology followed during the micromechanical analysis in this study is given as below:

1. Elastic constant prediction of the laminate
2. Back calculation of strength values of constituents with the application of unit strains
3. Back calculation of strength values of constituents with the application of unit stresses



4.1 Semi – empirical Mechanistic Micromechanics for Elastic Constant Prediction

The methodology for predicting the elastic constants of laminates starts mainly from the calculation of the properties for each ply. After having the knowledge of all the ply properties, i.e. modulus, strength, Poisson's ratio, thickness and angle, the Classical Lamination Theory (CLT) [5] is mainly used to obtain the properties of the laminates.

The equations for the prediction of both longitudinal and transverse moduli are given in table 4.1. The longitudinal modulus is predicted by all three models with (4.1). The models for the transverse modulus prediction are mainly discussed in the following sections.

4.1.1 Halpin – Tsai

In the equations for transverse modulus calculation (4.3) and (4.4), the geometrical factor ξ is very important. This factor depends on the stiffness and Poisson's ratio of the constituents elements. If $\xi=0$, then the transverse model becomes equal to the inverse model of Rule of Mixture. If $\xi=\infty$, then the transverse model of Halpin – Tsai becomes equal to the Rule of Mixture models. The value of ξ is also dependent on the fiber geometry, fiber distribution and loading conditions and taken as 2 according to the square array assumption [5].

Table 4.1- Axial and transverse modulus equations of semi - empirical models

Mechanistic/Semi-empirical Micromechanics Models			
Elastic Property	Mixture Rule Models	Halpin-Tsai	Chamis
Longitudinal Modulus	$E_{11} = E_f V_f + E_m V_m$ (4.1)		
Transverse Modulus	$E_{22} = \left(\frac{E_f E_m}{V_m E_f + V_f E_m} \right)$ (4.2)	$E_{22} = E_m \left(\frac{1 + \xi \eta V_f}{1 - \eta V_f} \right)$ (4.3) , where $\eta = \left(\frac{\frac{E_f}{E_m} - 1}{\frac{E_f}{E_m} + \xi} \right)$ (4.4) and $\xi = 2$ [5] for square array	$E_{22} = \frac{E_m}{1 - \sqrt{V_f} (1 - E_m / E_f)}$ (4.5)

4.1.2 Chamis

In the Chamis model, a cylindrical fiber model is assumed to be embedded in a homogenous matrix. A uniform load is applied at the infinity to this matrix and a strain field appears around the fiber, by means of which the elastic moduli are calculated [30]. The equation for the transverse moduli calculation for this model is given as (4.5) in table 4.1.

4.1.3 Rule of Mixture (ROM)

In the axial modulus calculation, the force is applied to the cross-section of the laminate (to the direction parallel to the fiber reinforcement) and the force is distributed between fibers and resin. Isostrain condition is assumed first. By dividing the force equation both with the area and strain, the equation regarding the axial modulus is

obtained (4.1). The formulation for the transverse modulus comes out as conveyance of the same stress through the fibers and resin if the load is applied transversely (isostress assumption). The relation regarding the strain is the summation of the strains of both the matrix and resin result in the total strain (4.2) [31].

4.2 FEM based Micromechanics for Elastic Constant Prediction

Finite Element based Unit Cell

As stated in Barbero [32], the elastic constants of the composite structures can be predicted with the creation of a suitable representative volume element (RVE) and periodic boundary conditions applied onto it. The basic procedure is to apply unit strain for each direction, i.e. X, Y, Z, XY, YZ and XZ. These boundary conditions are given in table 4.2. Then, the components of the stress tensors for each element calculated at the centroid are multiplied with the volume of the associated element. Next, these multiplied values for all elements are summed and divided with the total volume of the RVE, i.e. the volume average of the stress tensors are calculated for every 36 constants in the stiffness matrix of the composite laminate. Normally the stiffness tensor is a four ranked tensor but due to the symmetry in the structure, the 9x9 matrix reduces to 6x6. The required material properties are, as stated in the micromechanics review section, the volume fraction of the fiber and the elastic moduli and Poisson' s ratio of the isotropic constituent materials for elastic constant prediction.

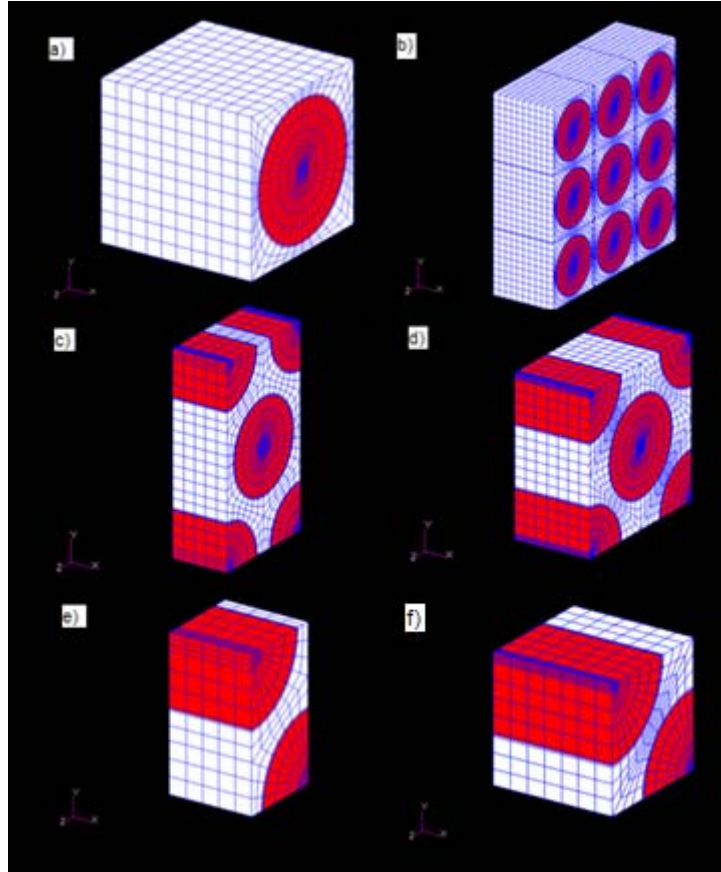


Figure 4.2- Possible Representative Volume Elements a) Single cube, b) Multiple cube, c) Hexagonal, d) Diamond, e) Quarter hexagonal and f) Quarter diamond, where the white part shows the matrix and the red part shows the reinforcement

The prescribed strain values applied to the representative unit element and the elastic constants of the structures are given table 4.2. All of the RVEs seen in figure 4.2 give approximately the same elastic constant values. For the sake of simplicity and frequency of use in the literature, the simple cube (Figure 4.2a) is used for further calculations. The stiffness matrix can be assumed as

$$C = \begin{bmatrix} C_{11} & C_{12} & C_{13} & C_{14} & C_{15} & C_{16} \\ C_{21} & C_{22} & C_{23} & C_{24} & C_{25} & C_{26} \\ C_{31} & C_{32} & C_{33} & C_{34} & C_{35} & C_{36} \\ C_{41} & C_{42} & C_{43} & C_{44} & C_{45} & C_{46} \\ C_{51} & C_{52} & C_{53} & C_{54} & C_{55} & C_{56} \\ C_{61} & C_{62} & C_{63} & C_{64} & C_{65} & C_{66} \end{bmatrix} \quad (4.6)$$

Table 4.2- The applied boundary conditions to the representative volume elements

Unit Strain Direction	Applied Strain Values
X(r=1)	$u(+x/2, ,) = (x, ,)$, $u(-x/2, ,) = (0, ,)$, $u(, +y/2,) = u(, -y/2,) = (, 0,)$, $u(, , +z/2) = u(, , -z/2) = (, , 0)$
Y(r=2)	$u(, +y/2,) = (, y,)$, $u(, -y/2,) = (, 0,)$, $u(+x/2, ,) = u(-x/2, ,) = (0, ,)$, $u(, , +z/2) = u(, , -z/2) = (, , 0)$
Z(r=3)	$u(, , +z/2) = (, , z)$, $u(, , -z/2) = (, , 0)$, $u(+x/2, ,) = u(-x/2, ,) = (0, ,)$, $u(, +y/2,) = u(, -y/2,) = (, 0,)$
XY(r=6)	$u(, +y/2,) = (x, ,)$, $u(, -y/2,) = (, 0,)$, $u(+x/2, ,) = u(-x/2, ,) = u(, , +z/2) = u(, , -z/2) = (, 0, 0)$
XZ(r=5)	$u(, , +z/2) = (x, ,)$, $u(, , -z/2) = (, , 0)$, $u(+x/2, ,) = u(-x/2, ,) = u(, +y/2,) = u(, -y/2,) = (, 0, 0)$
YZ(r=4)	$u(, , +z/2) = (, y,)$, $u(, , -z/2) = (, , 0)$, $u(+x/2, ,) = u(-x/2, ,) = u(, +y/2,) = u(, -y/2,) = (0, , 0)$

Where r is the boundary condition set number.

With the application of unit strains as given in table 4.2, C_{ij} values can be obtained, where i denotes the row and j denotes the column. With the application of one unit strain, one column of the stiffness tensor matrix can be obtained ($C_{1r}, C_{2r}, C_{3r}, C_{4r}, C_{5r}$ and C_{6r}). u is the displacement applied and x, y and z are dimensions of the representative volume element. The RVE stands at $(0,0,0)$ and $u(a,b,c) = (d,e,f)$ denotes the displacement of (d,e,f) applied to the face denoted with a,b,c . The representative volume element used in the study is mainly the square array type unit cell as in figure 4.3.

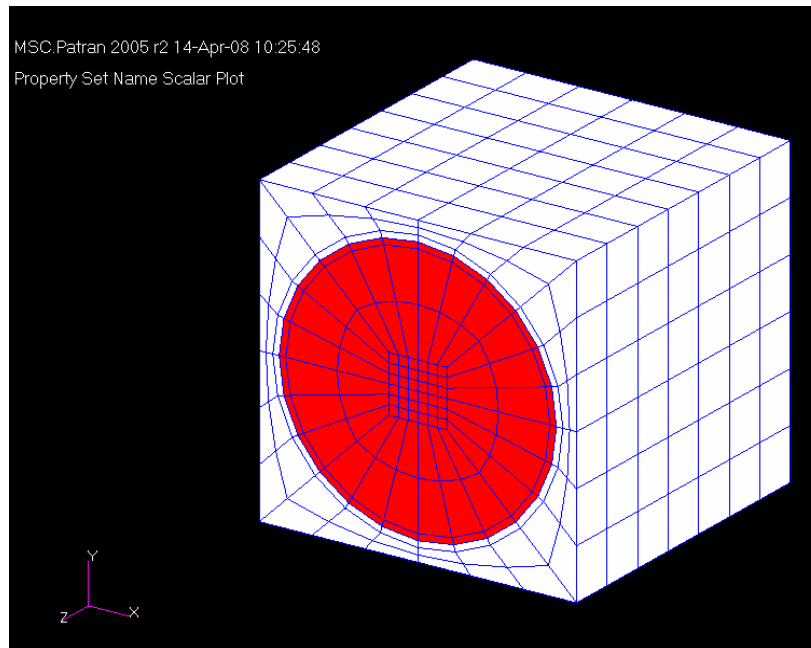


Figure 4.3- The representative volume element: square array type (where red part is for the fiber and the white part is for the resin)

The modulus and Poisson's ratio used in the verification of the elastic constant prediction are given in table 4.3. For the sake of model verification, the stiffness matrix obtained here via MSC NASTRAN and the ones given in Barbero [32] are compared in table 4.4.

Table 4.3- Properties of constituents for the verification of the methods described by Barbero

	Fiber	Matrix
E(GPa)	241	3.12
ν	0.2	0.38

The fiber volume fraction is taken as 0.4.

Table 4.4- The Comparison of the values found via FEM Method and the ones given in Barbero

	Found via FEM	Given in Barbero	%Dif.
C ₁₁	101.291	101.295	-0.004
C ₂₁	5.003	5.009	-0.120
C ₃₁	5.003	5.009	-0.120
C ₁₂	5.009	5.010	-0.020
C ₂₂	10.801	10.813	-0.111
C ₃₂	5.955	5.956	-0.017
C ₁₃	5.013	5.008	0.100
C ₂₃	5.957	5.955	0.034
C ₃₃	10.804	10.808	-0.037
E ₁	98.300	98.301	-0.001
E ₂	7.464	7.482	-0.241
G ₁₂	2.422	2.429	-0.288
v _L	0.299	0.299	0
v _T	0.541	0.540	0.185

After the verification of the finite element model and boundary condition implementation with the literature, the micromechanical model is used for further computations for the materials studied here by modifying the elastic constants and volume fraction input as measured in the experimental part of the thesis.

4.3 FEM based Failure Criterion

The values retrieved based on the unit applied strain directly gives the strain and stress amplification factors and their distribution due the existence of the fiber embedded into the matrix. The presence of a fiber in the RVE results in the variation of the stress and strain values when a unit strain or a unit stress is applied to any of the face of the RVE. These values deviated from the unity are called stress/or strain amplification factors since they are different than applied unit strain (or stress). Several key points are selected in the structure where the main behavior of the structure is tried to be examined. Figure 4.4, for instance, represents these points where the strains and/or

stresses can be evaluated and how much they vary when a unit strain [2] (Option 1) or a unit stress [3] (Option 2) is applied onto the RVE.

4.3.1 Methodology involving Application of Unit Strains [2], [3] (Option 1)

4.3.1.1 Strain Amplification Factors

The strain amplification factors are calculated by means of the same boundary conditions as also described in the previous chapter and summarized in table 4.5. Critical points for the strain amplification factors are illustrated in figure 4.4 and listed in table 4.6.

Table 4.5- Unit strain values are applied for each condition

r	Loading Direction	Boundary Conditions
1	1(=X) (longitudinal)	$\overline{\varepsilon}_{11} = 1, \overline{\varepsilon}_{22} = \overline{\varepsilon}_{33} = \overline{\gamma}_{12} = \overline{\gamma}_{23} = \overline{\gamma}_{13} = 0$
2	2(=Y) (transverse)	$\overline{\varepsilon}_{22} = 1, \overline{\varepsilon}_{11} = \overline{\varepsilon}_{33} = \overline{\gamma}_{12} = \overline{\gamma}_{23} = \overline{\gamma}_{13} = 0$
3	3(=Z) (transverse)	$\overline{\varepsilon}_{33} = 1, \overline{\varepsilon}_{11} = \overline{\varepsilon}_{22} = \overline{\gamma}_{12} = \overline{\gamma}_{23} = \overline{\gamma}_{13} = 0$
4	12(=XY) (in plane shear)	$\overline{\gamma}_{12} = 1, \overline{\varepsilon}_{11} = \overline{\varepsilon}_{22} = \overline{\varepsilon}_{33} = \overline{\gamma}_{23} = \overline{\gamma}_{13} = 0$
5	13(=XZ) (in plane shear)	$\overline{\gamma}_{13} = 1, \overline{\varepsilon}_{11} = \overline{\varepsilon}_{22} = \overline{\varepsilon}_{33} = \overline{\gamma}_{12} = \overline{\gamma}_{23} = 0$
6	23(=YZ) (out of plane shear)	$\overline{\gamma}_{23} = 1, \overline{\varepsilon}_{11} = \overline{\varepsilon}_{22} = \overline{\varepsilon}_{33} = \overline{\gamma}_{12} = \overline{\gamma}_{13} = 0$

Where $\overline{\varepsilon}$ is average axial strain and $\overline{\gamma}$ is the average shear strain and they are calculated as their volume average values. The amplified strain values are computed with the application unit strains to each face.

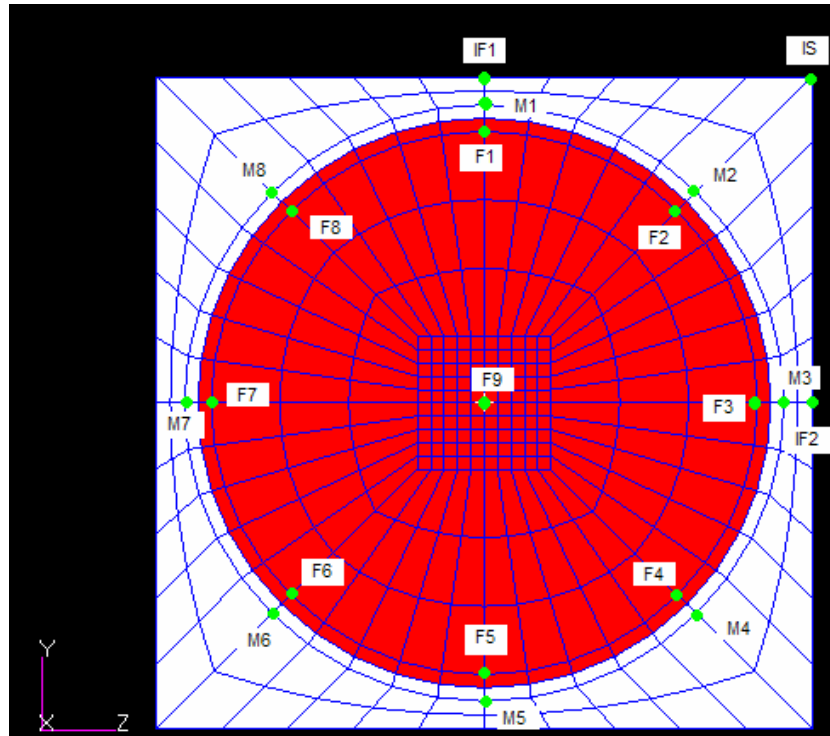


Figure 4.4- Critical points in the structure

Table 4.6- The list of critical points in the structure

#	Position	#	Position	#	Position	#	Position
1	IS	6	M3	11	M8	16	F5
2	IF1	7	M4	12	F1	17	F6
3	IF2	8	M5	13	F2	18	F7
4	M1	9	M6	14	F3	19	F8
5	M2	10	M7	15	F4	20	F9

4.3.1.2 Stress Amplification Factors

The critical failure locations throughout the specimen appear mainly as a result of stress amplifications in the structure. The levels in methodology during the calculation of stress factors can be summarized in figure 4.5.

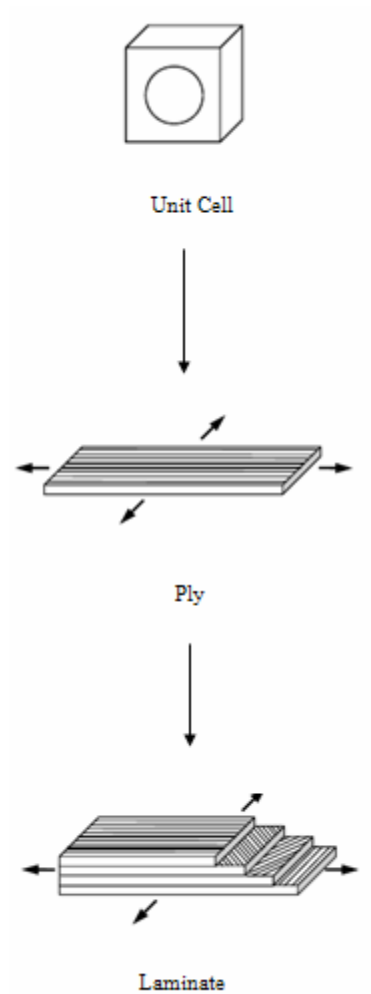


Figure 4.5- Top-bottom view in the Material Property Prediction

The strategy here is to start with the bottom-up approach, from RVE to the lamina and to laminate consequently. The equation to be used is given below:

$$AF_{Stress} = C_{Constituent} * AF_{Strain} * S_{Lamina} \quad (4.7)$$

Where AF is the amplification factor of strain or stress, C is the stiffness matrix and S is the compliance matrix of the laminate. The resin and glass fibers used are generally an isotropic material. For isotropic constituent materials the stiffness matrix (C) is [33]

$$\begin{bmatrix} \sigma_{xx} \\ \sigma_{yy} \\ \sigma_{zz} \\ \sigma_{yz} \\ \sigma_{xz} \\ \sigma_{xy} \end{bmatrix} = \frac{E}{(1+\nu)(1-2\nu)} \begin{bmatrix} 1-\nu & \nu & \nu & 0 & 0 & 0 \\ \nu & 1-\nu & \nu & 0 & 0 & 0 \\ \nu & \nu & 1-\nu & 0 & 0 & 0 \\ 0 & 0 & 0 & 1-2\nu & 0 & 0 \\ 0 & 0 & 0 & 0 & 1-2\nu & 0 \\ 0 & 0 & 0 & 0 & 0 & 1-2\nu \end{bmatrix} \begin{bmatrix} \varepsilon_{xx} \\ \varepsilon_{yy} \\ \varepsilon_{zz} \\ \varepsilon_{yz} \\ \varepsilon_{xz} \\ \varepsilon_{xy} \end{bmatrix} \quad (4.8)$$

↓
C matrix

For orthotropic materials, like the carbon fibers, the stiffness matrix is found by taking the inversion of S matrix [34].

$$\begin{bmatrix} \varepsilon_{xx} \\ \varepsilon_{yy} \\ \varepsilon_{zz} \\ \varepsilon_{yz} \\ \varepsilon_{xz} \\ \varepsilon_{xy} \end{bmatrix} = \begin{bmatrix} \frac{1}{E_x} & -\frac{\nu_{yx}}{E_y} & -\frac{\nu_{zx}}{E_z} & 0 & 0 & 0 \\ -\frac{\nu_{xy}}{E_x} & \frac{1}{E_y} & -\frac{\nu_{zy}}{E_z} & 0 & 0 & 0 \\ -\frac{\nu_{xz}}{E_x} & -\frac{\nu_{yz}}{E_y} & \frac{1}{E_z} & 0 & 0 & 0 \\ 0 & 0 & 0 & \frac{1}{2G_{yz}} & 0 & 0 \\ 0 & 0 & 0 & 0 & \frac{1}{2G_{xz}} & 0 \\ 0 & 0 & 0 & 0 & 0 & \frac{1}{2G_{xy}} \end{bmatrix} \begin{bmatrix} \sigma_{xx} \\ \sigma_{yy} \\ \sigma_{zz} \\ \sigma_{yz} \\ \sigma_{xz} \\ \sigma_{xy} \end{bmatrix} \quad (4.9)$$

↓
S matrix

After the application of the unit strains, the stress tensors at lamina level can be obtained from the stiffness matrix of the lamina using the following equation:

$$\bar{\sigma} = \bar{C}\bar{\varepsilon} \quad (4.10)$$

The stiffness matrix is obtained as given the C matrix

$$\begin{bmatrix} \bar{\sigma}_1 \\ \bar{\sigma}_2 \\ \bar{\sigma}_3 \\ \bar{\sigma}_4 \\ \bar{\sigma}_5 \\ \bar{\sigma}_6 \end{bmatrix} = \begin{bmatrix} \bar{C}_{11} & \bar{C}_{12} & \bar{C}_{13} & 0 & 0 & 0 \\ \bar{C}_{12} & \bar{C}_{22} & \bar{C}_{23} & 0 & 0 & 0 \\ \bar{C}_{13} & \bar{C}_{23} & \bar{C}_{33} & 0 & 0 & 0 \\ 0 & 0 & 0 & \bar{C}_{44} & 0 & 0 \\ 0 & 0 & 0 & 0 & \bar{C}_{55} & 0 \\ 0 & 0 & 0 & 0 & 0 & C_{66} \end{bmatrix} \begin{bmatrix} \bar{\varepsilon}_1 \\ \bar{\varepsilon}_2 \\ \bar{\varepsilon}_3 \\ \bar{\varepsilon}_4 \\ \bar{\varepsilon}_5 \\ \bar{\varepsilon}_6 \end{bmatrix} \quad (4.11)$$

Where \bar{C} describes the stiffness matrix of the lamina (equivalent to stiffness matrix of RVE) and the relation between the stress ($\bar{\sigma}$) and strain ($\bar{\varepsilon}$) values of the lamina. The strain amplification factors are obtained as a result of the application of unit strain to each face of the RVE one at a time.

$$\text{apply } \bar{\varepsilon}_i = 1 \Rightarrow \begin{pmatrix} AF_{strain1i} \\ AF_{strain2i} \\ AF_{strain3i} \\ AF_{strain4i} \\ AF_{strain5i} \\ AF_{strain6i} \end{pmatrix}_{j^{th} \text{ node}} = \begin{pmatrix} \varepsilon_1 = \varepsilon_{xx} \\ \varepsilon_2 = \varepsilon_{yy} \\ \varepsilon_3 = \varepsilon_{zz} \\ \varepsilon_4 = \varepsilon_{yz} \\ \varepsilon_5 = \varepsilon_{xz} \\ \varepsilon_6 = \varepsilon_{xy} \end{pmatrix}_{j^{th} \text{ node}} \quad (4.12)$$

where i is the compacted index of the strain tensor at which unit strain is applied while the other components are zero, j is the node of interest and the right hand side vector is the resultant strain vector at the jth node corresponding to applied unit average strain $\bar{\varepsilon}_i=1$. The index i being 1 to 6, leads to six AF vectors each is the respective column of the strain amplification factor matrix for the jth node. As a result, for any given average strain vector $\{\bar{\varepsilon}\}$ the strain vector at node j

$$\begin{pmatrix} \varepsilon_1 = \varepsilon_{xx} \\ \varepsilon_2 = \varepsilon_{yy} \\ \varepsilon_3 = \varepsilon_{zz} \\ \varepsilon_4 = \varepsilon_{yz} \\ \varepsilon_5 = \varepsilon_{xz} \\ \varepsilon_6 = \varepsilon_{xy} \end{pmatrix}_j = \begin{bmatrix} 1 & 0 & 0 & 0 & 0 & 0 \\ AF_{Strain\ 21} & AF_{Strain\ 22} & AF_{Strain\ 23} & AF_{Strain\ 24} & 0 & 0 \\ AF_{Strain\ 31} & AF_{Strain\ 32} & AF_{Strain\ 33} & AF_{Strain\ 34} & 0 & 0 \\ AF_{Strain\ 41} & AF_{Strain\ 42} & AF_{Strain\ 43} & AF_{Strain\ 44} & 0 & 0 \\ 0 & 0 & 0 & 0 & AF_{Strain\ 55} & AF_{Strain\ 56} \\ 0 & 0 & 0 & 0 & AF_{Strain\ 65} & AF_{Strain\ 66} \end{bmatrix}_j \begin{pmatrix} \bar{\varepsilon}_1 \\ \bar{\varepsilon}_2 \\ \bar{\varepsilon}_3 \\ \bar{\varepsilon}_4 \\ \bar{\varepsilon}_5 \\ \bar{\varepsilon}_6 \end{pmatrix} \quad (4.13)$$



Strain Amplification Matrix at the node j.

The local relation of the stress and strain in a constituent is given by (4.14).

$$\varepsilon_j = S\sigma_j, \quad (4.14)$$

Where ε_j is the strain at the related node and σ_j is the corresponding stress value calculated via the compliance matrix S . The average stress applied on the composite structure is calculated by means of equation (4.10). With the combination of equations (4.10), (4.11), (4.12), (4.13) and (4.14), (4.15) is obtained.

$$AF_{Stress\ j} = C_j AF_{Strain} \bar{S} \quad (4.15)$$

Where, as indicated earlier, C is the stiffness matrix of the constituent associated with the position on the RVE, and \bar{S} is the compliance of the RVE or lamina. The matrix of stress amplification factor is given in equation 4.16.

$$\begin{pmatrix} \sigma_1 = \sigma_{xx} \\ \sigma_2 = \sigma_{yy} \\ \sigma_3 = \sigma_{zz} \\ \sigma_4 = \sigma_{yz} \\ \sigma_5 = \sigma_{xz} \\ \sigma_6 = \sigma_{xy} \end{pmatrix}_j = \begin{bmatrix} AF_{Stress\ 11} & AF_{Stress\ 12} & AF_{Stress\ 13} & AF_{Stress\ 14} & 0 & 0 \\ AF_{Stress\ 21} & AF_{Stress\ 22} & AF_{Stress\ 23} & AF_{Stress\ 24} & 0 & 0 \\ AF_{Stress\ 31} & AF_{Stress\ 32} & AF_{Stress\ 33} & AF_{Stress\ 34} & 0 & 0 \\ AF_{Stress\ 41} & AF_{Stress\ 42} & AF_{Stress\ 43} & AF_{Stress\ 44} & 0 & 0 \\ 0 & 0 & 0 & 0 & AF_{Stress\ 55} & AF_{Stress\ 56} \\ 0 & 0 & 0 & 0 & AF_{Stress\ 65} & AF_{Stress\ 66} \end{bmatrix}_j \begin{pmatrix} \bar{\sigma}_1 \\ \bar{\sigma}_2 \\ \bar{\sigma}_3 \\ \bar{\sigma}_4 \\ \bar{\sigma}_5 \\ \bar{\sigma}_6 \end{pmatrix} \quad (4.16)$$



Stress Amplification Matrix at the node j.

Where x, y and z are the general coordinate system for the laminate and 1, 2 and 3 are the material directions for any given lamina as seen in figure 4.6.

The data in Ha *et al.* [3] and Jin *et al.* [2] are used for the verification. MD NASTRAN is used as processor program. For pre and post-processing, MSC PATRAN is used, which has a simple user interface. The RVE has a fiber content of 60%. Strain distributions of deformed structures are given in figure 4.6(a-f). The results match well with the results given in literature.

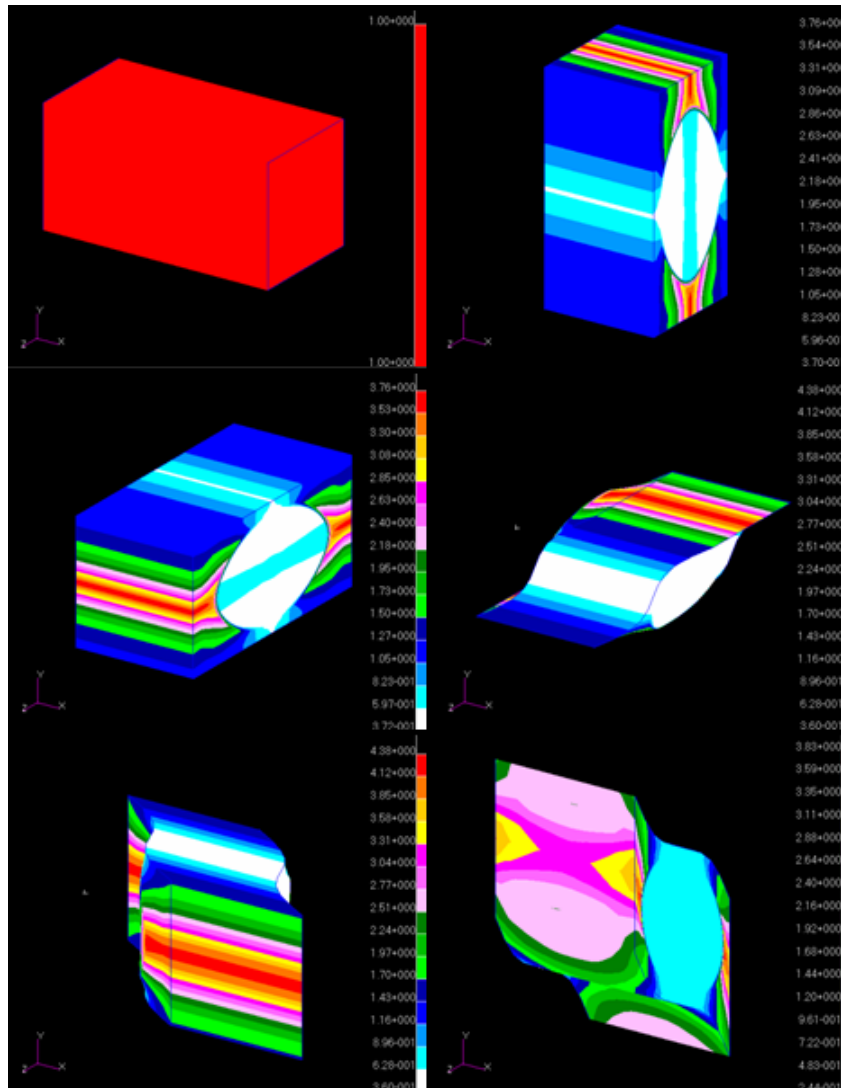


Figure 4.6- Unit strains are applied to each RVE. a) Unit strain in X direction is applied and resulting strain distribution in X direction is given b) Unit strain in Y direction is applied and resulting strain distribution in Y direction is given c) Unit strain in Z direction is applied and resulting strain distribution in Z direction is given d) Unit strain in XY direction is applied and resulting strain distribution in XY direction is given e) Unit strain in XZ direction is applied and resulting strain distribution in XZ direction is given f) Unit strain in YZ direction is applied and resulting strain distribution in YZ direction is given

4.3.2 Methodology involving Application of Unit Stress [4] (Option 2)

The stress amplification methodology can also be applied in another way. In this method, after the creation of the representative volume element, all nodes on each face are constrained to the node located at the center of that face. The motions of all the nodes on the faces in the perpendicular direction to those faces become dependent to the center nodes present on each face. The RBE2 Multiple Point Constraint (MPC) is used in this method. The Inertia Relief Method has to be used in this method. Generally, for static analyses, the FEM program cannot solve the stiffness matrix if it becomes singular. Singularity comes into practice when there is a mechanism in the structure or it moves as a rigid body, i.e. without strain [35]. The Inertia Relief Method requires the introduction of density values of the constituents to be entered to the MSC PATRAN, which are $1.8\text{e-}15\text{kg}/\mu\text{m}^3$ and $1\text{e-}15\text{kg}/\mu\text{m}^3$ for carbon fiber and epoxy resin, respectively. The implementation of MPCs to the RVE can be seen in the figure below:

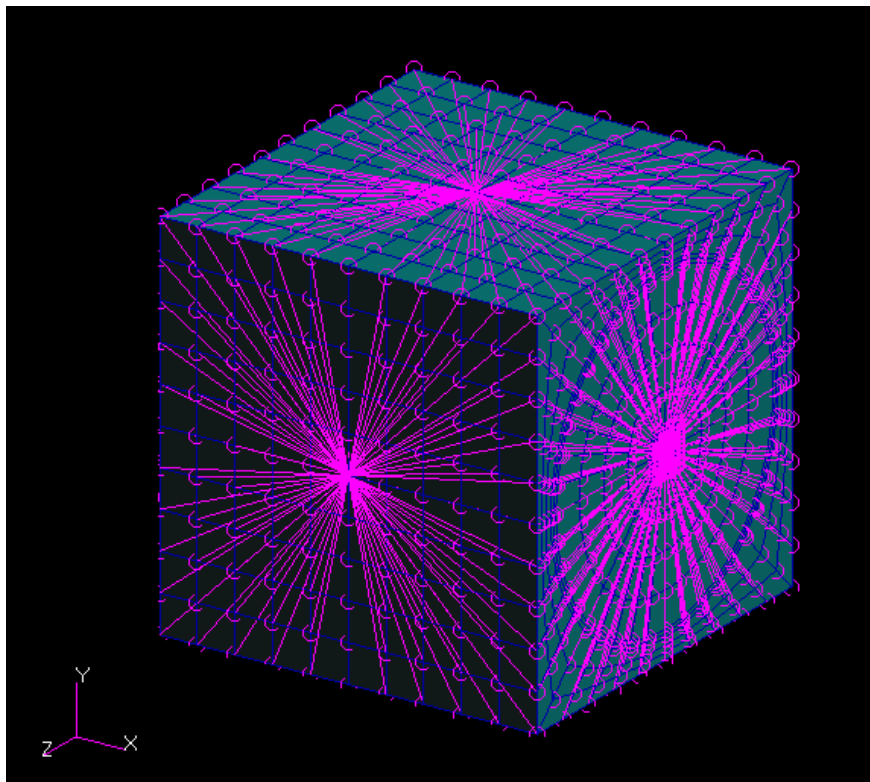


Figure 4.7-The multiple point constraints on each face of RVE

The unit stress is applied to opposite faces at $+x/2$ and $-x/2$ to obtain a deformation in x direction.

Case 1

Case 1 studied by *et al.* uses the T700 carbon fiber and epoxy resin, the properties of which are given in table 4.7[3].

Table 4.7- The properties of the constituents used in case 1

Properties	T700 Carbon Fiber	Epoxy Resin
E_{11} (GPa)	232	3.46
$E_{22}=E_{33}$ (GPa)	23.1	
G_{12} (GPa)	8.96	
G_{23} (GPa)	8.27	
ν_{12}	0.2	0.35
ν_{23}	0.4	

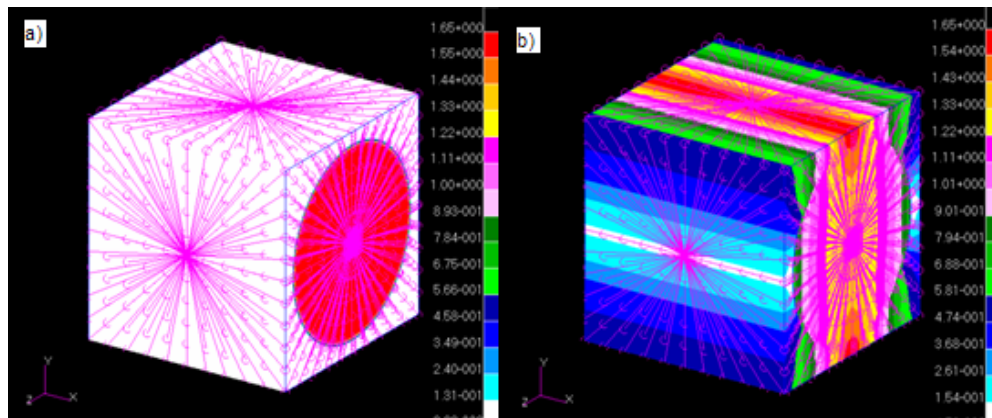


Figure 4.8- Resulting amplified stress values for Case 1 a) Stresses are applied in x direction and resulting corresponding stress values in x direction b) Stresses are applied in y direction and resulting corresponding stress values in y direction

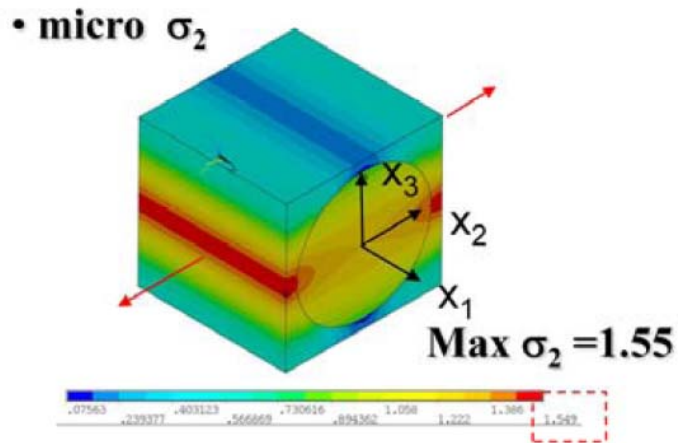


Figure 4.9- Stress Amplification Distribution Deformation in direction 2, when unit stresses are applied in 2 direction [3]

Case 2

Case 2 includes the same volume fraction of different type carbon fibers with a different type of an epoxy resin used by Jin et al. The mechanical properties of the constituents are given in table 4.8[2].

Table 4.8- The properties of the constituents used in case 2

Properties	Carbon Fiber	Epoxy Resin
E_{11} (GPa)	303	3.31
$E_{22}=E_{33}$ (GPa)	15.2	
$G_{12}= G_{23}$ (GPa)	9.65	
ν_{12}	0.2	0.35
ν_{23}	0.2	

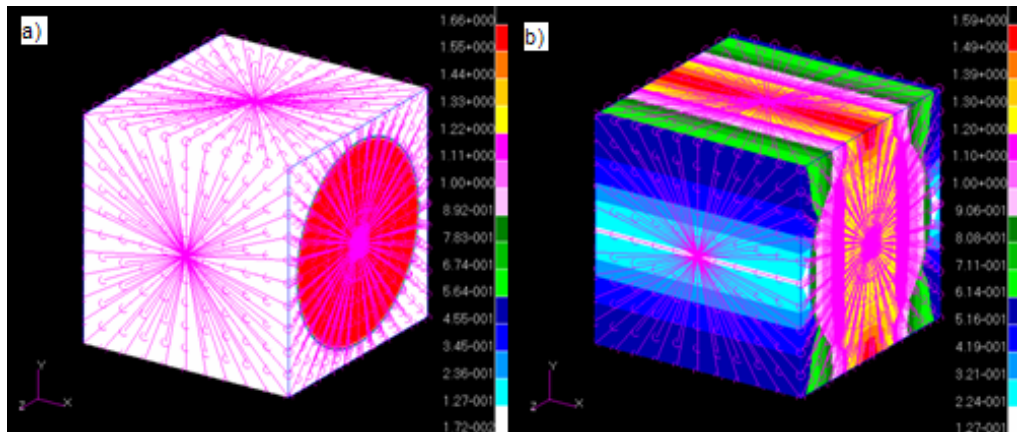


Figure 4.10- Resulting amplified stress values for Case 2 a) Stresses are applied in x direction and resulting corresponding stress values in x direction b) Stresses are applied in y direction and resulting corresponding stress values in y direction

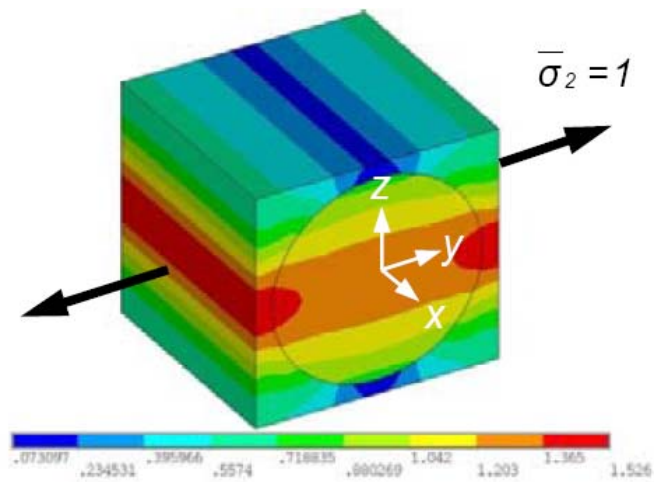


Figure 4.11- Stress Amplification Distribution Deformation in direction 2, when unit stresses are applied in 2 direction

The comparison of the results obtained via application of unit strains and stresses are compared in the figures below

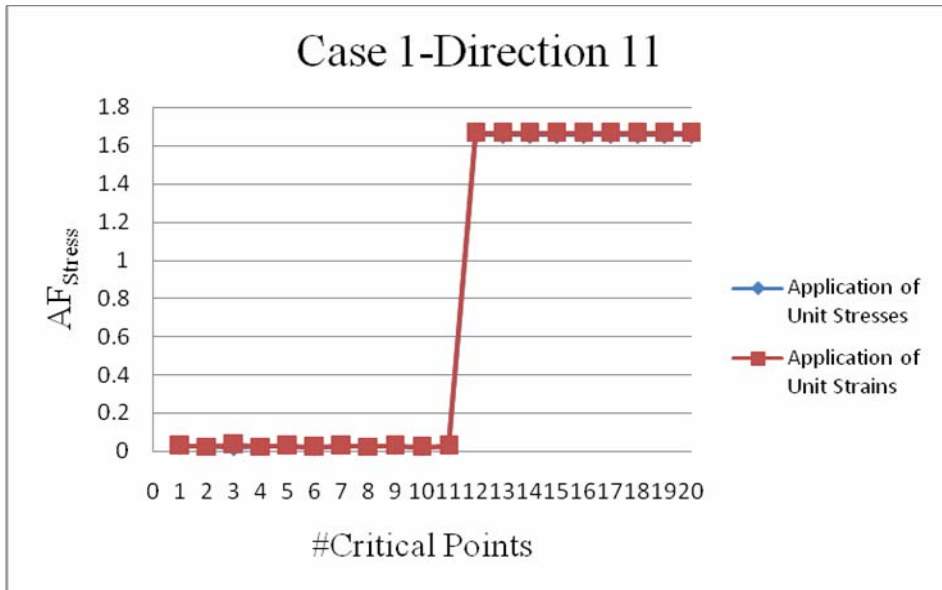


Figure 4.12- Comparison of amplified stress values in X direction for Case 1 resulting from both application of unit strains and stresses in X direction

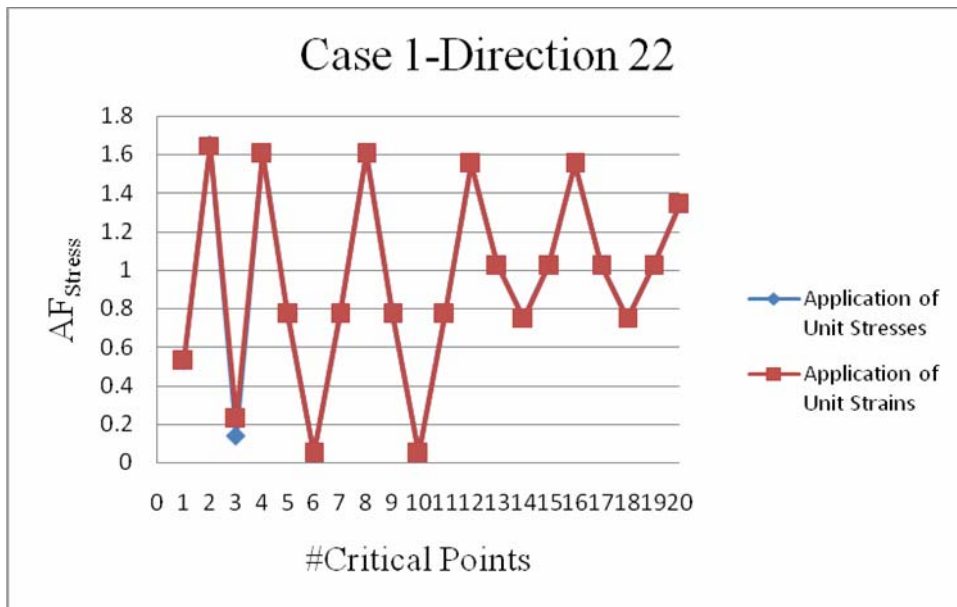


Figure 4.13- Comparison of amplified stress values in Y direction for Case 1 resulting from both application of unit strains and stresses in Y direction

As seen in figures 4-12 and 4-13, the applied two methodologies result in same outputs.

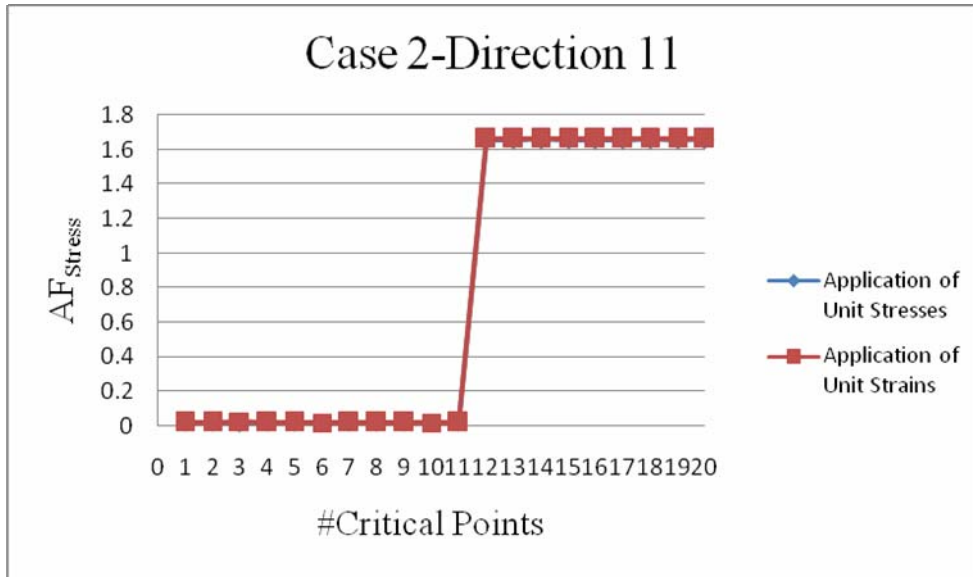


Figure 4.14- Comparison of amplified stress values in X direction for Case 2 resulting from both application of unit strains and stresses in X direction

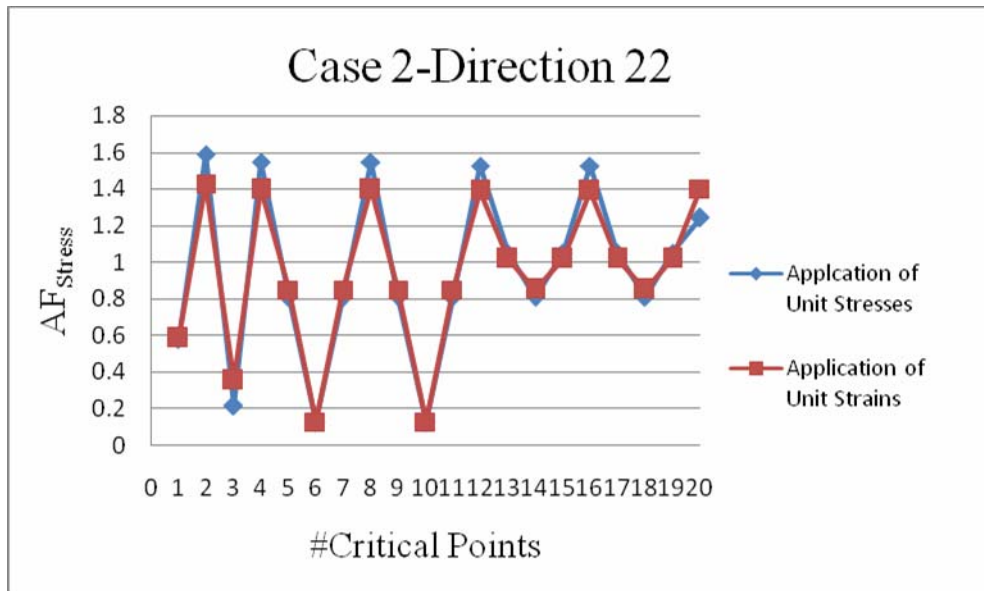


Figure 4.15- Comparison of amplified stress values in Y direction for Case 2 resulting from both application of unit strains and stresses in Y direction

In figures 4.12, 4.13 and 4.14, the same results are obtained. Figure 4.15 illustrates the slight difference in almost all values. For the sake of accuracy, the further stress amplification factors are calculated with the application of unit strain values, and then with further computations the stress amplification factors are obtained. For the back calculation methodology, for the application of deformation in x direction, the point 20(F9) is required (Figures 4.8a and 4.10a) and for the application of deformation

in y direction, the point 2(IF1) (Figures 4.8b and 4.10b) is required. Because, these points result in highest amount of stress values as also verified by Jin *et al.* and Ha *et al.* Further computations in this thesis are done according to the first methodology, which involves application of unit strains to the representative volume element.

CHAPTER 5

5 RESULTS

5.1 Case Study 1 (Examination of composites having loosely warp-knitted 600, 1200 and 2400TEX non-crimp reinforcement)

The composite laminates are manufactured with eight unidirectional (UD) plies. The constituent materials are loosely warp knitted 600, 1200 and 2400TEX fibers and Crystic Scott Bader T671 vinyl ester resin. The effects of TEX [1] on the final mechanical properties of unidirectional reinforced laminates were examined here. The back calculation methodology [3], [4] is also applied to the laminates with different TEX values in order to back-calculate the mechanical properties of constituents using the measured final strength values and fiber volume fraction of the laminates. Note that, in design the opposite will be required, that is, knowing the properties of the constituents and fiber volume fraction, strength of any laminates can be predicted.

5.1.1 Mechanical Properties of the Constituent Materials

The mechanical behavior analyses of the fibers were done at Cam Elyaf Co. with a special setup for fiber tensile testing at Cam Elyaf Co. (Figures 5.1, 5.2 and 5.3) according to the factory standards. The mechanical properties of the resin are examined and results are given in figure 5.4. The tension test of the laminates is done with the 100kN load cell installed on the UTM device, whereas 10kN load cells are used for the

tension test of resin. The average moduli of 600TEX, 1200TEX, 2400TEX fibers and Crystic Scott Bader T671 vinyl ester resin, which are 17923.8, 18760.1, 17875.0 and 593.8MPa, respectively, were used in the following FEM computations (Table 9.1). The detailed results are given in Appendix/Case Study 1. To see the statistical variance in the elastic modulus of fibers, eight specimens were tested for each fiber with a given TEX. The curves have to be moved to the origin of the axes to examine for their stress and strain values.

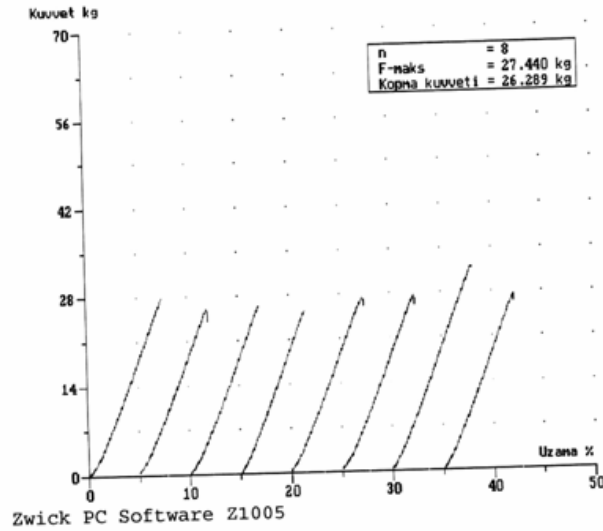


Figure 5.1- Tension test of 600TEX glass fibers

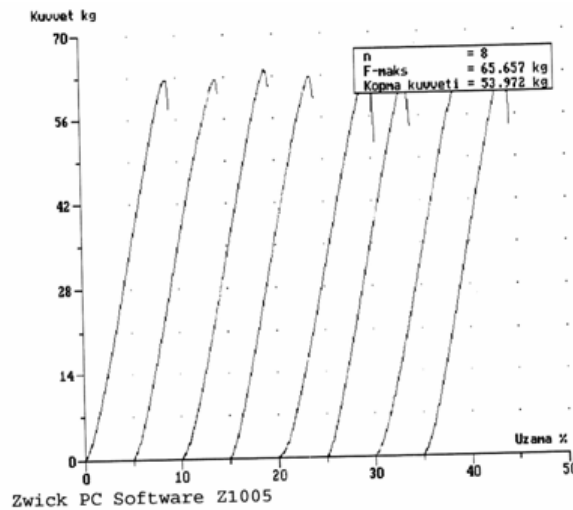


Figure 5.2- Tension test of 1200TEX glass fibers

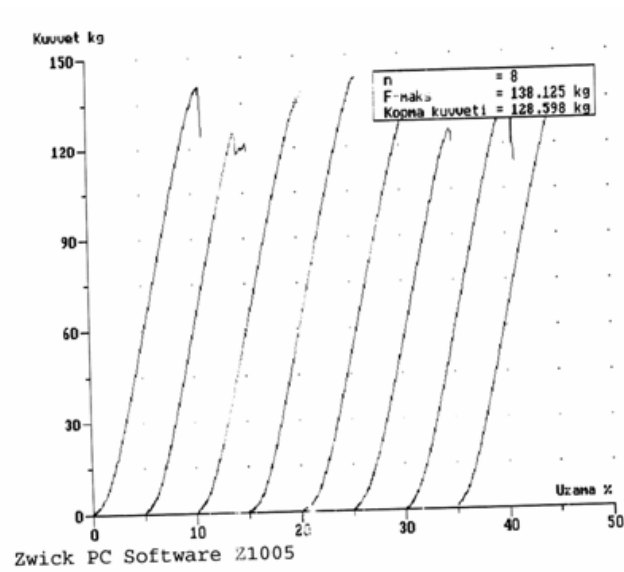


Figure 5.3- Tension test of 2400TEX glass fibers

As seen in figures 5.1, 5.2 and 5.3, the behavior of the glass fibers is completely brittle.

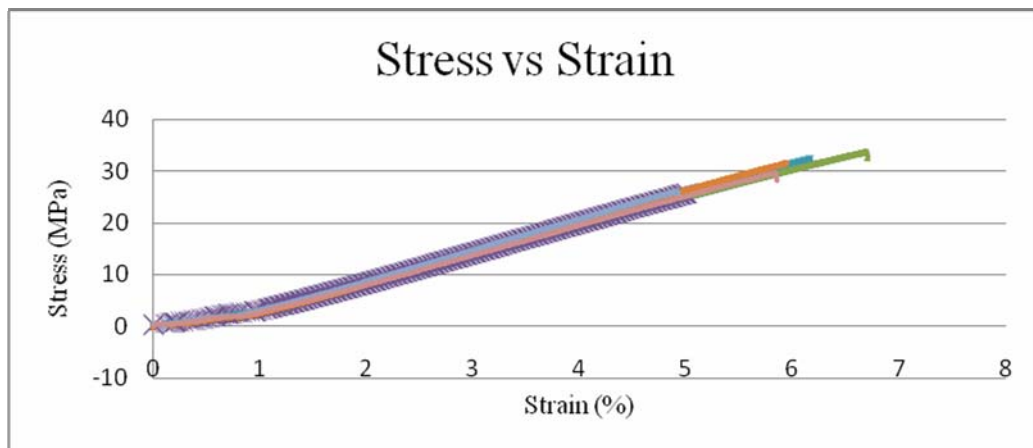


Figure 5.4- Tension test of the cured Crystic Scott Bader T671 vinyl ester resin

The ductile behavior of the resin can easily be recognized.

The ductile behavior of the T671 can be recognized easily as given in figure 5.4.

5.1.2 Mechanical Testing of the Laminates

The laminates specimens are manufactured via vacuum infusion and tested according to ASTM D3039 with the 100kN load cell is installed on the Zwick UTM device. The results of these tests are given in figures 5.(5-10). The statistics of the tension sets is summarized in table 9.2.

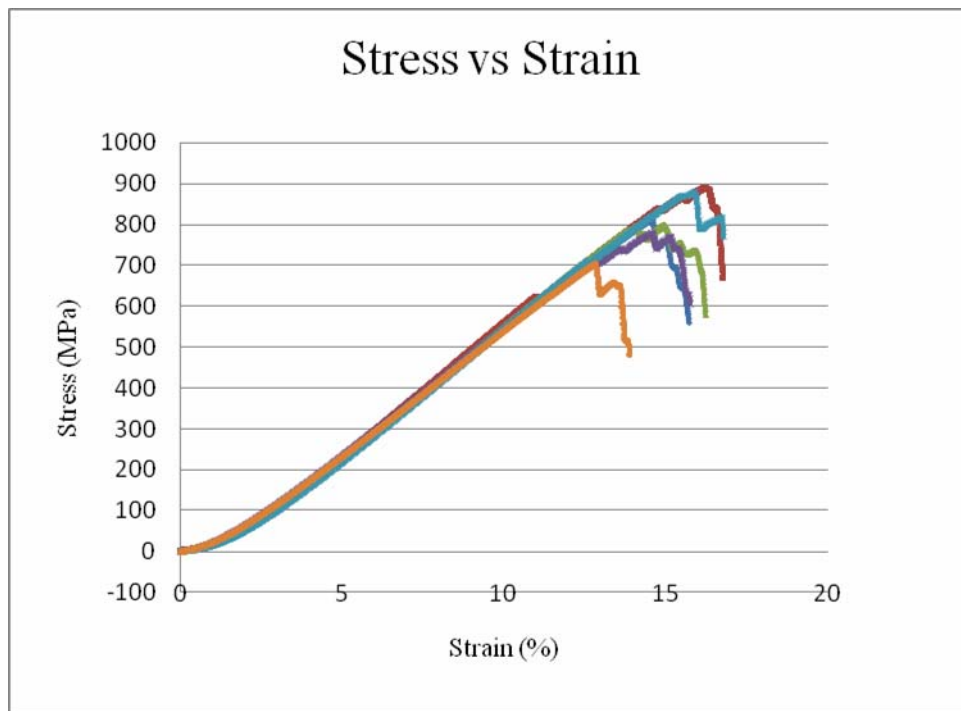


Figure 5.5- Longitudinal tension test of $(0)_8$ laminates with 600TEX fibers

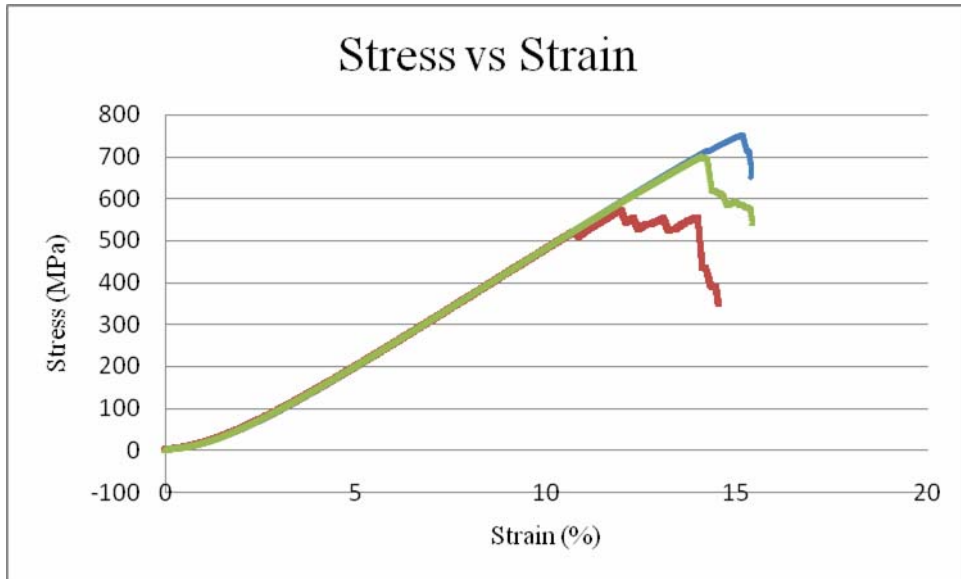


Figure 5.6- Longitudinal tension test of $(0)_8$ laminates with 1200TEX fibers,

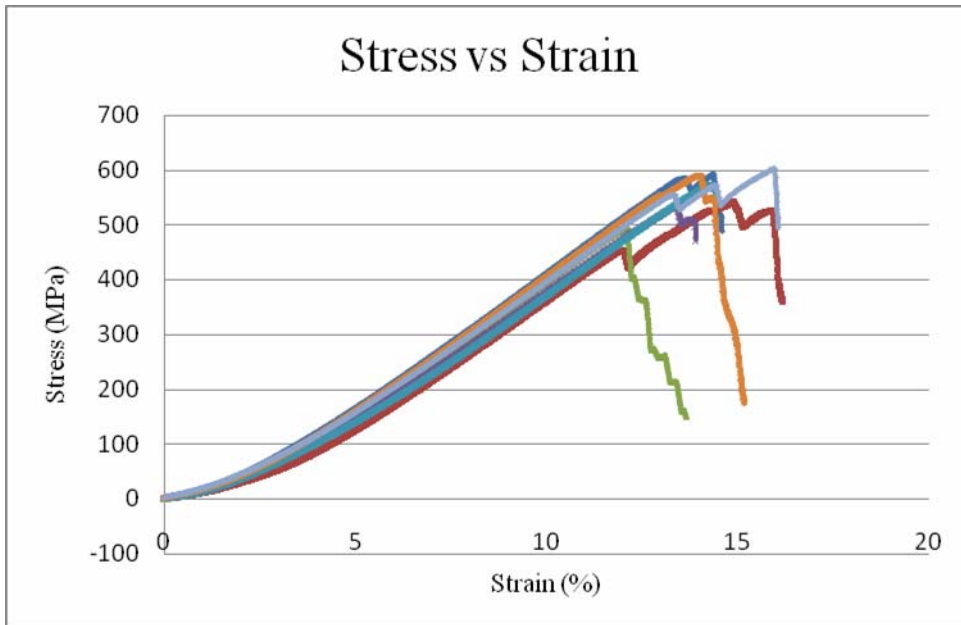


Figure 5.7- Longitudinal tension test of $(0)_8$ laminates with 2400TEX fibers

Where $(0)_8$ means there are 8 plies, all have 0° angles with respect to the longitudinal direction.

As can be seen in figures 5.5, 5.6 and 5.7, fiber pull out can easily be recognized with the stepwise decrease in the stress with the increasing strain value.

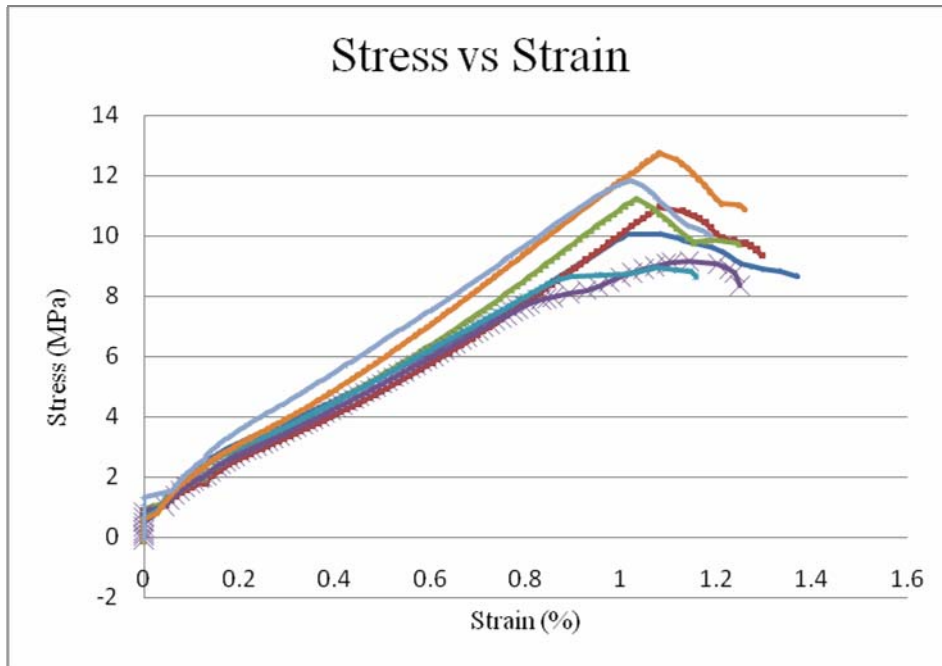


Figure 5.8- Transverse tension test of $(0)_8$ laminates with 600TEX fibers

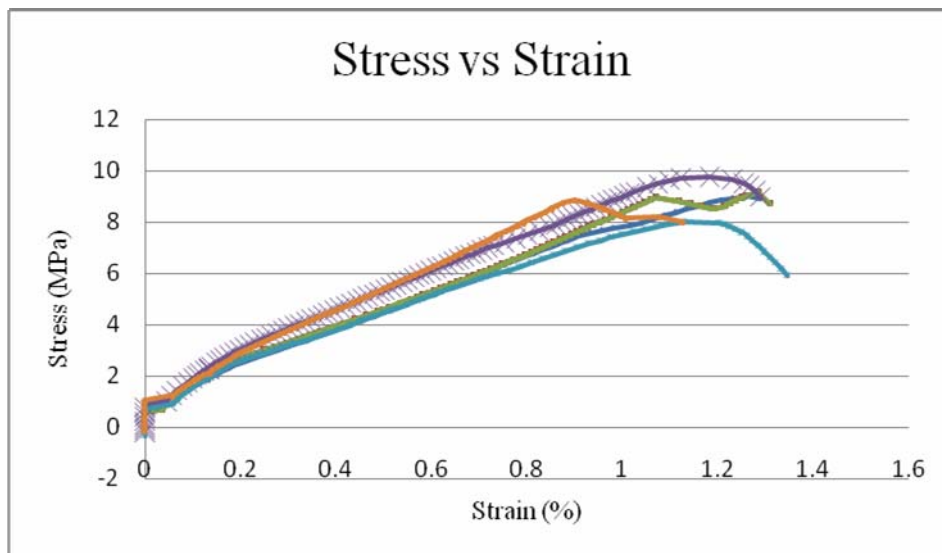


Figure 5.9- Transverse tension test of $(0)_8$ laminates with 1200TEX fibers

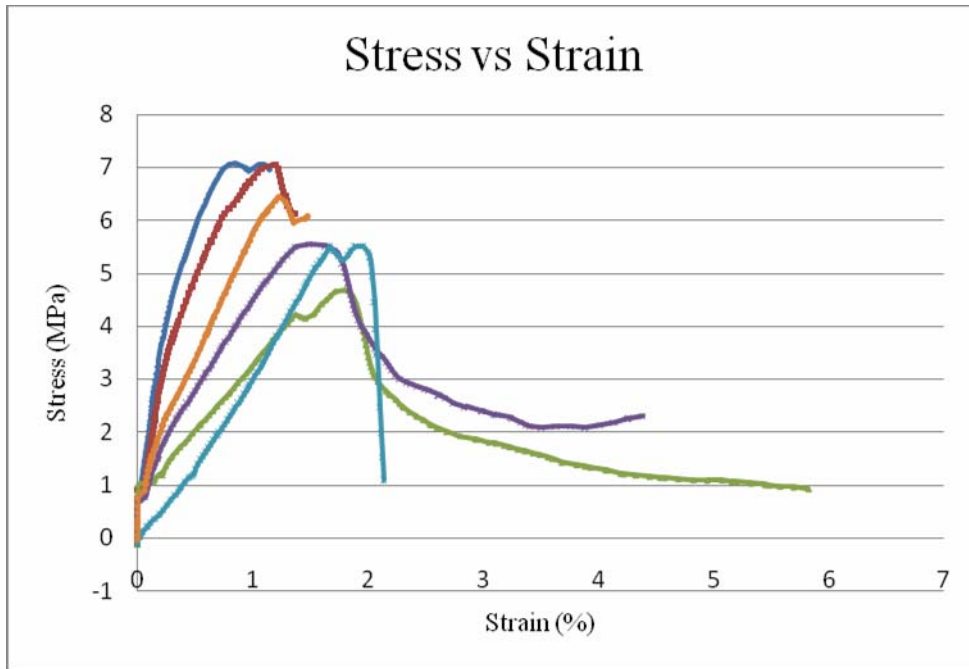


Figure 5.10- Transverse tension test of (0)₈ laminates with 2400TEX fibers

The ductile behavior of the resin is recognizable in figures 5.8, 5.9 and 5.10. The failure mechanism here may be the breakage of interfacial bonds. The two curves having failure strain values as high as 4 and 6 show that the tension test samples for those curves are taken from resin rich regions.

5.1.3 Determination of Fiber Volume Fraction

The Loss on Ignition (LOI) is applied for the determination of volume fraction of the fibers in the laminate. The mean fiber volume fractions of the laminates of (0)₈ stacking sequence with 600, 1200 and 2400TEX fiber reinforcement are measured as 0.4353, 0.4156 and 0.4121, respectively (see table 9.3).

5.1.4 Micromechanical Predictions using Monte Carlo Technique

With the uncertainty data measured concerning the stiffness values of the fibers and resins, volume fraction of fiber in the laminate, the uncertainty in longitudinal and transverse stiffness values of the laminates were computed. The maximum and minimum values of these factors are taken as limits and a uniform distribution is assumed and applied with the help of the RAND () function in MS EXCEL. Then with the Rule of Mixture (ROM), Halpin-Tsai, and Chamis models, the stiffness values were calculated for each sample within the context of Monte Carlo Simulation. The main purpose of using Monte Carlo Simulation is the assumption that the properties of each constituent and fiber volume fraction of fiber in each laminate is not a single value and can only be simulated randomly in a given interval. Equation (5.1) is used with the stiffness and fiber volume fractions given in tables 5.1 and 5.2. Note the longitudinal stiffness calculation is the same for these three criteria as stated previously. The results are summarized in table 5.3.

$$Y=Y_{\min}+(Y_{\max}-Y_{\min})*\text{RAND}() \quad (5.1)$$

Table 5.1- Minimum and maximum values stiffness and fiber volume fraction of fibers used in the MC Simulations

TEX	Vol% Min	Vol% Max	E Min (in MPa)	E Max (in MPa)
600	37.47	45.61	17244.59	18633.04
1200	36.46	45.63	17773.45	20091.72
2400	37.27	43.68	16145.13	18939.48

Table 5.2- Minimum and maximum stiffness values of the resin used in the MC Simulations

Resin	E Min (in MPa)	E Max (in MPa)
	579.7	613.1

Table 5.3- Stiffness predictions via Monte Carlo Simulation

	Statistics	Axial Modulus (in MPa)			Transverse Modulus (in MPa)		
		600 TEX	1200 TEX	2400 TEX	600 TEX	1200 TEX	2400 TEX
Rule of Mixture	Min	6854	6870	6389	910	898	906
	Max	8832	9481	8622	1094	1101	1061
	Mean	7793	8134	7455	997	992	981
	Std	459	572	468	42	47	33
Halpin - Tsai	Min	6854	6870	6389	1412	1355	1370
	Max	8832	9481	8622	1977	2030	2079
	Mean	7793	8134	7455	1681	1671	1635
	Std	459	572	468	88	105	100
Chamis	Min	6854	6870	6389	1427	1397	1416
	Max	8832	9481	8622	1765	1763	1693
	Mean	7793	8134	7455	1584	1573	1549
	Std	459	572	468	79	88	62

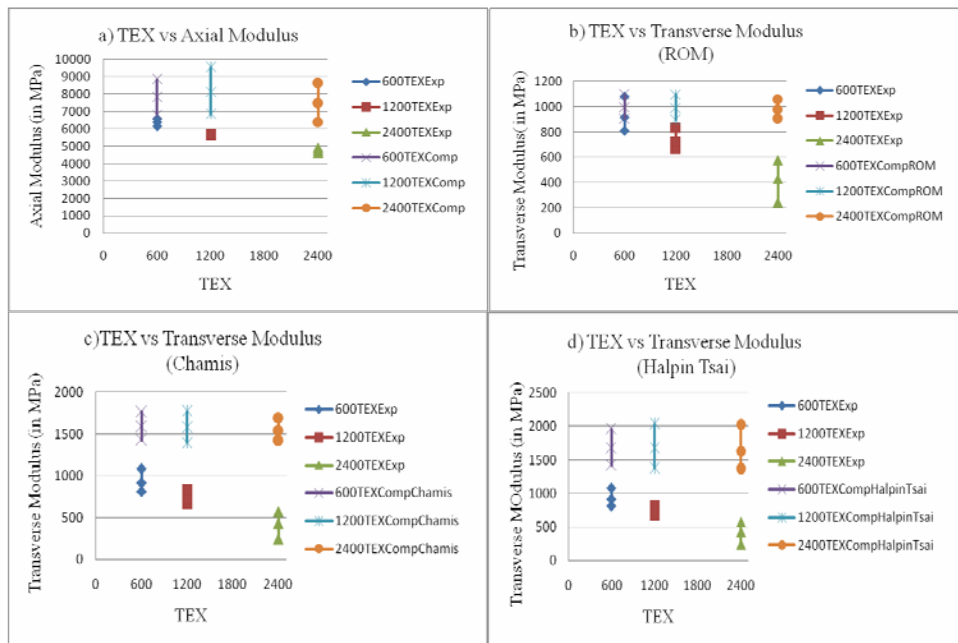


Figure 5.11- Comparison of experimental and computed values modulus of laminates - transverse moduli a) Experimental vs inverse ROM, b) Experimental vs Halpin-Tsai, c) Experimental vs Chamis and d) Longitudinal modulus experimental vs predicted

For Laminates with 600TEX Fiber Reinforcement: In the longitudinal direction, all of the values obtained via Monte Carlo Simulation are higher than the experimental values. In the transverse direction, Inverse Rule of Mixture can predict the stiffness in a

desired manner, but the other two approaches result in much higher values than the experimental ones.

For Laminates with 1200TEX Fiber Reinforcement: In the longitudinal direction, the computed values are higher than the experimental values. In the transverse direction, the Inverse Rule of Mixture is again the closest one that estimates the stiffness values closest to the experimental ones. Halpin-Tsai and Chamis give much higher stiffness values.

For Laminates with 2400TEX Fiber Reinforcement: In the longitudinal direction, the calculated values are higher than the experimental ones. In the transverse direction, all of the computed values are higher than the experimental ones, but again, the one that most closely predicting the stiffness value is the Inverse Rule of Mixture.

As can be seen in figure 5.11d, the longitudinal modulus values of the laminates decrease as the TEX value increases. Since the moduli of the 1200TEX fiber is higher than both 600 and 2400TEX fibers, the predicted axial moduli of the UD laminate of 1200 is higher than others.

The uncertainty band for the results showed correlation with the TEX. 2400 TEX has the highest variation in moduli, both experimental and computed. This is attributed to the fact that its fiber diameter is the largest which increases the effect of imperfections.

5.1.5 Back Calculation of Strength Values of Constituents

The aim here is to be able to make use of experimental data on the longitudinal and transverse specimens from $(0)_8$ laminate and evaluate how the micromechanics of failure criterion are effective. The measured stress at failure of the laminate is used to back- calculate the failure strengths of the constituents which then can be compared with the dedicated test results for the strengths of constituents. As stated previously,

when the Back Calculation Method is conducted with the application of unit strains, first the strain amplification factors are obtained with the creation of the representative volume element in the FEM Program. Then, the required boundary conditions are applied as in table 4.5. Since the unit strain is applied, the resultant strain values computed in the specified points of the unit cell give the strain amplification factors. Following the procedure described in section 4.3.1.2, stress amplification factors are obtained. As, also stated by Jin *et al.* [2] and Ha *et al.* [3], the maximum stress amplification occurs in the IF1 position if unit strain is applied transversely in the 22 direction. The maximum stress amplification occurs, however, in the F9 position if the strain is applied in the axial 11 direction. Detailed results concerning this case study are given in Appendix/Case Study 1. The back calculated strength values of both fiber and resin are given in tables 5.4 and 5.5. The Poisson's ratio for resin and fiber are taken as 0.35 and 0.2, respectively [36], [37].

Table 5.4- Comparison of strength values of the fibers with the values found via back calculation

#TEX	Statistics	Longitudinal Strength (in MPa)	Critical AF_{Stress}	Longitudinal Strength* AF_{Stress} (inMPa)	Fiber Strength (in MPa)
600	Max	890.7	2.22	1977.4	1374.9
	Average	810.8		1800.0	1176.0
	Min	704.5		1564.0	1080.4
1200	Max	750.0	2.30	1725.0	1406.3
	Average	674.1		1550.4	1359.3
	Min	572.5		1316.8	1322.1
2400	Max	602.8	2.23	1344.2	1524.9
	Average	561.2		1251.5	1455.6
	Min	497.4		1109.2	1337.8

Table 5.5- Comparison of strength values of the resin with the values found via back calculation

#TEX	Statistics	Transverse Strength (in MPa)	Critical AF_{Stress}	TransverseStrength* AF_{Stress} (inMPa)	Resin Strength (in MPa)
600	Max	12.7	1.71	21.7	33.7
	Average	10.7		18.3	29.3
	Min	8.9		15.2	23.2
1200	Max	9.8	1.69	16.6	33.7
	Average	9.0		15.2	29.3
	Min	8.0		13.5	23.2
2400	Max	7.1	1.69	12.0	33.7
	Average	6.2		10.5	29.3
	Min	4.7		7.9	23.2

The actual and predicted strength of fibers are given in the figure below:

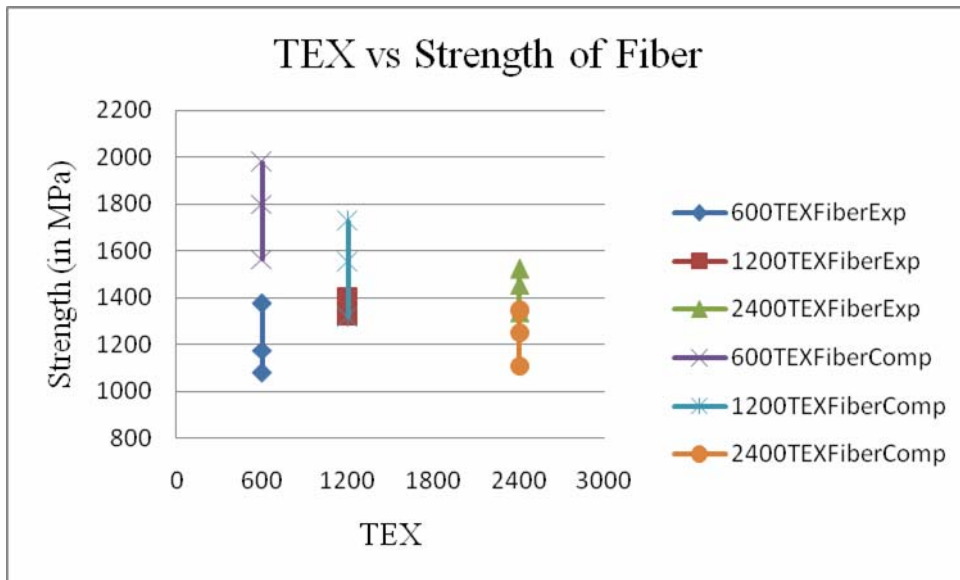


Figure 5.12- Comparison of experimental and back calculated fiber strength values

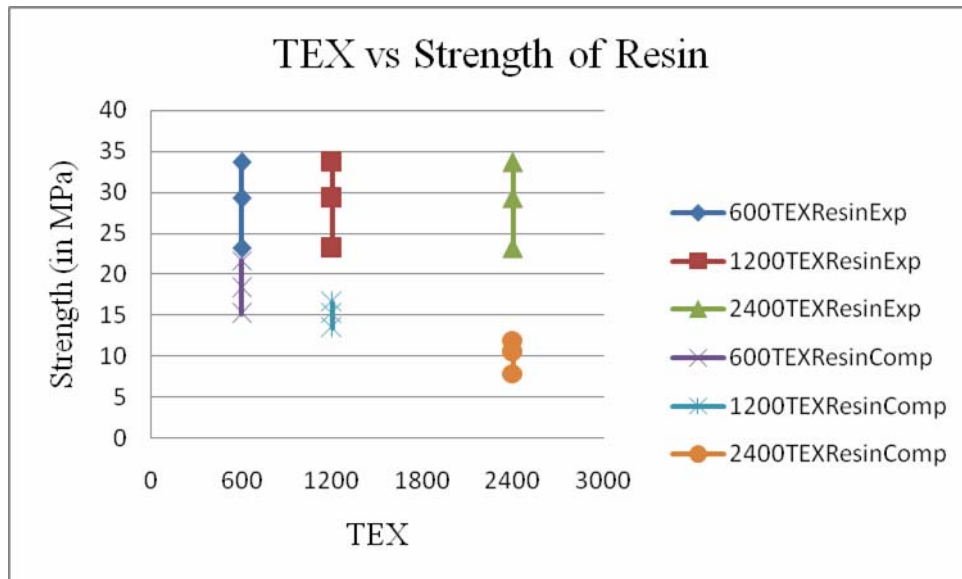


Figure 5.13- Comparison of experimental and back calculated resin strength values

Fiber Strength: The strength values of the fibers are reasonably well predicted for laminates with 1200 and 2400TEX fibers.

Resin Strength: The strength of the resin predicted is always lower than the actual value, specifically; it is most closely predicted for the laminate with 600TEX fibers.

The applied micromechanical model assumes the homogenous distribution of fibers throughout the resin. The difference in the experimental and computed resin strength may appear as a result of resin pockets in the laminate structure (Figure 6.1).

5.2 Case Study 2 (Axial Strength Prediction of the UD Laminate by tightly warp-knitted NCF: Application of Back Calculation Methodology)

In the second case study, the back calculation methodology is examined for another type of NCF reinforcement. The constituents are 1200TEX tightly warp knitted fibers with Scott Bader Crystic T676 NA Vacuum Infusion Resin. 12 UD plies are used in the stacking.

5.2.1 Mechanical Testing of the Constituent Materials

The mechanical analysis of the Scott Bader Crystic T676 NA vacuum infusion resin is done as described in previous case study and the elastic modulus and tensile strength are obtained as 445.7MPa and 26.66MPa (Figure 5.14 and table 9.4), respectively. The fibers used in this study are 1200TEX, just like the previous case study, but they have also transverse assistance as given in figure 2.7b. The results of the tests are given figure 5.2 and table 8.1.

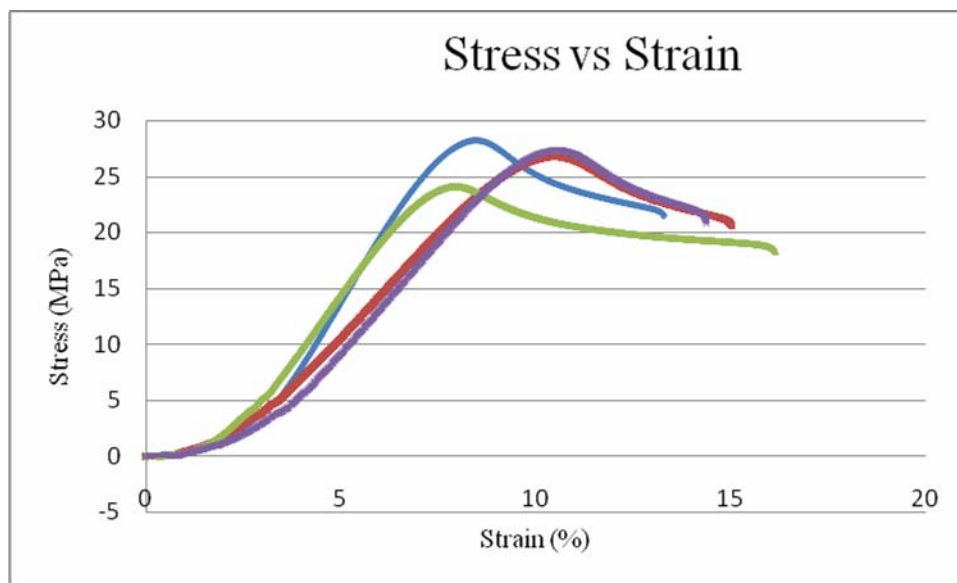


Figure 5.14- Tension test of Scott Bader Crystic T676 NA vacuum infusion resin

As can be seen in figure 5.14, the resin undergoes ductile behavior when longitudinally tested.

5.2.2 Mechanical Examination of the UD Composite Laminates

The mechanical tests of the laminates are done as described in previous case study. As seen in figure 5.15, the longitudinal behavior of the laminates is completely brittle, i.e. a sudden fracture appears without yielding.

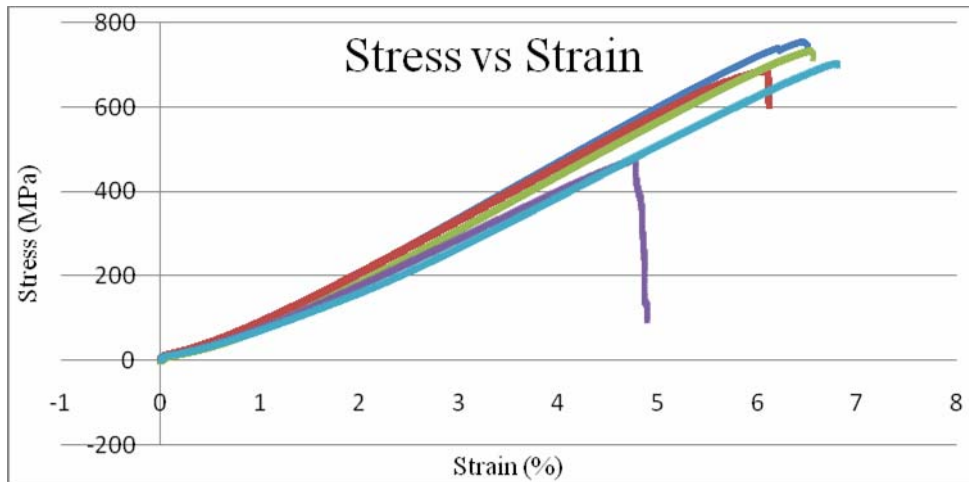


Figure 5.15- Longitudinal tension test of $(0)_{12}$ UD laminates

The behavior of the UD laminate is completely brittle here. When figure 5.16 is examined, it can be concluded that the failure two steps appear as a result of the presence of extra transverse fiber reinforcement.

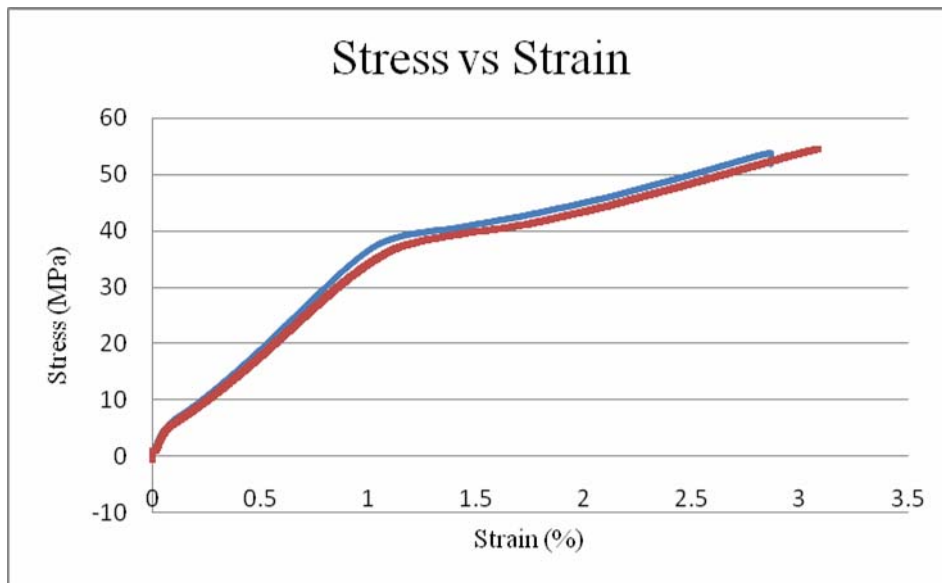


Figure 5.16- Transverse tension test of $(0)_{12}$ UD laminates

Effect of the transverse reinforcement comes into picture here. The slope change may also appear due to the failure of the resin and the ultimate failure may appear due to the failure of interfacial bonds. The modulus values of the UD laminates are given in table 9.5.

5.2.3 Determination of Fiber Volume Fraction

The difference of the reinforcing NCF here is the distribution of the fiber bundles throughout the fabric. This reinforcing layer consists of 472g/mm² longitudinal, 37g/mm² transverse glass fibers rovings and 5g/mm² stitching polyester yarn. That is, individual NCF reinforcing layer is actually made of a 1200TEX glass fiber running in the longitudinal direction and a much less amount of glass fibers in the transverse direction held together by the stitching polyester yarns (Figure 2.7b).

With the Loss on Ignition Methodology, the weight fraction of the fiber is measured to be 71% which includes both longitudinal and transverse glass fibers. For the determination of the glass fiber volume fraction, the transverse roving and stitching yarn are proposed to eliminate from the calculations and the effective volume fraction of the major UD or longitudinal reinforcing fibers is determined with a proposed equation:

$$V_f = \frac{w_f * \frac{LFTEX}{LFTEX + TFTEX} * \frac{1}{d_f}}{w_f * \frac{LFTEX}{LFTEX + TFTEX} * \frac{1}{d_f} + (1 - w_f * \frac{LFTEX}{LFTEX + TFTEX}) * \frac{1}{d_r}} \quad (5.2)$$

where LFTEX is the TEX of longitudinal fibers(in g/m²) and TFTEX is the TEX of fibers located transversely, w_f and V_f are the weight and volume fractions of fibers, and d_f and d_r and the densities of fiber and resin, respectively.

The overall volume fraction of the fiber is taken as 55.5% and the longitudinally effective volume fraction of fiber is taken as 49.5% both in the mathematical models and Finite Element Method based Failure Criterion and the predicted fiber strength results are compared with the experimental fiber strength.

5.2.4 Back Calculation of Strength Values of Constituents

The stiffness matrices for the fiber and resin, global compliance matrix of the composite and strain and stress amplification factors for locations F9 and IF1 are given in the Appendix/Case Study 2. The results of the back calculation are given in table 5.6 and figure 5.17. The elastic modulus of the resin is measured as 445.7MPa. For the computation in the FEM model this value is taken as the modulus of resin with a Poisson's ratio of 0.35[36]. The elastic modulus and Poisson's ratio of the fiber are 18760.1MPa and 0.2[37], respectively, in the FEM model with both effective (=0.495) and overall volume fractions (=0.555). Detailed results concerning this case study are given in Appendix/Case Study 2.

Table 5.6- Comparison of predicted and experimental fiber strength values both with overall and effective fiber volume fractions

	Laminate Strength (Exp) (in MPa)	Fiber Strength (Exp) (in MPa)	Overall			Effective		
			AF _{Stress}	Fiber Strength (Pred.) (in MPa)	% Dif.	AF _{Stress}	Fiber Strength (Pred.) (in MPa)	% Dif.
Max	754.0	1406.3	1.77	1337.8	4.87	1.98	1492.3	-6.11
Av.	718.9	1359.3		1275.5	6.17		1422.8	-4.67
Min	684.6	1322.1		1214.5	8.15		1354.8	-2.47

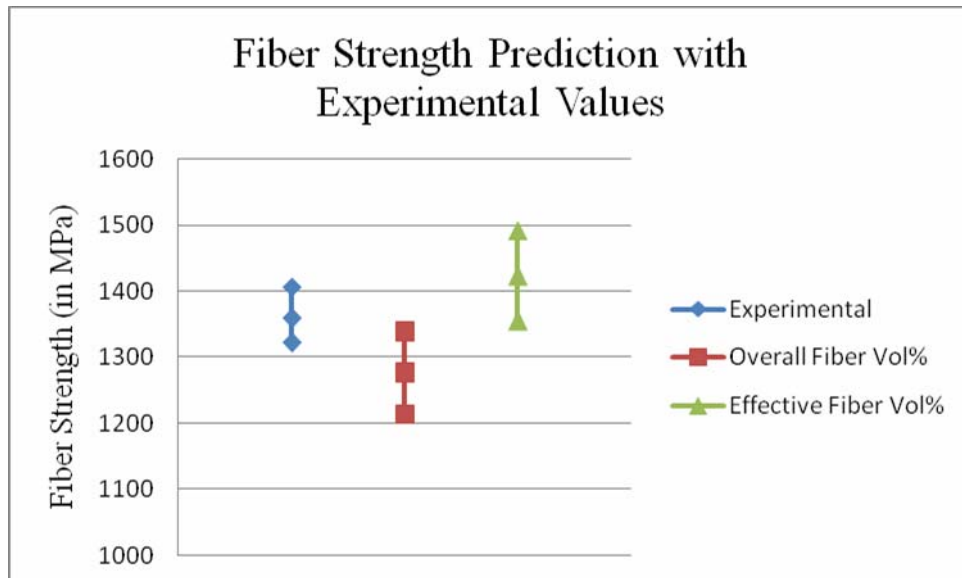


Figure 5.17- Comparison of predicted and experimental fiber strength values both with reduced (effective) and unreduced (overall) fiber volume fractions

The differences between the average experimental and unreduced and reduced predicted fiber strengths are 6.165% and -4.671%, respectively, which provides a projection on the efficiency of the methodology in predicting the longitudinal strength of the laminate if the properties of constituents and fiber volume fraction are correctly measured. Both differences and errors are reasonable, but as the prior logic necessitates, the fibers placed transversely do not have a contribution on the final longitudinal strength of the laminate. With the back-calculation methodology, if the laminates longitudinal strength is predicted, the effective stress amplification factors give more conservative values, since the stress amplification factor for the effective fiber volume fraction is higher.

5.3 Case Study 3(Verification of the Strength of Fiber and Resin of Laminates with 1200TEX fiber reinforcement having $((0/90)_3)_s$ stacking sequence)

In the final study, $((0/90)_3)_s$, the tension test of the laminates is done and the RVE of the lamina is created with the properties of the constituents. The modulus of it is predicted with this RVE and the moduli of the laminates are computed via CLT [5]. The stress amplification factors are calculated and the strength values of both fiber and resin are back-calculated which again verifies the efficiency of this method. In this method, the laminate's strength is applied to the laminate and the maximum value of the average stresses in each ply is taken. After that, this value is multiplied with the required stress amplification factor to obtain the strength of the constituents.

In the term $((0/90)_3)_s$ the subscript 3 denotes that there are three layers of the repeating stacking, which is $(0^\circ/90^\circ)$ here. The subscript s is for the symmetry relative to the mid-plane of the laminate. So the stacking here is $0/90/0/90/0/90/90/0/90/0/90/0$.

5.3.1 Mechanical Examination of the Laminates

Longitudinal behavior of the laminate is brittle as seen in figure 5.18. The stiffness values obtained via these tensile tests are given in table 5.7.

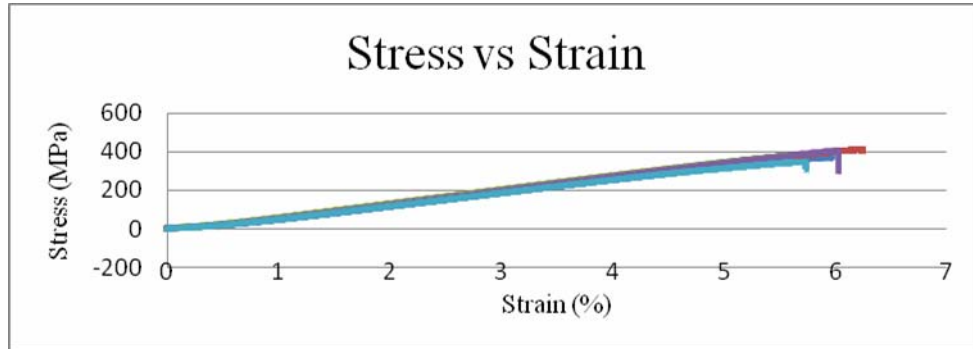


Figure 5.18- Tension testing of $((0/90)_3)_s$ laminates

Table 5.7- Elastic Moduli of biaxial reinforced laminates obtained via UTM Device

	Modulus (in MPa)
#Spec	$(0/90)_3)_s$
1	7010.8
2	7174.5
3	7240.3
4	7296.8
5	6933.7
Average	7131.2
StDev	153.875

5.3.2 Determination of Fiber Volume Fraction

The Loss on Ignition Procedure is applied and the fiber volume fraction is found as 0.556 for $(0/90)_3)_s$ laminate. All the volume fractions of these laminates tested are given Appendix/Case Study 3. Again the effective fiber volume is also found as 0.505, with the same approach described in previous case study.

5.3.3 Classical Lamination Theory via FEM

For the prediction of the stiffness of the laminate via CLT, the moduli and Poisson's ratio of the constituents are needed. With the usage of all these material constants, the ply properties are calculated via the RVE in FEM. After calculating the elastic constants via FEM, the CLT is applied in order to predict the elastic constants of the laminate. Again, as it is done in Chapter 5.2. Case Study 2, all the predictions are also done not only with the overall but also with the effective volume fiber fractions.

Table 5.8- Laminate Properties predicted via CLT

Stacking	Laminate Properties	
	Overall (0/90) ₃ _s	Effective (0/90) ₃ _s
V _f	0.566	0.505
E ₁₁ =E ₂₂ (MPa)	6370	5663

Where the modulus of the laminate is measured as 7131 MPa.

The overall fiber assumption predicts the longitudinal modulus of the laminate with an error of %10.67, whereas it is %20.59 with the effective assumption. Detailed results concerning this case study are given in Appendix/Case Study 3.

Table 5.9- Prediction of fiber strength in ((0/90)₃)_s laminates

Vol%	Longitudinal Strength (in MPa)	Average Stress (in MPa)	Critical AF_{Stress}	Average Stress * AF_{Stress} (inMPa)	Fiber Strength (in MPa)
0.566	380.96	647.00	1.74	1125.78	1359.30
0.505		655.00	1.95	1277.25	

With the overall fiber assumption, the longitudinal strength of the laminate is predicted with an error of %16.52, whereas it is %6.12 with the effective fiber assumption.

Table 5.10- Prediction of resin strength in ((0/90)₃)_s laminates

Vol%	Longitudinal Strength (in MPa)	Average Stress (in MPa)	Critical AF_{Stress}	Average Stress * AF_{Stress} (in MPa)	Resin Strength (in MPa)
0.566	380.960	115.0	1.90	218.50	26.66
0.505		107.0	1.80	192.60	

As it's seen in table 5.10, the resin strength is more than seven fold of the actual value.

CHAPTER 6

6 DISCUSSION

The application of unit strains and unit stresses separately give the same results for both 11 and 22 directions. As far as the longitudinal tensile behavior of the laminates is considered, the main failure mechanism is the fiber pull-out. With the isostrain approach, fibers try to move as much as the resin and they elongate together, but since the stiffness of the fiber is much higher than the resin, shear stress appears at the interface. As the resulting shear stress is higher than the interfacial shear strength between the fiber and resin, fiber pull-out is observed. The highest stress amplification factors appeared at the nodes located in the fiber in 11 direction with the application of longitudinal loading. Some of the fibers undergo fracture and the remaining stress is distributed between the remaining fibers. These laminates fail at strain values bigger than the sole fiber fracture strain since curing of the resin results in tensile residual stresses at the interface and helps in the more elongation of fibers with the resulting longitudinal stress. The amplified stress values in 22 direction with the application of unit stress (or strain) in 22 direction again show that the IF1 position has the highest stress value meaning that with the application of the prescribed load in that direction the highest stress amplification is in the matrix at the axis of the applied load. Actually, this increase in the stress values is due to the change in the material properties which results in that amplification at the interface and that IF1 point is close to that interface.

As seen in the second and third case studies, with the same properties of the constituents, when the fiber volume fraction increases, the stress amplification decreases. The increase in the fiber volume fraction results in the increase in the strain

amplification factors. However, the calculations of stress amplification from the application of unit strains require the multiplication of the strain amplification factors, the stiffness matrix of the constituents and the compliance matrix of the lamina, and the effect of reduction of in the compliance matrix overwhelms the increase in the strain amplification factors. This results in the lower stress amplification factors if the fiber volume fraction is higher.

As discussed in Case Study 1 (Examination of composites having loosely warp knitted 600, 1200 and 2400TEX non-crimp reinforcement), the diameter of the fibers in the higher TEX NCF was higher, which results in the lower amount of surface between the fiber and the resin when the volume fraction is the same. The reduced surface area here associated with the increase in TEX results in the decrease in the longitudinal stiffness as the volume fraction remain almost the same.. In addition to the lower amount of interface, the reduction of fiber volume fraction reduces the longitudinal modulus as expected. For the application of load in transverse direction, no relation between the TEX and stiffness is observed.

As far as the longitudinal tension tests of the laminates are considered, the fiber pull-out behavior can be recognized with the stepwise reduction in stress value with an increase in strain which is typical for polymer matrix glass fiber reinforced laminates when the fiber volume fraction is between 40% and 65% [19]. The shrinkage at cure of the resin is also very important. The presence of the fibers in the curing resin hinders this shrinkage. Fiber failure may appear in the regions where resin volume fraction is relatively low, disturbing the stress conveyance in the structure. The presence of resin rich regions on the other hand lowers the stiffness and strength values. When the behavior of the laminates under transverse loading is considered, the applied load becomes again higher than the interfacial strength between the fiber and resin.

When the Monte Carlo simulations are discussed, as can be seen in figure 5.11, the longitudinal predictions give higher values than the experimental values, which are expected. Longitudinal mechanistic micromechanical models assume perfect bonding between the fiber and resin, which result in higher longitudinal stiffness values than

experimental values. The experimental results for longitudinal stiffness here were lower than Rule of Mixture predictions as expected as the latter provides the upper bound. Their difference from upper bound is not significant and this is attributed to the cure shrinkage and resulting associated tensile residual stresses in the structure which may elevate stiffness values in longitudinal direction. Figure 2.7a and b show the differences in two types of fibers. The gap present between the two fiber bundles in the loosely warp knitted figure 2.7a is bigger than the one given in 2.7b. That gap allows the resin to shrink during curing and imposes more tensile residual reinforcement in the longitudinal direction and helps in the prevention of fiber failure during the curing process. That may be the cause for the closer predictions of Rule of Mixtures in the longitudinal direction. For the predictions made in the transverse directions, the simulations give higher values than the experimental values. Normally, those mechanistic micromechanical models assume homogenous distribution of fibers in the resin which is not valid for real life cases where the fibers are randomly distributed as given in figure 6.1. The closest transverse stiffness predictions are made with the inverse Rule of Mixture model.

As far as the back-calculation results for the strength of fibers predictions are considered, the computations give promising results. The main motivation for this work is the ability to predict the longitudinal strength of laminates with the knowledge of the strength of fibers. The work done here is to predict the strength of the constituents which directly contributes to our motivation by demonstrating the effectiveness of the MMF in an inverse setting.

When the 5.2. Case Study 2 (Axial Strength Prediction of the UD laminates by tightly warp-knitted NCF: Application of Back Calculation Methodology) is considered, the strength of fibers can again be well predicted with both the effective (reduced) and overall (as measured) fiber volume fractions. The closest predictions are made with the effective fiber volume assumption since the fibers located transversely do not have a contribution to the longitudinal direction in UD laminates.

In the transverse tension test of the laminates, it is seen that the laminate undergoes a two-step behavior which may be due to the presence of the structural fibers in the transverse direction. This change may also appear due to the failure of the resin since the stress value where the slope change happens exceeds the strength of the sole resin. The ultimate failure is likely to be due to the failed interfacial bonds.

As seen in the Case Study 3 (Verification of the strength of both fiber and the resin of laminates with 1200TEX fiber reinforcement having $((0/90)_3)_s$ stacking sequence), the longitudinal tensile failure of $((0/90)_3)_s$ laminates is completely in brittle manner with sudden fracture. The logic of removing the effect of fibers located transversely to each local axis in every ply is applicable here. The strength of the laminate is multiplied with the thickness of the laminate and applied as a load to the laminate in CLT. The highest value of the resulting average stress in all plies is taken as the critical average lamina stress and it is multiplied with the highest stress amplification value among all plies in longitudinal direction, which corresponds to the strength of fibers if the fiber breakage happens. CLT has to be applied here in order to retrieve the average lamina stresses in material coordinate system. The strength of the fiber is again well predicted. The strength of the resin, however, is well below the back-calculated resin strength values. The presence of transverse fibers located in tightly warp knitted fibers increase the transverse strength of the laminate, which in turn gives high lamina average stresses and back-calculated transverse strength estimates, in fact not appropriate to compare with the neat resin strength.

As far as the stiffness of the $((0/90)_3)_s$ laminate is considered, again the closest prediction is made with the overall fiber volume assumption since for this case, the locally transverse (longitudinal in global axes) fibers located at the ply n above the mid-plane have a contribution to the ply $n+1$ above the mid-plane in the longitudinal direction in global axes. So the reduction of extra transverse fibers during the computations is not suitable in the prediction of stiffness.

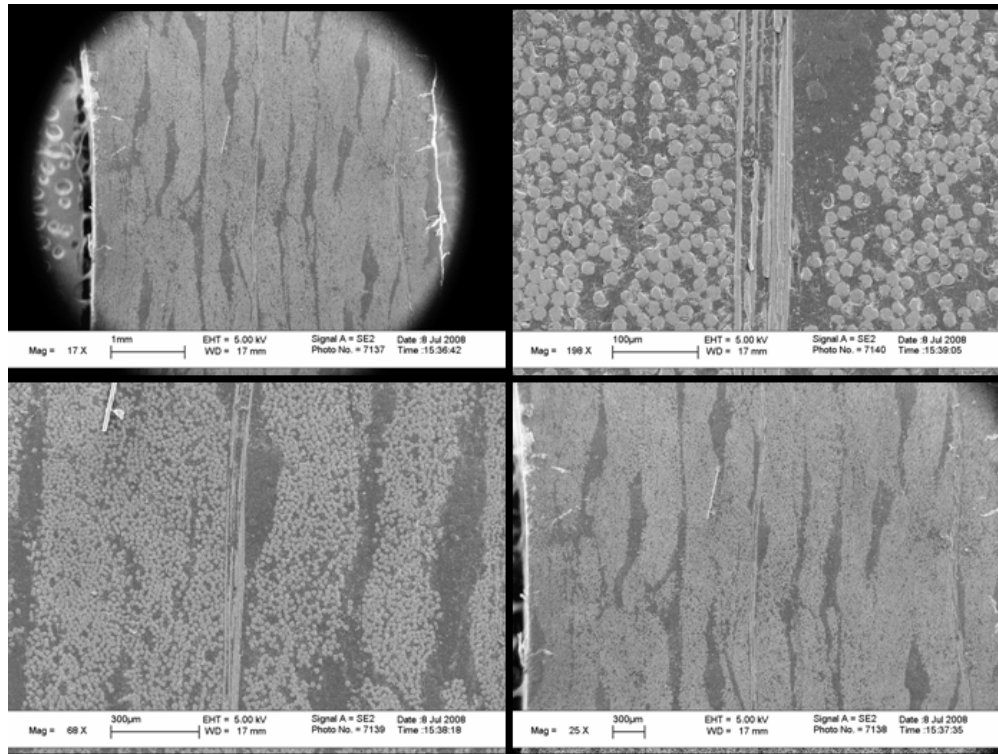


Figure 6.1- Waviness of fiber bundles in the structure and resin pockets prevents the efficiency of isotress condition.

Where \updownarrow is the transverse direction in figure 6-1 and the longitudinal direction is perpendicular to the sheet.

In biaxial reinforced NCF composites, when the load is applied in longitudinal direction, the intralaminar failure is mainly seen in plies having fiber reinforcement in the transverse direction relative to the loading direction which is not usually seen for laminates manufactured via traditional methods. The micro cracks propagate in the thickness direction in the 90° ply and when they come to the interface between the two plies of 0° and 90° angles, they cannot pass to the ply with 0° and a localized delamination is seen with the increased tensile load. That increase in the tensile load increases the transverse cracks in the thickness direction. These cracks in the NCF occur in the fiber bundles and propagate toward other bundles or propagate longitudinally [38].

The experimental studies show that the fiber pull-out is the main failure mechanism in longitudinal tension test. With the FEM based micromechanics model, by

means of the knowledge of the properties of constituents and fiber volume fraction, the longitudinal strength and stiffness values can be predicted with lower variance. As far as the transverse behavior is considered, the main failure mechanism is the breakage of interfacial bonds with the application of higher stress values than the interfacial strength. For the strength and stiffness predictions in transverse direction, the real-life distribution of the fibers throughout the structure should be ameliorated. The Monte Carlo simulation should be implemented into the input file of MD PATRAN and the effect of this randomness in the distribution and the presence of resin pockets should be well implemented.

CHAPTER 7

7 SUGGESTIONS

With the further improvements in this methodology, the necessity of testing the laminates may be limited, which results in much money and time savings.

Random distribution of the fibers within the matrix can be implemented and the laminates can be modeled more realistically.

For further verification the back calculation methodology can be applied to the other types of resins and fiber reinforcements. Other conventional stacking sequences such as $(\pm 45)_s$ or quasi isotropic structures $(0/45/90/-45)_s$ should also be investigated.

CHAPTER 8

8 REFERENCES

1. M. Baiardo, E. Zini, Mariastella Scandola, Flax Fibre-Polyester Composites, *Composites Part A: Applied Science and Manufacturing*, Vol. 35, pp 703-710, 2004,
2. K-K. Jin, Y. Huang, Y-H. Lee and S. K. Ha, Distribution of Micro Stresses and Interfacial Traction in Unidirectional Composites, *Journal of Composite Materials*, 2008
3. S. K. Ha, Online Composites Design Tutorial at Stanford University, *Micromechanics of Failure (MMF): Theory and Application*, 2007,
4. H. Cai, Y. Miyano, M. Nakada and S. K. Ha, Long-term Strength Prediction of CFRP Structure Based on Micromechanics of Failure, *Journal of Composite Materials*, Vol.42, 2008,
5. K. K. Chawla, *Composite Materials, Science and Engineering*, Chapters 11.2 and 11.3, pp 351-357, Springer, 1998,
6. Vacuum Infusion, *ASM Handbook Volume 21:Composites*, 2001,
7. Manufacturing Processes - Structural Reaction Injection Molding, <http://www.engineershandbook.com/MfgMethods/srim.htm>, accessed on 23-06-2008,
8. Materials Solutions – Polymer Composites, http://www.rapra.net/vircon/2_1_4.asp, accessed on 23-06-2008,
9. SCRIMP Construction, JBoats, <http://www.jboats.com/j100/j100scrimp.htm>, accessed on 08-07- 2008,
10. A. Cocquyt, Vacuum Infusion Process, GRP Guru, <http://www.grpguru.com/vipupdate.asp>, accessed on 13-07-2008,

11. R.D.Hale, VARTM,
http://www.engr.ku.edu/~rhale/ae510/websites_f02/vartmwebsite/, accessed on 08-07-2008,
12. H. Heß, Y.C. Roth, N. Himmel, Elastic constants estimation of stitched NCF CFRP laminates based on a finite element unit-cell model, *Composites Science and Technology*, Vol. 67, pp. 1081-1095, 2006,
13. Stephan Adden, Peter Horst, Damage propagation in non-crimp fabrics under bi-axial static and fatigue loading, *Composites Science and Technology*, Vol. 66, pp 626-633, 2006,
14. Gonzalez, A. / Graciani, E. / Paris, F. , Prediction of in-plane stiffness properties of non-crimp fabric laminates by means of 3D finite element analysis, *Composites Science and Technology*, Vol. 68, pp. 121-131, 01- 2008,
15. David Mattsson, Roberts Joffe, Janis Varna, Methodology for characterization of internal structure parameters governing performance in NCF composites, *Composites Part B: Engineering*, Volume 38, Issue 1, pp. 44-57, 2007,
16. Marvin B. Dow, H. Benson Dexter, Development of stitched, braided and woven Composite Structures in the ACT Program and at Langley Research Center, NASA/TP-97-206234, 1985-1997, 1997,
17. Y. Wang, Mechanical Properties of Stitched Multiaxial Fabric Reinforced Composites from Manual Layup Process, *Applied Composite Materials*, Vol.9, pp. 81-97, 2002,
18. Arief Yudhanto, Master's Thesis, 2005,
19. Basic Failure Modes of Continuous Fiber Composites, ASM Engineered Materials Handbook, pp. 782-783, 1987,
20. M. J. Hinton, A. S. Kaddour, P. D. Soden, Failure Criteria in Fibre Reinforced Polymer Composites: The World-Wide Exercise, A Composites Science and Technology Compendium, Elsevier, 2004,
21. T. E. Tay, S. H. N. Tan, V.B.C. Tan, J. H. Gosse, Damage Progression by the Element-Failure Method (EFM) and Strain Invariant Failure Theory(SIFT), *Composites Science and Technology*, Vol. 65, pp. 935-944, 2005,
22. Scott Bader VE 671 and VA 676 Vinyl Ester Resins,

23. Netcomposites, Guide to Composites, Vinylester Resins,
<http://www.netcomposites.com/education.asp?sequence=10>, accessed on 08 -07- 2008,
24. SP Sytems, SP Guide to Composites, <http://sp-na.com/>, accessed on 08 -07-2008,
25. PPG Industries UD Glass Fibers,
26. Vacuum Infusion – Fibre Glast-Developments Corporation, The Equipment and Process of Resin Infusion, <http://www.fibreglast.com/documents/361.pdf>, accessed on 23-06-2008,
27. ASTM D 638 Standard Test Method for Tensile Properties of Plastics,
28. ASTM D3039 Standard Test Method for Tensile Properties of Polymer Matrix Composite Materials,
29. ISO 1887 Textile Glass – Determination of Combustible Matter Content,
30. Christos C. Chamis, Louis M. Handler, Jane M. Manderscheid, COMP2007–002, Proceedings of COMP07: 6th International Symposium on Advanced Composites, 2007,
31. Angelo G.Facca, Marc T. Kortschot, Ning Yan, Predicting the Elastic Modulus of Fibre Reinforced Thermoplastics, *Composites Part A: Applied Science and Manufacturing*, Vol. 37, pp. 1660-1671, 2006,
32. E. J. Barbero, Finite Element Analysis of Composite Materials, Chp. 6: Computational Micromechanics, pp. 139-166, CRC Press, 2007,
33. Hooke’s Law for Isotropic Materials,
http://www.efunda.com/formulae/solid_mechanics/mat_mechanics/hooke_isotropic.cfm, accessed on 23-06-2008,
34. Hooke’s Law for Orthotropic Materials,
http://www.efunda.com/formulae/solid_mechanics/mat_mechanics/hooke_orthotropic.cfm, accessed on 23-06-2008,
35. MSC NASTRAN 105 Exercise Workbook,Workshop 17-Inertia Relief Method
http://www.mssoftware.com/support/online_ex/NASTRAN/Nas105/workshop_17.pdf, accessed on 23-06-2008,

36. Toughened Vinyl Ester Resins, World Intellectual Property Organization, <http://www.wipo.int/pctdb/en/wo.jsp?IA=US2005004527&DISPLAY=DESC>, accessed on 23-06-2008,
37. E-Glass Fiber, Generic, Matweb, www.matweb.com, accessed on 23-06-2008,
38. F. Edgren, D. Mattson, L. E. Asp and J. Varna, Formation of damage and its effects on non-crimp fabric reinforced composites loaded in tension, *Composites Science and Technology*, Vol. 64, pp 675-692, 2004.

CHAPTER 9

9 APPENDIX

9.1 Case Study 1

Table 9.1- Stiffness values of the loosely warp knitted fibers and Crystic Scott Bader T671 vinyl ester resin

#of Spec	Measured Modulus (in MPa)			
	600TEX Fiber	1200TEX Fiber	2400TEX Fiber	Resin
1	17883.3	18836.0	18939.5	585.9
2	17411.2	18546.2	18939.5	600.4
3	17883.3	18430.3	18628.0	580.0
4	18633.0	18724.5	18008.0	585.7
5	18022.1	17773.5	17387.1	600.0
6	17244.6	17883.8	16145.1	613.1
7	17985.5	20091.7	17387.1	605.7
8	18327.6	19794.5	17564.5	579.7
Average	17923.8	18760.1	17875.0	593.8
Std dev	448.3	823.4	957.5	12.6

Table 9.2- Longitudinal and transverse stiffness values of laminates with UD reinforcement having loosely warp knitted fibers and Crystic Scott Bader T671 vinyl ester resin

#of Spec	Longitudinal Modulus (in MPa)			Transverse Modulus (in MPa)		
	L600(0) ₈	L1200(0) ₈	L2400(0) ₈	L600(0) ₈	L1200(0) ₈	L2400(0) ₈
1	6547.8	5833.1	5206.8	838.7	1127.7	1207.3
2	6621.9	5894.0	5032.9	950.2	1075.2	790.9
3	6480.3	5904.3	4597.5	976.3	1130.8	267.4
4	6229.1		5027.2	868.7		168.5
5	6545.1		4166.4	879.8		199.0
6	6170.0			1087.5		
7				1018.2		
Average	6432.4	5877.1	4806.2	945.6	1111.2	526.6
Std dev	186.8	38.5	422.4	89.5	31.3	457.2

Table 9.3- Fiber volume fractions of UD reinforcement having loosely warp knitted fibers and Crystic Scott Bader T671 vinyl ester resin

#of Spec	Fiber Volume Fraction of Laminates (%)		
	600Tex	1200Tex	2400Tex
1	45.61	45.63	42.03
2	37.47	45.45	41.21
3	45.32	36.46	41.03
4	44.64	42.31	42.02
5	43.90	38.72	43.68
6	44.25	40.79	37.27
Average	43.53	41.56	41.21
Std. Dev.	3.04	3.66	2.14

Stiffness matrices of the Constituents:

$$C_{\text{Crystic Scott Bader T671 Vinyl Ester Resin}} = \begin{bmatrix} 0.95 & 0.51 & 0.51 & 0.00 & 0.00 & 0.00 \\ 0.51 & 0.95 & 0.51 & 0.00 & 0.00 & 0.00 \\ 0.51 & 0.51 & 0.95 & 0.00 & 0.00 & 0.00 \\ 0.00 & 0.00 & 0.00 & 0.44 & 0.00 & 0.00 \\ 0.00 & 0.00 & 0.00 & 0.00 & 0.44 & 0.00 \\ 0.00 & 0.00 & 0.00 & 0.00 & 0.00 & 0.44 \end{bmatrix} \text{ (GPa)} \quad (9.1)$$

$$C_{600\text{TEXFibers}} = \begin{bmatrix} 19.92 & 4.98 & 4.98 & 0.00 & 0.00 & 0.00 \\ 4.98 & 19.92 & 4.98 & 0.00 & 0.00 & 0.00 \\ 4.98 & 4.98 & 19.92 & 0.00 & 0.00 & 0.00 \\ 0.00 & 0.00 & 0.00 & 14.94 & 0.00 & 0.00 \\ 0.00 & 0.00 & 0.00 & 0.00 & 14.94 & 0.00 \\ 0.00 & 0.00 & 0.00 & 0.00 & 0.00 & 14.94 \end{bmatrix} \text{ (GPa)} \quad (9.2)$$

$$C_{1200\text{TEXFibers}} = \begin{bmatrix} 20.84 & 5.21 & 5.21 & 0.00 & 0.00 & 0.00 \\ 5.21 & 20.84 & 5.21 & 0.00 & 0.00 & 0.00 \\ 5.21 & 5.21 & 20.84 & 0.00 & 0.00 & 0.00 \\ 0.00 & 0.00 & 0.00 & 15.63 & 0.00 & 0.00 \\ 0.00 & 0.00 & 0.00 & 0.00 & 15.63 & 0.00 \\ 0.00 & 0.00 & 0.00 & 0.00 & 0.00 & 15.63 \end{bmatrix} \text{ (GPa)} \quad (9.3)$$

$$C_{2400\text{TEXFibers}} = \begin{bmatrix} 19.86 & 4.97 & 4.97 & 0.00 & 0.00 & 0.00 \\ 4.97 & 19.86 & 4.97 & 0.00 & 0.00 & 0.00 \\ 4.97 & 4.97 & 19.86 & 0.00 & 0.00 & 0.00 \\ 0.00 & 0.00 & 0.00 & 14.90 & 0.00 & 0.00 \\ 0.00 & 0.00 & 0.00 & 0.00 & 14.90 & 0.00 \\ 0.00 & 0.00 & 0.00 & 0.00 & 0.00 & 14.90 \end{bmatrix} \text{ (GPa)} \quad (9.4)$$

Strain Amplification Factors for the node at IF1 of the Laminate

$$AF_{\text{Strain}600\text{TEXFibers}} = \begin{bmatrix} 1.00 & 0.00 & 0.00 & 0.00 & 0.00 & 0.00 \\ 0.48 & 3.73 & -0.23 & 0.00 & 0.00 & 0.00 \\ -0.18 & -1.01 & 1.07 & 0.00 & 0.00 & 0.00 \\ 0.00 & 0.00 & 0.00 & 0.17 & 0.00 & 0.00 \\ 0.00 & 0.00 & 0.00 & 0.00 & 0.37 & 0.00 \\ 0.00 & 0.00 & 0.00 & 0.00 & 0.00 & 3.49 \end{bmatrix} \quad (9.5)$$

$$AF_{\text{Strain}1200\text{TEXFibers}} = \begin{bmatrix} 1.00 & 0.00 & 0.00 & 0.00 & 0.00 & 0.00 \\ 0.44 & 3.51 & -0.22 & 0.00 & 0.00 & 0.00 \\ -0.17 & -0.95 & 1.07 & 0.00 & 0.00 & 0.00 \\ 0.00 & 0.00 & 0.00 & 0.18 & 0.00 & 0.00 \\ 0.00 & 0.00 & 0.00 & 0.00 & 0.37 & 0.00 \\ 0.00 & 0.00 & 0.00 & 0.00 & 0.00 & 3.26 \end{bmatrix} \quad (9.6)$$

$$AF_{\text{Strain2400TEXFibers}} = \begin{bmatrix} 1.00 & 0.00 & 0.00 & 0.00 & 0.00 & 0.00 \\ 0.46 & 3.65 & -0.21 & 0.00 & 0.00 & 0.00 \\ -0.18 & -0.98 & 1.04 & 0.00 & 0.00 & 0.00 \\ 0.00 & 0.00 & 0.00 & 0.18 & 0.00 & 0.00 \\ 0.00 & 0.00 & 0.00 & 0.00 & 0.35 & 0.00 \\ 0.00 & 0.00 & 0.00 & 0.00 & 0.00 & 3.41 \end{bmatrix} \quad (9.7)$$

Strain Amplification Factors for the node at F9 of the Laminate

$$AF_{\text{Strain600TEXFibers}} = \begin{bmatrix} 1.00 & 0.00 & 0.00 & 0.00 & 0.00 & 0.00 \\ -0.17 & 0.14 & -0.01 & 0.00 & 0.00 & 0.00 \\ -0.17 & -0.01 & 0.14 & 0.00 & 0.00 & 0.00 \\ 0.00 & 0.00 & 0.00 & 0.22 & 0.00 & 0.00 \\ 0.00 & 0.00 & 0.00 & 0.00 & 0.10 & 0.00 \\ 0.00 & 0.00 & 0.00 & 0.00 & 0.00 & 0.10 \end{bmatrix} \quad (9.8)$$

$$AF_{\text{Strain1200TEXFibers}} = \begin{bmatrix} 1.00 & 0.00 & 0.00 & 0.00 & 0.00 & 0.00 \\ -0.17 & 0.12 & -0.01 & 0.00 & 0.00 & 0.00 \\ -0.17 & -0.01 & 0.12 & 0.00 & 0.00 & 0.00 \\ 0.00 & 0.00 & 0.00 & 0.21 & 0.00 & 0.00 \\ 0.00 & 0.00 & 0.00 & 0.00 & 0.09 & 0.00 \\ 0.00 & 0.00 & 0.00 & 0.00 & 0.00 & 0.09 \end{bmatrix} \quad (9.9)$$

$$AF_{\text{Strain2400TEXFibers}} = \begin{bmatrix} 1.00 & 0.00 & 0.00 & 0.00 & 0.00 & 0.00 \\ -0.17 & 0.13 & -0.01 & 0.00 & 0.00 & 0.00 \\ -0.17 & -0.01 & 0.13 & 0.00 & 0.00 & 0.00 \\ 0.00 & 0.00 & 0.00 & 0.22 & 0.00 & 0.00 \\ 0.00 & 0.00 & 0.00 & 0.00 & 0.10 & 0.00 \\ 0.00 & 0.00 & 0.00 & 0.00 & 0.00 & 0.10 \end{bmatrix} \quad (9.10)$$

Laminate Compliance Matrices

$$S_{\text{Laminatewith600TEXFibers}} = \begin{bmatrix} 0.12 & -0.03 & -0.03 & 0.00 & 0.00 & 0.00 \\ -0.03 & 0.60 & -0.21 & 0.00 & 0.00 & 0.00 \\ -0.03 & -0.21 & 0.60 & 0.00 & 0.00 & 0.00 \\ 0.00 & 0.00 & 0.00 & 0.96 & 0.00 & 0.00 \\ 0.00 & 0.00 & 0.00 & 0.00 & 0.94 & 0.00 \\ 0.00 & 0.00 & 0.00 & 0.00 & 0.00 & 0.94 \end{bmatrix} (\text{GPa}^{-1}) \quad (9.11)$$

$$S_{\text{Laminatewith1200TEXFibers}} = \begin{bmatrix} 0.12 & -0.03 & -0.03 & 0.00 & 0.00 & 0.00 \\ -0.03 & 0.63 & -0.24 & 0.00 & 0.00 & 0.00 \\ -0.03 & -0.24 & 0.63 & 0.00 & 0.00 & 0.00 \\ 0.00 & 0.00 & 0.00 & 1.00 & 0.00 & 0.00 \\ 0.00 & 0.00 & 0.00 & 0.00 & 0.99 & 0.00 \\ 0.00 & 0.00 & 0.00 & 0.00 & 0.00 & 0.99 \end{bmatrix} (\text{GPa}^{-1}) \quad (9.12)$$

$$S_{\text{Laminatewith2400TEXFibers}} = \begin{bmatrix} 0.12 & -0.03 & -0.03 & 0.00 & 0.00 & 0.00 \\ -0.03 & 0.60 & -0.22 & 0.00 & 0.00 & 0.00 \\ -0.03 & -0.22 & 0.60 & 0.00 & 0.00 & 0.00 \\ 0.00 & 0.00 & 0.00 & 0.97 & 0.00 & 0.00 \\ 0.00 & 0.00 & 0.00 & 0.00 & 0.95 & 0.00 \\ 0.00 & 0.00 & 0.00 & 0.00 & 0.00 & 0.95 \end{bmatrix} (\text{GPa}^{-1}) \quad (9.13)$$

Stress Amplification Factors for the node at IF1 of the Laminate

$$AF_{\text{Stress600TEXFibers}} = \begin{bmatrix} 0.07 & 0.70 & -0.08 & 0.00 & 0.00 & 0.00 \\ -0.01 & 1.71 & -0.48 & 0.00 & 0.00 & 0.00 \\ 0.01 & 0.36 & 0.31 & 0.00 & 0.00 & 0.00 \\ 0.00 & 0.00 & 0.00 & 0.07 & 0.00 & 0.00 \\ 0.00 & 0.00 & 0.00 & 0.00 & 0.15 & 0.00 \\ 0.00 & 0.00 & 0.00 & 0.00 & 0.00 & 1.44 \end{bmatrix} \quad (9.14)$$

$$AF_{\text{Stress1200TEXFibers}} = \begin{bmatrix} 0.07 & 0.69 & -0.07 & 0.00 & 0.00 & 0.00 \\ -0.01 & 1.69 & -0.49 & 0.00 & 0.00 & 0.00 \\ 0.01 & 0.33 & 0.34 & 0.00 & 0.00 & 0.00 \\ 0.00 & 0.00 & 0.00 & 0.08 & 0.00 & 0.00 \\ 0.00 & 0.00 & 0.00 & 0.00 & 0.16 & 0.00 \\ 0.00 & 0.00 & 0.00 & 0.00 & 0.00 & 1.42 \end{bmatrix} \quad (9.15)$$

$$AF_{\text{Stress2400TEXFibers}} = \begin{bmatrix} 0.08 & 0.69 & -0.08 & 0.00 & 0.00 & 0.00 \\ -0.01 & 1.69 & -0.48 & 0.00 & 0.00 & 0.00 \\ 0.01 & 0.35 & 0.31 & 0.00 & 0.00 & 0.00 \\ 0.00 & 0.00 & 0.00 & 0.08 & 0.00 & 0.00 \\ 0.00 & 0.00 & 0.00 & 0.00 & 0.15 & 0.00 \\ 0.00 & 0.00 & 0.00 & 0.00 & 0.00 & 1.43 \end{bmatrix} \quad (9.16)$$

Stress Amplification Factors for the node at F9 of the Laminate

$$AF_{\text{Stress600TEXFibers}} = \begin{bmatrix} 2.20 & -0.38 & -0.38 & 0.00 & 0.00 & 0.00 \\ 0.00 & 1.45 & -0.30 & 0.00 & 0.00 & 0.00 \\ 0.00 & -0.30 & 1.45 & 0.00 & 0.00 & 0.00 \\ 0.00 & 0.00 & 0.00 & 3.14 & 0.00 & 0.00 \\ 0.00 & 0.00 & 0.00 & 0.00 & 1.38 & 0.00 \\ 0.00 & 0.00 & 0.00 & 0.00 & 0.00 & 1.38 \end{bmatrix} \quad (9.17)$$

$$AF_{\text{Stress1200TEXFibers}} = \begin{bmatrix} 2.30 & -0.41 & -0.41 & 0.00 & 0.00 & 0.00 \\ 0.00 & 1.46 & -0.31 & 0.00 & 0.00 & 0.00 \\ 0.00 & -0.31 & 1.46 & 0.00 & 0.00 & 0.00 \\ 0.00 & 0.00 & 0.00 & 3.28 & 0.00 & 0.00 \\ 0.00 & 0.00 & 0.00 & 0.00 & 1.41 & 0.00 \\ 0.00 & 0.00 & 0.00 & 0.00 & 0.00 & 1.41 \end{bmatrix} \quad (9.18)$$

$$AF_{\text{Stress2400TEXFibers}} = \begin{bmatrix} 2.23 & -0.39 & -0.39 & 0.00 & 0.00 & 0.00 \\ 0.00 & 1.45 & -0.30 & 0.00 & 0.00 & 0.00 \\ 0.00 & -0.30 & 1.45 & 0.00 & 0.00 & 0.00 \\ 0.00 & 0.00 & 0.00 & 3.17 & 0.00 & 0.00 \\ 0.00 & 0.00 & 0.00 & 0.00 & 1.39 & 0.00 \\ 0.00 & 0.00 & 0.00 & 0.00 & 0.00 & 1.39 \end{bmatrix} \quad (9.19)$$

9.2 Case Study 2

Table 9.4- Elastic moduli and stiffness of Crystic Scott BaderT671 vinyl ester resin

Specimen	Elastic Modulus (in MPa)	Tensile Strength (in MPa)
1	578.6	28.5
2	353.2	26.7
3	486.8	24.1
4	364.2	27.3
Average	445.7	26.7
Std dev	107.3	1.9

Table 9.5- Axial and transverse moduli of UD laminates

Specimen	Axial Elastic Modulus (in MPa)	Transverse Elastic Modulus (in MPa)
1	13032.0	3375.8
2	12587.5	3178.3
3	12451.2	
4	10774.4	
Average	12211.3	3277.1
StdDev	989.5	139.7

Stiffness matrices of the Constituents:

$$C_{1200\text{TEXTiglyStitchedFiber}} = \begin{bmatrix} 20.84 & 5.21 & 5.21 & 0.00 & 0.00 & 0.00 \\ 5.21 & 20.84 & 5.21 & 0.00 & 0.00 & 0.00 \\ 5.21 & 5.21 & 20.84 & 0.00 & 0.00 & 0.00 \\ 0.00 & 0.00 & 0.00 & 15.63 & 0.00 & 0.00 \\ 0.00 & 0.00 & 0.00 & 0.00 & 15.63 & 0.00 \\ 0.00 & 0.00 & 0.00 & 0.00 & 0.00 & 15.63 \end{bmatrix} \text{ (GPa)} \quad (9.20)$$

$$C_{\text{Crystic Scott Bader T676NA Vinyl Ester Resin}} = \begin{bmatrix} 0.72 & 0.39 & 0.39 & 0.00 & 0.00 & 0.00 \\ 0.39 & 0.72 & 0.39 & 0.00 & 0.00 & 0.00 \\ 0.39 & 0.39 & 0.72 & 0.00 & 0.00 & 0.00 \\ 0.00 & 0.00 & 0.00 & 0.33 & 0.00 & 0.00 \\ 0.00 & 0.00 & 0.00 & 0.00 & 0.33 & 0.00 \\ 0.00 & 0.00 & 0.00 & 0.00 & 0.00 & 0.33 \end{bmatrix} \text{ (GPa)} \quad (9.21)$$

$$S_{\text{LaminateOverall}} = \begin{bmatrix} 0.09 & -0.02 & -0.02 & 0.00 & 0.00 & 0.00 \\ -0.02 & 0.53 & -0.15 & 0.00 & 0.00 & 0.00 \\ -0.02 & -0.15 & 0.53 & 0.00 & 0.00 & 0.00 \\ 0.00 & 0.00 & 0.00 & 0.92 & 0.00 & 0.00 \\ 0.00 & 0.00 & 0.00 & 0.00 & 0.89 & 0.00 \\ 0.00 & 0.00 & 0.00 & 0.00 & 0.00 & 0.89 \end{bmatrix} \text{ (GPa}^{-1}\text{)} \quad (9.22)$$

Strain Amplification Factors for the node at F9 of the Laminate

$$AF_{\text{StrainOverall}} = \begin{bmatrix} 1.00 & 0.00 & 0.00 & 0.00 & 0.00 & 0.00 \\ -0.17 & 0.14 & -0.03 & 0.00 & 0.00 & 0.00 \\ -0.17 & -0.03 & 0.14 & 0.00 & 0.00 & 0.00 \\ 0.00 & 0.00 & 0.00 & 0.20 & 0.00 & 0.00 \\ 0.00 & 0.00 & 0.00 & 0.00 & 0.09 & 0.00 \\ 0.00 & 0.00 & 0.00 & 0.00 & 0.00 & 0.09 \end{bmatrix} \quad (9.23)$$

Strain Amplification Factors for the node at IF1 of the Laminate

$$AF_{\text{StrainOverall}} = \begin{bmatrix} 1.00 & 0.00 & 0.00 & 0.00 & 0.00 & 0.00 \\ 0.92 & 5.87 & -0.10 & 0.00 & 0.00 & 0.00 \\ -0.33 & -1.45 & 0.74 & 0.00 & 0.00 & 0.00 \\ 0.00 & 0.00 & 0.00 & 0.15 & 0.00 & 0.00 \\ 0.00 & 0.00 & 0.00 & 0.00 & 0.16 & 0.00 \\ 0.00 & 0.00 & 0.00 & 0.00 & 0.00 & 5.64 \end{bmatrix} \quad (9.24)$$

Stress Amplification Factors for the node at F9 of the Laminate

$$AF_{\text{StressOverall}} = \begin{bmatrix} 1.77 & -0.23 & -0.23 & 0.00 & 0.00 & 0.00 \\ 0.00 & 1.47 & -0.34 & 0.00 & 0.00 & 0.00 \\ 0.00 & -0.34 & 1.47 & 0.00 & 0.00 & 0.00 \\ 0.00 & 0.00 & 0.00 & 2.81 & 0.00 & 0.00 \\ 0.00 & 0.00 & 0.00 & 0.00 & 1.30 & 0.00 \\ 0.00 & 0.00 & 0.00 & 0.00 & 0.00 & 1.30 \end{bmatrix} \quad (9.25)$$

Stress Amplification Factors for the node at IF1 of the Laminate

$$AF_{\text{StressOverall}} = \begin{bmatrix} 0.04 & 0.84 & -0.15 & 0.00 & 0.00 & 0.00 \\ -0.01 & 1.88 & -0.46 & 0.00 & 0.00 & 0.00 \\ 0.01 & 0.56 & 0.06 & 0.00 & 0.00 & 0.00 \\ 0.00 & 0.00 & 0.00 & 0.05 & 0.00 & 0.00 \\ 0.00 & 0.00 & 0.00 & 0.00 & 0.05 & 0.00 \\ 0.00 & 0.00 & 0.00 & 0.00 & 0.00 & 1.65 \end{bmatrix} \quad (9.26)$$

$$S_{\text{LaminateEffective}} = \begin{bmatrix} 0.11 & -0.03 & -0.03 & 0.00 & 0.00 & 0.00 \\ -0.03 & 0.64 & -0.21 & 0.00 & 0.00 & 0.00 \\ -0.03 & -0.21 & 0.64 & 0.00 & 0.00 & 0.00 \\ 0.00 & 0.00 & 0.00 & 1.08 & 0.00 & 0.00 \\ 0.00 & 0.00 & 0.00 & 0.00 & 1.06 & 0.00 \\ 0.00 & 0.00 & 0.00 & 0.00 & 0.00 & 1.06 \end{bmatrix} (\text{GPa}^{-1}) \quad (9.27)$$

Strain Amplification Factors for the node at F9 of the Laminate

$$AF_{\text{StrainEffective}} = \begin{bmatrix} 1.00 & 0.00 & 0.00 & 0.00 & 0.00 & 0.00 \\ -0.17 & 0.12 & -0.02 & 0.00 & 0.00 & 0.00 \\ -0.17 & -0.02 & 0.12 & 0.00 & 0.00 & 0.00 \\ 0.00 & 0.00 & 0.00 & 0.18 & 0.00 & 0.00 \\ 0.00 & 0.00 & 0.00 & 0.00 & 0.08 & 0.00 \\ 0.00 & 0.00 & 0.00 & 0.00 & 0.00 & 0.08 \end{bmatrix} \quad (9.28)$$

Strain Amplification Factors for the node at IF1 of the Laminate

$$AF_{\text{StrainEffective}} = \begin{bmatrix} 1.00 & 0.00 & 0.00 & 0.00 & 0.00 & 0.00 \\ 0.67 & 4.67 & -0.18 & 0.00 & 0.00 & 0.00 \\ -0.25 & -1.23 & 0.92 & 0.00 & 0.00 & 0.00 \\ 0.00 & 0.00 & 0.00 & 0.14 & 0.00 & 0.00 \\ 0.00 & 0.00 & 0.00 & 0.00 & 0.24 & 0.00 \\ 0.00 & 0.00 & 0.00 & 0.00 & 0.00 & 4.40 \end{bmatrix} \quad (9.29)$$

Stress Amplification Factors for the node at F9 of the Laminate

$$AF_{\text{StressEffective}} = \begin{bmatrix} 1.98 & -0.30 & -0.30 & 0.00 & 0.00 & 0.00 \\ 0.00 & 1.46 & -0.32 & 0.00 & 0.00 & 0.00 \\ 0.00 & -0.32 & 1.46 & 0.00 & 0.00 & 0.00 \\ 0.00 & 0.00 & 0.00 & 3.07 & 0.00 & 0.00 \\ 0.00 & 0.00 & 0.00 & 0.00 & 1.34 & 0.00 \\ 0.00 & 0.00 & 0.00 & 0.00 & 0.00 & 1.34 \end{bmatrix} \quad (9.30)$$

Stress Amplification Factors for the node at IF1 of the Laminate

$$AF_{\text{StressEffective}} = \begin{bmatrix} 0.05 & 0.77 & -0.12 & 0.00 & 0.00 & 0.00 \\ -0.01 & 1.78 & -0.47 & 0.00 & 0.00 & 0.00 \\ 0.01 & 0.46 & 0.17 & 0.00 & 0.00 & 0.00 \\ 0.00 & 0.00 & 0.00 & 0.05 & 0.00 & 0.00 \\ 0.00 & 0.00 & 0.00 & 0.00 & 0.08 & 0.00 \\ 0.00 & 0.00 & 0.00 & 0.00 & 0.00 & 1.53 \end{bmatrix} \quad (9.31)$$

9.3 Case Study 3

$$S_{\text{LaminateOverall}} = \begin{bmatrix} 0.09 & -0.02 & -0.02 & 0.00 & 0.00 & 0.00 \\ -0.02 & 0.51 & -0.14 & 0.00 & 0.00 & 0.00 \\ -0.02 & -0.14 & 0.51 & 0.00 & 0.00 & 0.00 \\ 0.00 & 0.00 & 0.00 & 0.89 & 0.00 & 0.00 \\ 0.00 & 0.00 & 0.00 & 0.00 & 0.86 & 0.00 \\ 0.00 & 0.00 & 0.00 & 0.00 & 0.00 & 0.86 \end{bmatrix} \text{ (GPa}^{-1}\text{)} \quad (9.32)$$

$$S_{\text{LaminateEffective}} = \begin{bmatrix} 0.10 & -0.03 & -0.03 & 0.00 & 0.00 & 0.00 \\ -0.03 & 0.63 & -0.20 & 0.00 & 0.00 & 0.00 \\ -0.03 & -0.20 & 0.63 & 0.00 & 0.00 & 0.00 \\ 0.00 & 0.00 & 0.00 & 1.05 & 0.00 & 0.00 \\ 0.00 & 0.00 & 0.00 & 0.00 & 1.03 & 0.00 \\ 0.00 & 0.00 & 0.00 & 0.00 & 0.00 & 1.03 \end{bmatrix} \text{ (GPa}^{-1}\text{)} \quad (9.33)$$

Strain Amplification Factors for the node at F9 of the Laminate

$$AF_{\text{StrainOverall}} = \begin{bmatrix} 1.00 & 0.00 & 0.00 & 0.00 & 0.00 & 0.00 \\ -0.17 & 0.15 & -0.03 & 0.00 & 0.00 & 0.00 \\ -0.17 & -0.03 & 0.15 & 0.00 & 0.00 & 0.00 \\ 0.00 & 0.00 & 0.00 & 0.20 & 0.00 & 0.00 \\ 0.00 & 0.00 & 0.00 & 0.00 & 0.10 & 0.00 \\ 0.00 & 0.00 & 0.00 & 0.00 & 0.00 & 0.10 \end{bmatrix} \quad (9.34)$$

$$AF_{\text{StrainEffective}} = \begin{bmatrix} 1.00 & 0.00 & 0.00 & 0.00 & 0.00 & 0.00 \\ -0.17 & 0.12 & -0.02 & 0.00 & 0.00 & 0.00 \\ -0.17 & -0.02 & 0.12 & 0.00 & 0.00 & 0.00 \\ 0.00 & 0.00 & 0.00 & 0.18 & 0.00 & 0.00 \\ 0.00 & 0.00 & 0.00 & 0.00 & 0.08 & 0.00 \\ 0.00 & 0.00 & 0.00 & 0.00 & 0.00 & 0.08 \end{bmatrix} \quad (9.35)$$

Strain Amplification Factors for the node at IF1 of the Laminate

$$AF_{\text{StrainOverall}} = \begin{bmatrix} 1.00 & 0.00 & 0.00 & 0.00 & 0.00 & 0.00 \\ 0.98 & 6.15 & -0.08 & 0.00 & 0.00 & 0.00 \\ -0.35 & -1.49 & 0.70 & 0.00 & 0.00 & 0.00 \\ 0.00 & 0.00 & 0.00 & 0.16 & 0.00 & 0.00 \\ 0.00 & 0.00 & 0.00 & 0.00 & 0.15 & 0.00 \\ 0.00 & 0.00 & 0.00 & 0.00 & 0.00 & 5.93 \end{bmatrix} \quad (9.36)$$

$$AF_{\text{StrainEffective}} = \begin{bmatrix} 1.00 & 0.00 & 0.00 & 0.00 & 0.00 & 0.00 \\ 0.71 & 4.84 & -0.17 & 0.00 & 0.00 & 0.00 \\ -0.26 & -1.26 & 0.89 & 0.00 & 0.00 & 0.00 \\ 0.00 & 0.00 & 0.00 & 0.14 & 0.00 & 0.00 \\ 0.00 & 0.00 & 0.00 & 0.00 & 0.22 & 0.00 \\ 0.00 & 0.00 & 0.00 & 0.00 & 0.00 & 4.56 \end{bmatrix} \quad (9.37)$$

Stress Amplification Factors for the node at F9 of the Laminate

$$AF_{\text{StressOverall}} = \begin{bmatrix} 1.74 & -0.22 & -0.22 & 0.00 & 0.00 & 0.00 \\ 0.00 & 1.47 & -0.35 & 0.00 & 0.00 & 0.00 \\ 0.00 & -0.35 & 1.47 & 0.00 & 0.00 & 0.00 \\ 0.00 & 0.00 & 0.00 & 2.77 & 0.00 & 0.00 \\ 0.00 & 0.00 & 0.00 & 0.00 & 1.30 & 0.00 \\ 0.00 & 0.00 & 0.00 & 0.00 & 0.00 & 1.30 \end{bmatrix} \quad (9.38)$$

$$AF_{\text{StressEffective}} = \begin{bmatrix} 1.95 & -0.29 & -0.29 & 0.00 & 0.00 & 0.00 \\ 0.00 & 1.46 & -0.33 & 0.00 & 0.00 & 0.00 \\ 0.00 & -0.33 & 1.46 & 0.00 & 0.00 & 0.00 \\ 0.00 & 0.00 & 0.00 & 3.03 & 0.00 & 0.00 \\ 0.00 & 0.00 & 0.00 & 0.00 & 1.34 & 0.00 \\ 0.00 & 0.00 & 0.00 & 0.00 & 0.00 & 1.34 \end{bmatrix} \quad (9.39)$$

Stress Amplification Factors for the node at IF1 of the Laminate

$$AF_{\text{StressOverall}} = \begin{bmatrix} 0.04 & 0.86 & -0.15 & 0.00 & 0.00 & 0.00 \\ -0.01 & 1.90 & -0.45 & 0.00 & 0.00 & 0.00 \\ 0.01 & 0.59 & 0.04 & 0.00 & 0.00 & 0.00 \\ 0.00 & 0.00 & 0.00 & 0.05 & 0.00 & 0.00 \\ 0.00 & 0.00 & 0.00 & 0.00 & 0.04 & 0.00 \\ 0.00 & 0.00 & 0.00 & 0.00 & 0.00 & 1.69 \end{bmatrix} \quad (9.40)$$

$$AF_{\text{StressEffective}} = \begin{bmatrix} 0.05 & 0.78 & -0.13 & 0.00 & 0.00 & 0.00 \\ -0.01 & 1.80 & -0.48 & 0.00 & 0.00 & 0.00 \\ 0.01 & 0.47 & 0.15 & 0.00 & 0.00 & 0.00 \\ 0.00 & 0.00 & 0.00 & 0.05 & 0.00 & 0.00 \\ 0.00 & 0.00 & 0.00 & 0.00 & 0.08 & 0.00 \\ 0.00 & 0.00 & 0.00 & 0.00 & 0.00 & 1.56 \end{bmatrix} \quad (9.41)$$

Table 9.6- Fiber volume fraction of biaxial reinforced laminates

	(0/90)3s
1	0.566
2	0.556
3	0.568
Average	0.563
StDev	0.006

Table 9.7- Axial and transverse moduli of UD laminates

Specimen	Axial Elastic Modulus (in MPa)
1	13032.0
2	12587.5
3	12451.2
4	10774.4
Average	12211.3
StdDev	989.5

CLT Code for Elastic Constant Prediction via MATLAB

```

E11=Input (Eaxial of the lamina)
E22= Input (Etransverse of the lamina)
v12= Input (v12 of the lamina)
G12= Input (G12 of the lamina)
v21=v12*E22/E11
Angles=zeros(12,1)
Qbar=zeros(3,3,12)
Ex=0
Ey=0
Q11=E11/(1-v12*v21)
Q12=v21*E11/(1-v12*v21)
Q21=v12*E22/(1-v12*v21)
Q22=E22/(1-v12*v21)
Q66=G12
    Angles=[Input(Angle1)/180*pi; Input(Angle2)/180*pi; Input(Angle3)/180*pi;
Input(Angle4)/180*pi; Input(Angle5)/180*pi; Input(Angle6)/180*pi;
Input(Angle7)/180*pi; Input(Angle8)/180*pi; Input(Angle9)/180*pi;
Input(Angle10)/180*pi; Input(Angle11)/180*pi; Input(Angle12)/180*pi]
    for i=1:12
Qbar(1,1,i)=Q11*(cos(Angles(i,1)))^4+2*(Q12+2*Q66)*(sin(Angles(i,1)))^2*(cos(Ang
les(i,1)))^2+Q22*(sin(Angles(i,1)))^4
    Qbar(1,2,i)=(Q11+Q22-
4*Q66)*(sin(Angles(i,1)))^2*(cos(Angles(i,1)))^2+Q12*((sin(Angles(i,1)))^4+(cos(An
gles(i,1)))^2)
Qbar(2,2,i)=Q11*(sin(Angles(i,1)))^4+2*(Q12+2*Q66)*(sin(Angles(i,1)))^2*(cos(Ang
les(i,1)))^2+Q22*(cos(Angles(i,1)))^4
    Qbar(1,3,i)=(Q11-Q12-2*Q66)*(sin(Angles(i,1)))*(cos(Angles(i,1)))^3+(Q12-
Q22+2*Q66)*(sin(Angles(i,1)))^3*(cos(Angles(i,1)))
    Qbar(2,3,i)=(Q11-Q12-2*Q66)*(sin(Angles(i,1)))^3*(cos(Angles(i,1)))+(Q12-
Q22+2*Q66)*(sin(Angles(i,1)))*(cos(Angles(i,1)))^3

```

```

    Qbar(3,3,i)=(Q11+Q22-2*Q12-
2*Q66)*(sin(Angles(i,1)))^2*(cos(Angles(i,1)))^2+Q66*((sin(Angles(i,1)))^4+(cos(Angles(i,1)))^4)
    Qbar(2,1,i)=Qbar(1,2,i)
    Qbar(3,1,i)=Qbar(1,3,i)
    Qbar(3,2,i)=Qbar(2,3,i)
end
A=zeros(3,3)
B=zeros(3,3)
D=zeros(3,3)
for j=1:3
    for k=1:3
        for l=1:12
            A(j,k)=A(j,k)+Input(thickness of the laminate/12)*Qbar(j,k,l)
        end
    end
end
for j=1:3
    for k=1:3
        for l=1:6
            B(j,k)=B(j,k)+(-(7-l)^2+(6-l)^2)* ( Input(thickness of the laminate/12))^2)
            *Qbar(j,k,l)
        end
        for l=7:12
            B(j,k)=B(j,k)+((l-6)^2-(l-7)^2)* ( Input(thickness of the laminate/12))^2)
            *Qbar(j,k,l)
        end
    end
end
B=0.5*B
for j=1:3
    for k=1:3
        for l=1:6
            D(j,k)=D(j,k)+((7-l)^3-(6-l)^3)* ( Input(thickness of the laminate/12))^3)
            *Qbar(j,k,l)
        end
        for l=7:12
            D(j,k)=D(j,k)+((l-6)^3-(l-7)^3)* ( Input(thickness of the laminate/12))^3)
            *Qbar(j,k,l)
        end
    end
end
D=D*1/3
Ex=(A(1,1)*A(2,2)-A(1,2)^2)/( Input(thickness of the laminate) *A(2,2))
Ey=(A(1,1)*A(2,2)-A(1,2)^2)/( Input(thickness of the laminate) *A(1,1))
Gxy=A(3,3)/ Input(thickness of the laminate)

```